Modeling of Axial Piston Pump Input Torque and Output Flow Rate using MATLAB® Simulink

by

Pawan Panwar

A Report Submitted to the Faculty of the

Milwaukee School of Engineering

in Partial Fulfillment of the

Requirements for the Degree of

Master of Science in Engineering

Milwaukee, Wisconsin

August 2018

Abstract

The purpose of this project was to examine and to develop a steady-state MATLAB Simulink model of the variable displacement axial piston pump. Axial piston pumps are widely used both in industry and off-highway machinery because of their design's compactness, flexibility in power transfer, a broad range of operating pressure and speed, variable flow rate, and high efficiencies as compared to their manufacturing costs.

Work was carried out with the goal of developing detailed steady-state Simulink models of the axial piston pump using physical parameters based on first principles (i.e., actual measurements) to assist in determining the pump outlet flow, leakage flow, and torque input. The pressure and temperature dependent fluid properties that influence the efficiency of hydraulic machinery were also incorporated to validate the model for multiple fluids and to determine the most energy efficient hydraulic oil. In the first phase of the project, fluid properties that affects the performance of the hydraulic system were developed as a function of pressure and temperature of the fluid. In the second phase, the empirical models for the discharge flow and torque input were developed using best subset regression analysis. Finally, the MATLAB Simulink of discharge flow and torque on the shaft was developed using the dimensions of a pump.

Four fluids that differ in their physical properties were evaluated in a dynamometer at 80°C using a modified ISO 4409 procedure. The dynamometer consists of an open-loop axial piston swash plate type pump, to test hydraulic fluid efficiency for off-highway machinery. For developing a robust and high-fidelity empirical model, a Latin Hypercube sampling (LHS) based design of experiment (DOE) was planned and to validate the developed MATLAB model, a full factorial based DOE was implemented.

The fluid properties model developed for this project very well correlated fluid properties for a broad range of operating conditions. Empirical models based upon LHS DOE were shown very effective in predicting both discharge flow and torque input and in distinguishing the fluids that differ in their physical properties. Hence, they could be used in predicting energy efficient fluid for off-highway machinery. In addition, the MATLAB Simulink models that were developed for this project, which incorporate the developed fluid properties model, were successful in forecasting discharge flow and torque input. However, the developed torque input model has a considerable difference as compared to the flow rate model. A higher fidelity model for gap height and viscous friction would enhance the accuracy of torque model.

Acknowledgments

It gives me great pleasure to express my sincere gratitude to everyone who has supported and contributed to making this capstone project possible.

I would like first to acknowledge my direct supervisor and advisor Mr. Paul Michael for his enthusiasm, inspiration and huge efforts to explain things clearly and simply and my technical advisor Dr. Daniel Williams for providing significant help in implementing mathematical models into MATLAB Simulink. Without these gentlemen's immense assistance, this project could not have been completed.

I would also like to thank Prof. Gary Shimek for his fantastic technical writing assistance and his guidance on which areas of my project to focus on. I would also like to thank Dr. Kumpaty for putting my excellent team of advisors together.

I also thank Mr. Tim Kerrigan, Mr. Joseph Munski, Mr. Jon Shibilski, Mr. Russell Steinmetz, and Mr. Levi Wagner of the MSOE Fluid Power Institute (FPI) for test stand design, construction, control, instrumentation, troubleshooting and data collection. Furthermore, a special thanks to Mr. Tim Kerrigan, who is a Director of FPI, for giving me a spare axial piston pump and pushing me to work on a project I knew I would enjoy, instead of one I already knew how to complete.

This research was supported by the MSOE Fluid Power Institute and the research grant given by the Society of Tribologists and Lubrication Engineers (STLE), Chicago Section. I also wish to acknowledge the scholarship support provided by MSOE throughout my B.S. and M.S. Program.

Lastly and most importantly, I dedicate this capstone project to my parents, Mr. Laxminarayan and Mrs. Kiran Panwar, and my best friends, Radheshyam and Sarita Panwar, who supported, taught, motivated and loved me throughout my entire life.

Milwaukee, 2018
Pawan Panwar

Table of Contents

List of Figures 6

List of Tables 8

Nomenclature 9

Chapter 1: Introduction 15

Chapter 2: Background and Literature Review 17

2.1 Positive Displacement Machine 17

2.2 Axial Piston Swash-Plate Pump 17

2.3 Empirical Modeling 22

Chapter 3: Physical and Thermal Properties of the Hydraulic Fluids 26

3.1 Introduction 26

3.2 Bulk Modulus 27

3.3 Viscosity 29

3.3.1 Kinematic Viscosity 32

3.4 Density 32

3.5 Thermal Properties 33

Chapter 4: Mathematical Modeling of Axial Piston Pump 34

4.1 Pump Kinematics 34

4.2 Volumetric Flow Rate 37

4.2.1 Theoretical Flow Rate and Ripple 37

4.2.2 Instantaneous Displacement Chamber Pressure 40

4.2.3 Overall Flow Rate of the Pump 48

4.3 Torque Input on the Shaft and Swash Plate 49

4.3.1 Piston Dynamic Loading 49

4.3.2 Instantaneous Torque on the Shaft 52

4.3.3 Overall Torque on the Shaft of the Pump 53

4.4 MATLAB Simulink Models 54

Chapter 5: Experimental Methodology 69

Chapter 6: Results and Discussion 75

6.1 Empirical Modeling 75

6.1.1 Pump Discharge Flow Model 75

6.1.2 Pump Torque Model 77

6.2 Mathematical Modeling in MATLAB Simulink 79

Chapter 7: Summary 91

References 93

APPENDIX 97

Appendix A: MATLAB Function to Determine Fluid Properties Model 97

Appendix B: MATLAB Function to Acquire Parameters of the Fluids 99

Appendix C: MATLAB Function to Determine Theoretical Flow Ripple 101

Appendix D: MATLAB Function for TOET Method 102

Appendix E: MATLAB Script for Empirical Model of Flow and Torque 104

Appendix F: MATLAB Function for Best Subset Regression 108

List of Figures

Figure 1: Exploded View of Variable Displacement Axial Piston Pump. 18
Figure 2: Sectional View of a Rotating Group of Pumps. 19
Figure 3: Sectional View of Axial Piston Swash-Plate Pump. 20
Figure 4: Bulk Modulus at 25 MPa and 20, 50 and 80º C. 29
Figure 5: Viscosity for Conventional AW 46 Hydraulic Fluid at 80°C. 30
Figure 6: Schematic of an Axial Piston Pump to Explain the Kinematics 34
Figure 7: Control Volume of Displacement Chamber. 40
Figure 8: Piston States in a Displacement Chamber. 42
Figure 9: Leakage through Slipper Pad. 43
Figure 10: Geometry of Valve Plate with Nine Kidney Ports. 46
Figure 11: External Forces Acting on the Piston. 49
Figure 12: Integrated Model. 54
Figure 13: Phase Angle Model. 55
Figure 14: Piston Configuration Model (Overall Flow). 56
Figure 15: Instantaneous Displacement Chamber Pressure (Piston) Model. 57
Figure 16: Fluid Properties Model. 58
Figure 17: Bulk Modulus Model. 58
Figure 18: Effective Bulk Modulus Model. 59
Figure 19: Density Model. 59
Figure 20: Kinematic Viscosity Model. 60
Figure 21: Specific Heat and Thermal Conductivity Model. 61
Figure 22: Pump Kinematics Model. 61
Figure 23: Discharge and Suction Area Model. 62
Figure 24: Discharge Area Model. 62
Figure 25: Flow Rates Model. 63
Figure 26: Swivel Torque Model. 64
Figure 27: Piston Subsystem Block of Swivel Torque Model. 64
Figure 28: Torque on the Shaft Model. 65
Figure 29: Instantaneous Torque on the Shaft by a Single Piston. 66
Figure 30: Swashplate Mass Moment of Inertia. 67

Figure 31: Hydraulic Test Rig at the Fluid Power Institute, MSOE. 69
Figure 32: Hydraulic Circuit Schematic of the Test Rig. 70
Figure 33: Orthogonal and Latin Hypercube-Based Design of Experiments. 71
Figure 34: First Step of the Toet Method. 73
Figure 35: Second Step of the Toet Method. 74
Figure 36: Comparison of the Four- and Five-Term Models. 77
Figure 37: Density of the PP11D Fluid. 79
Figure 38: Pump Kinematics Parameters at Maximum Swash Plate Angle and 13 rpm.. 81
Figure 39: Theoretical Flow Ripple based on Kinematics. 82
Figure 40: Instantaneous Discharge or Suction Area of the Valve Plate Opening. 83
Figure 41: Displacement Chamber Pressure. 84
Figure 42: Pump Discharge Flow at 1000 rpm and 2000 psi for 100% Displacement. ... 85
Figure 43: Pump Leakage Flow at 1000 rpm and 2000 psi for 100% Displacement. 86
Figure 44: Moment on Swash Plate at 1000 rpm and 2000 psi for 100% Displacement. 86
Figure 45: Torque by a Piston at 1000 rpm and 2000 psi for 100% Displacement. 87
Figure 46: Torque on the Shaft at 1000 rpm and 2000 psi for 100% Displacement. 88
Figure 47: Steady State Discharge Flow for PP11D at 100% Displacement. 89
Figure 48: Steady State Discharge Flow for PP10D at 100% Displacement. 89
Figure 49: Steady State Shaft Torque at 100% Displacement. 90

List of Tables

Table 1: Terms for Empirical Flow and Torque Models. 23
Table 2: Parameters Used in Modeling. 68
Table 3: Instruments and Sensors Used in the Test Stand. 70
Table 4: Descriptions of Hydraulic Oils and their Properties. 72
Table 5: Pump Discharge Flow Models. 76
Table 6: Pump Torque Models. 78
Table 7: Linear Regression Fit for Density. 80

Nomenclature

Symbol	Definition	Unit
A	cross sectional area	m^2
A_G	area of slipper pad in contact with swash plate	m^2
A_k	area of a piston	m^2
a_k	piston Acceleration	m/s^2
a_u	radial acceleration	m/s^2
A_{rHPi}	instantaneous discharge orifice area for i^{th} displacement chamber	m^2
A_{rLPi}	instantaneous suction orifice area for i^{th} displacement chamber	m^2
A_s & A_l	area of small and large actuator	m^2
a_V	thermal expansivity defined for volume linear with temperature	K^{-1}
a	acceleration	m/s^2
C	coefficient of viscous damping	N.s/m
C_k	Damping coefficient of piston	N.s/m
c_p	specific heat of the fluid	J/kg.K
D	displacement	m^3/rev
D_l	diameter of the large actuator	m
D_s	diameter of the small actuator	m
d_d	diameter of the capillary opening in the piston	m
d_k	diameter of a single piston	m
d_{xi}	horizontal distance of the i^{th} piston away from the y-axis	m
E	energy	J
F	force	N
f	frequency	Hz
F_{AKz}	sum of axial forces	N
F_{aKz}	axial inertial force due to acceleration of the piston	N
F_l	forces exerted on the swashplate by large actuator	N
F_{TC}	viscous friction on the kidney port	N
F_{DK}	displacement chamber pressure force	N
F_s	forces exerted on the swashplate by small actuator	N

Symbol	Definition	Unit
F_{SKy}	transverse force on the piston by swash plate	N
F_{SK}	swash plate reaction force acting on the piston	N
F_{TG}	external viscous friction on the slipper pad	N
F_{TK}	viscous friction force between cylinder and piston	N
$F_{\omega K}$	centrifugal force acting on the piston and slipper	N
g	acceleration due to gravity	m/s^2
H	stroke	m
h	clearance	m
H_k	piston stroke	m
$H_{k\max}$	maximum piston stroke	m
h_G	gap between slipper pad and swash plate	m
h_k	clearance between piston and bore	m
I	swashplate mass moment of inertia	$kg \cdot m^2$
K	isothermal bulk modulus of the fluid without any entrapped air	Pa
k	bias-spring constant	N/m
k	thermal conductivity of mineral oil	W/m.K
k_T	viscosity temperature coefficient, $-\partial \ln \mu / \partial T$	K^{-1}
K_0	isothermal bulk modulus at $p = 0$	Pa
K_{00}	K_0 at zero absolute temperature	Pa
K^*	bulk modulus of the fluid-air mixture	Pa
L	distance from the actuator to the swashplate pivot	m
l_A	length of the piston/cylinder interface at IDC or internal gap length	m
l_b	bushing length	m
l_d	total length of the piston	m
l_k	dynamic length of piston	m
M	moment	$N \cdot m$
m	mass	kg
$\dot{m}$	mass flow rate	kg/s
M_l	mass of the large actuator	kg
M_s	mass of the small actuator	kg
m_k	mass of a single psiton with slipper pad	kg

Symbol	Definition	Unit
N	shaft or rotational speed	rpm
P	power	W
p	absolute pressure	Pa
p_c	control pressure applied to the piston of the large actuator to control the swashplate angle	Pa
P_d	discharge pressure	Pa
P_i	displacement chamber pressure	Pa
P_{in}	intake pressure	Pa
p_e	Pressure of the fluid in case of the pump	Pa
Δp	Pressure differential	Pa
p_R	reference pressure	Pa
p_s	varying discharge pressure in small actuator	Pa
p_∞	pressure for which the viscosity diverges	Pa
Q_a	Instantaneous Volumetric flow rate	m^3/s
Q	volumetric flow rate	m^3/s
Q_g	geometric flow rate	m^3/s
Q_{thp}	theoretical flow rate	m^3/s
Q_{po}	actual outlet/inlet flow	m^3/s
Q_{Lp}	leakage flow	m^3/s
Q_{ri}	sum of the flow rate leaving from and entering in i^{th} displacement chamber through discharge and suction port	m^3/s
Q_{leaki}	sum of the external leakage flow through three different lubricating paths of the i^{th} displacement chamber	m^3/s
Q_{rHPi}	flow through high pressure side	m^3/s
Q_{rLPi}	flow through low pressure side	m^3/s
Q_{SKi}	leakage flow from radial clearance between piston and bore	m^3/s
Q_{SBi}	leakage flow due to gap height between cylinder and valve plate	m^3/s
Q_{SGi}	leakage flow due to gap height between slipper and swash plate	m^3/s
Q_{net}	net flow into the actuator	m^3/s
$\dot{Q}$	heat transfer rate	W
R_G	outer radius of the slipper land pad	m

Symbol	Definition	Unit
r_G	Inner radius of the slipper lad pad	m
R	pitch circle or piston pitch radius	m
s_k	Piston displacement	m
T	temperature of the fluid	°C or K
T	Net instantaneous or overall torque	$N \cdot m$
T_{avg}	average torque exerted on the pump shaft	$N \cdot m$
T_s	swivel Torque	$N \cdot m$
t	time	s
t_s	settling time	s
T_∞	temperature for which the viscosity diverges	K
T_R	reference temperature	K
V	volume of fluid at any temperature and pressure	m^3
V_{air}	volume of air in the fluid-air mixture	m^3
V_F	volume of fluid in the fluid-air mixture	m^3
V_i	instantaneous volume of the piston chamber	m^3
V_0	volume of fluid at $p = 0$	m^3
V_R	volume of fluid at reference state, T_R, $p = 0$	m^3
V_D	dead volume of a displacement chamber	m^3
V_0	volume of a displacement chamber at ODC	m^3
V_{sweep}	volume swept by the piston when it travels distance s_k	m^3
$V_{g\max}$	maximum geometric displacement of the pump	m^3
v_u	circumferential Velocity	rad/s
v	linear velocity	m/s
W	work done	J
z	total number of pistons	#
α	angular acceleration	rad/s^2
α_p	viscosity pressure coefficient, $\partial \ln \mu / \partial p$	Pa^{-1}
α^*	reciprocal isoviscous pressure viscosity coefficient	Pa^{-1}
β_1	angle at which the silencing groove area starts to open	rad
β_2	angle at which the major slot of the valve plate of discharge side starts to open to kidney port	rad
β_3	angle at which the major slot open to area equals to the area of the circle formed by the kidney port of radius equals to the kidney port radius r_{kp}	rad

Symbol	Definition	Unit
β_4	angle at which the kidney port starts to open completely, and it remain completely open till the angular position equals to β_5	rad
β_5	angle at which the complete opening of kidney port start to close	rad
β_6	angle at which the major slot start to close	rad
β_7	angle at which the major slot closes	rad
β	swash plate angle	rad
$\beta_{\max}$	maximum swashplate angle	rad
β_o	desired swashplate angle	rad
β_p	isothermal coefficient of compressibility	Pa^{-1}
β_T or β_K	isobaric thermal coefficient of volume expansion	K^{-1}
$\ddot{\beta}$	angular acceleration of the swash plate	rad/s^2
ρ	density of the fluid	kg/m^3
ρ_R	reference density of the fluid at reference state, $\rho_R = \rho(T_R, p = 0)$	kg/m^3
γ	thermodynamic interaction parameter at reference state	$Pa \cdot s$
γ	pressure carry over angle on the valve plate	rad
μ	dynamic viscosity	$Pa \cdot s$
μ_0	low-shear viscosity at $p = 0$	$Pa \cdot s$
μ_R	reference dynamic viscosity of the fluid $\mu_R = \mu(T_R, p = 0)$	$Pa \cdot s$
μ_∞	parameter in viscosity formulas	$Pa \cdot s$
ν	kinematic viscosity	m^2/s or cSt
φ	phase angle	rad
ω	Angular velocity or rotational frequency	rad/s
$\Delta\varphi$	piston pitch or phase angle	rad
ε	error in swashplate angle	rad
API	American Petroleum Institute	-
A and B	constants in Walther's equation	-
B_F	fragility parameter in the viscosity equation	-
C_d	orifice flow discharge coefficient	-
C_L	empirical (generic) flow loss coefficient	-
K_c	gain constant of the pump controller	-

Symbol	Definition	Unit
K_0'	pressure rate of change of isothermal bulk modulus at $p = 0$	-
SG	specific gravity	-
Re	Reynolds number	-
ϕ	dimensionless scaling parameter for viscosity	-
ϕ_∞	scaling parameter for unbounded viscosity	-
γ	specific weight	-
η_m	mechanical efficiency	-
η_v	volumetric efficiency	-
η_o	overall efficiency	-

Chapter 1: Introduction

Tribology is the branch of science that focuses on friction, lubrication, and wear of interacting surfaces in relative motion. It applies an operational analysis to problems of great economic significance, such as efficiency, reliability, and wear [1]. The Department of Energy reports that fluid power applications account for 2-3% of the nation's energy consumption [2]. In this, hydraulic systems have more than 90% contribution. Hydraulic equipment is mainly used in agriculture, construction, and mining applications. The efficiency of hydraulic power transmission is affected by internal leakage flow losses in pumps and motors, the pressure drops through flow control valves and fluid conduits, and friction in hydraulic motors and cylinders. These losses generate heat and reduce the power available to engage the payload. In addition, heat or friction caused by wear is a major cause of material wastage and mechanical energy dissipation in the form of heat such as within internal combustion engines [1]. Currently, lubrication is an effective means of controlling wear and reducing friction. It is vital to focus on tribology in hydraulic systems because fluid functions as both a lubricant and a power transmission medium. Also, any reduction in wear control can result in a considerable economic saving.

While many are concerned with on-highway machine fuel economy, hydraulic system fuel efficiency has long been unheeded. It is well known that a significant amount of efficiency depends on the design of the system rather than on the fluid/fuel [3]. However, there is a limit to which the design can be enhanced to increase the efficiency. Therefore, it is vital to focus on the fuel, as well, which generates energy or helps in the transfer of energy. Additionally, it is important to reduce the environmental effects. When hydraulic fluids are involved, the first image that comes to mind is a lubricating substance. Nevertheless, hydraulic fluid has many other applications in a system other than simple lubrication for the system. In a hydraulic system, the major role of fluid is to transfer energy. Minute changes in the fluid formulation result in efficiency gains, which have led to significant increases in low-speed high-torque (LSHT) hydrostatic mechanical efficiency [3]. These gains indicate that greater advances are possible in this area. While

fluid power is being utilized in many applications today, further research can lead to increased efficiency improvements. MSOE's unique Shell test stand is the epitome of this potential; however, testing is time-consuming and expensive. According to Paul Michael of FPI, the Shell test stand costs over $16,800 for a test fluid, excluding the cost of fluid and labor [4]. It usually takes one to two weeks for the completion of tests for a fluid. The goal of this test procedure is to see which fluid might provide better efficiency in off-highway machinery. This is done by quantifying the performance of an axial piston pump with various fluids as per ISO 4409 test procedure because in most hydraulic systems, often the pump is the main component of hydraulic power. The main function of a hydraulic pump is to convert input mechanical power into the fluid or hydraulic power.

The primary goal of this project was to develop a steady-state MATLAB Simulink model of an axial piston pump that relates fluid properties to pump performance. The pump performance mainly is quantified by pump input torque and discharge flow as a function of operating condition and major fluid properties. The secondary goal of this project was to facilitate the development MATLAB Simulink tool that can assist in selecting hydraulic fluids for off-highway fluid power equipment. The goal was to be accomplished by evaluating hydraulic fluids in a dynamometer and creating steady-state models that relate fluid properties to pump performance. Pump performance was to be evaluated in a dynamometer. Dynamometer testing can assess the effects of fluid properties--such as viscosity, density, and shear stability--on hydraulic pump efficiency. A similar approach has been used to simulate fluid performance in the hydraulic system of an agricultural machine [5] and gear pumps [6]. The personal purpose of this project was to learn the pump mechanics and enhance modeling capability.

Chapter 2: Background and Literature Review

2.1 Positive Displacement Machine

An Axial piston pump is a positive displacement machine that works on the displacement principle. The displacement machines are divided into five main classifications-- piston machines, gear machines, screw machines, vane machines, and other machines. Most of the machines can operate either as a pump or a motor. The piston machines use moving pistons to displace fluid from the displacement chambers which are formed between the cylinders and the moving pistons. Axial piston pumps are widely used as the efficient input power source for hydraulic circuitry because of their high output pressure and power. They can efficiently operate in a broad range of operating pressures and speeds; however, they are costly and generate a high level of noise. Axial piston pumps can be classified into two categories based on the relationship between the line of action of the pistons and the center line of the drive shaft. The axial piston pumps in which the line of action of the pistons is inclined to the centerline of the drive shaft are classified as axial piston bent-axis pumps, whereas the axial piston pumps in which the line of action of the pistons is parallel to the centerline of the drive shaft are classified as axial piston swash plate pumps [7].

2.2 Axial Piston Swash-Plate Pump

Figure 1 shows the exploded view of an axial piston swash plate pump assembly. Generally, the pumps are comprised of a shaft with a bearing locked in a position, a swash plate to vary the geometrical displacement of the pump, a pair of bearing shelves or bush on which the swashplate resides, and a discrete number of pistons equally spaced and longitudinally equidistant and parallel to the central driving shaft in the cylindrical block or barrel. The ends of the pistons are connected to shoes (slipper pads) with a spherical joint (a ball and socket joint). Pistons with their slipper pads right through a retaining ring--called a retainer--are in a position in the cylinder barrel or block. The slipper retainer ensures the slipper pads are always equally spaced and longitudinally

equidistant from each other and retain their position. The cylinder barrel also has a load spring and multiple load pins, and both are locked in position inside the barrel. There is a spherical washer that resides on these three load pins. The spring in the barrel is naturally loaded or compressed. It ensures that the slipper pads of the pistons are pressed hard against the swashplate. The retaining ring pushes against the spherical washer and three tiny load pins, which ensures that the porting face of the cylinder barrel is pressed against the port or valve plate. The port plate is locked in position, and a control piston and a biased piston are on the front housing cap.

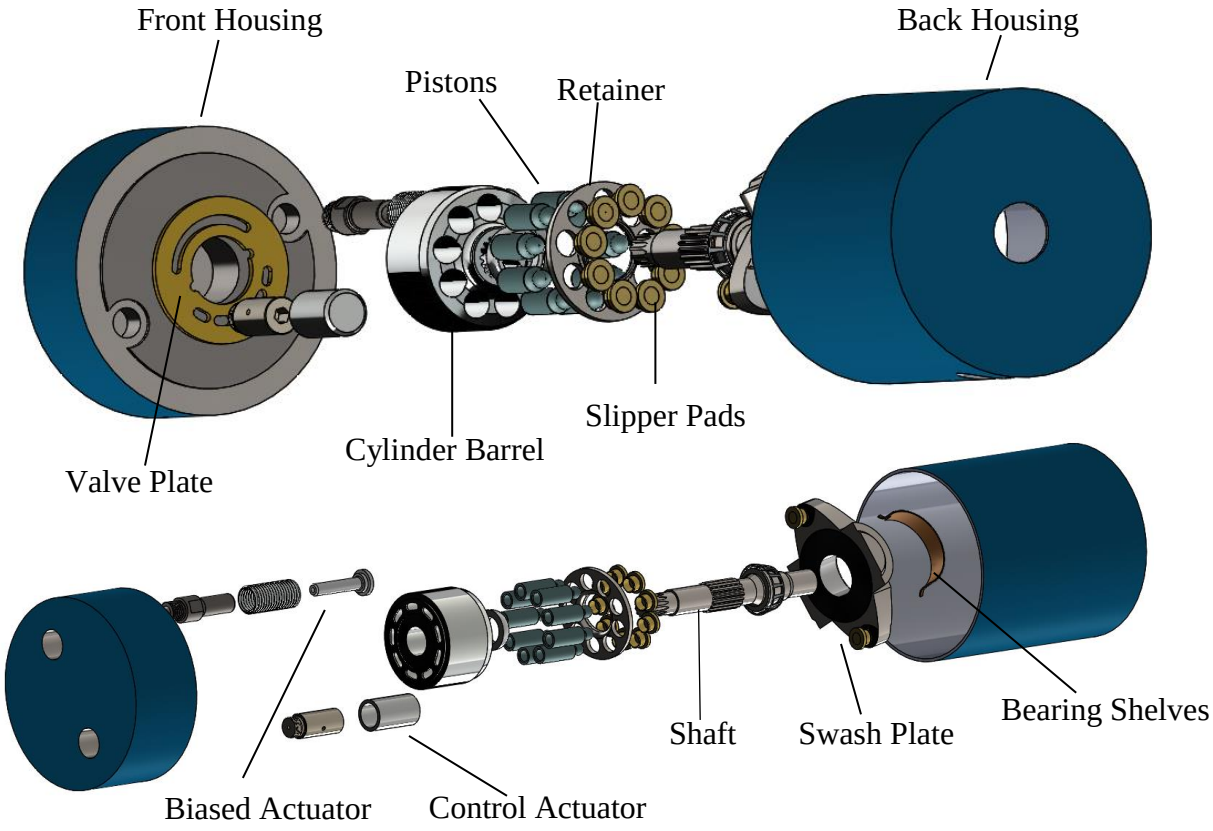

Figure 1: Exploded View of Variable Displacement Axial Piston Pump.

The barrel is connected to the drive shaft by a spline. The rotation of the drive shaft causes the rotary group--consisting of cylinder blocks, pistons, retaining plate--to revolve. This can be clearly seen in the sectional view of the rotatory group, as shown in Figure 2. Because of the inclination of the swash plate, the pistons are forced to reciprocate in a sinusoidal fashion to displace and suck the fluid in one revolution [7]. The slipper pads connected to pistons slide on an inclined swash plate. During one revolution, the piston moves inside the barrel from the outer dead center (ODC) to the inner dead center (IDC) and back to the starting point. The positions at which a piston is fully expanded and retracted in the cylinder, respectively, are known as the inner dead center (IDC) and outer dead center (ODC). Two openings on the valve plate covering almost 180° angles each are provided for suction and discharge manifolds and ports for the pump. Because of the inclined swash plate, each piston gets a chance to advance in the displacement chamber, formed between piston and cylinder, in one half of the rotation delivering the high-pressure fluid through the outlet port on the valve plate. In the remaining half revolution, the pistons are withdrawn from their positions drawing low-pressure fluid in through the suction port on the valve plate [7, 8].

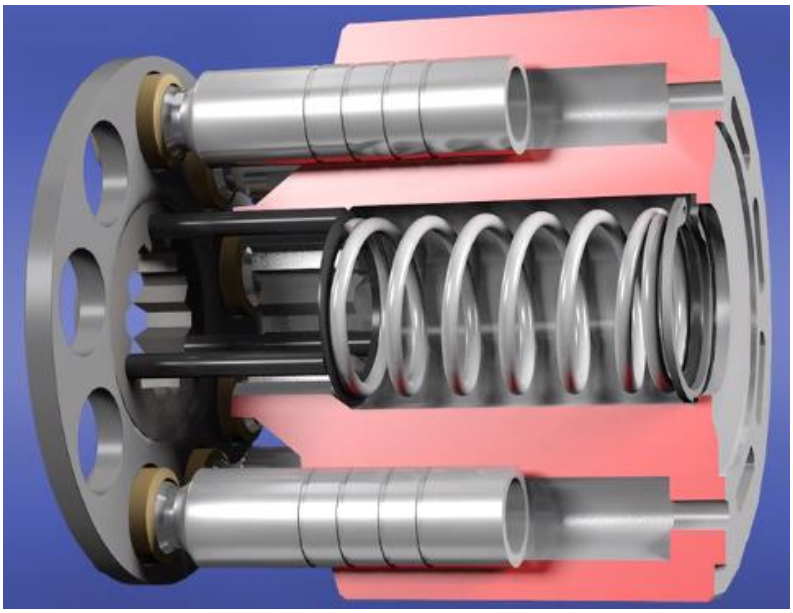

Figure 2: Sectional View of a Rotating Group of Pumps [9].

The maximum distance the piston can travel in a revolution--known as a stroke--is dependent on the angle of inclination of the swash plate. The amount of fluid that is displaced or swept by the pump in a revolution is known as geometric displacement per revolution. It remains constant for the constant swash plate angle. The geometric displacement is varied by changing the inclination angle of the swash plate through the control mechanism. A pump consisting of a swash plate angle control mechanism is known as the variable displacement axial piston swash-plate pump [10]. There are various types of control mechanisms on piston pumps, used to achieve different goals by changing the swash plate angle. The pressure compensator is the most basic and perhaps the most popular control on piston pumps. There are also other controls such as remote pressure compensation, the flow compensation (or the load sensing pump), and the horsepower or torque limiting pump. Some pumps also consist of a stroke limiting adjustment. It is an additional feature that allows the user to limit the maximum geometric displacement of the pump by manually adjusting the screw [9], as shown in Figure 3.

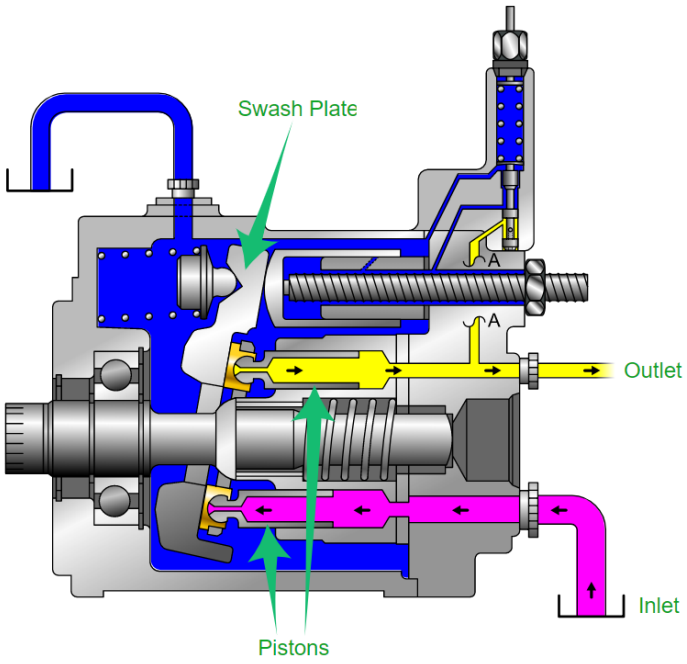

Figure 3: Sectional View of Axial Piston Swash-Plate Pump [9].

The pump shown in Figure 3 has a pressure compensating mechanism. The control mechanisms consist of two actuators commonly known as a small (bias) actuator and a large (control) actuator, as shown in Figures 1 and 3. The bias actuator tries to keep the pump on-stroke by pushing the swash plate. When the system pressure rises to maximum set pressure, the pressure compensator spool shifts against the compensator set spring and allows some discharge fluid at system pressure to extend the piston of the control actuator so that the pump's displacement can be reduced to near zero by reducing the swash plate angle close to zero. During this period, the pump slightly comes on-stroke and goes off-stroke to displace adequate fluid to maintain the maximum system pressure. When the system pressure falls below the maximum set pressure, the compensator spring pushes the spool back to its resting position and allows the bias spring to bring the pump back on-stroke. The fluid inside the control piston vents through the compensator to the inside of the pump's case while it retracts [9]. Having the pump reduce its output to near zero when the system pressure reaches a maximum, is more energy efficient than relying only on a relief valve. This reduction in displacement conserves input energy and prevents the buildup of excess heat [8, 9].

The main source of power loss in an axial piston machine are the lubricating gaps. The power loss due to viscous friction and gap occur in these lubricating interfaces. The main lubricating gaps are located between the cylinder block and valve plate, piston and cylinder, and between slipper and swash plate. It is very important to take this into account when the pump is designed.

2.3 Empirical Modeling

The main function of a hydraulic pump is to convert input mechanical power into fluid or hydraulic power. The ideal discharge flow of a pump can be given by the product of the pump geometric displacement and the rotation speed, i.e., $Q_{po,ideal} = D_p N_p$. Similarly, the ideal torque input of a pump can be given by the product of the pump geometric displacement, D_p, and the differential pressure, Δp_p, across the pump inlet and outlet ports, i.e., $T_{p,ideal} = D_p \Delta p_p$.

The mechanical power is characterized by the input-shaft torque, *T*, times the rotational speed, N_p, of the shaft. The hydraulic power is given by the discharge pressure, p_d, of the pump times the discharge flow rate, Q_{po}. Hence, the overall efficiency of the pump can be defined [7] as

$$\eta_{op} = \frac{P_{out}}{P_{in}} = \frac{\Delta p_p Q_{po,act}}{T_{p,act} N_p} \quad \text{or} \quad \eta_{op} = \eta_{vp} \times \eta_{Tp}. \tag{1}$$

Therefore, to determine hydraulic system performance, it is necessary to quantify the volumetric flow rate and the shaft torque. One way to quantify the volumetric flow rate and shaft torque is through a steady-state model generated either physically, numerically, experimentally, or analytically. The easiest way to quantify the performance of the pump is through the ISO 4409 [11] test procedure. It is steady-state pump testing procedure, and the data obtained through this procedure can be used to generate the performance curves, which are governed [7] by Equations (2), (3), (4), and (5):

$$Q_{po,act} = \eta_{vp} D_p N_p \quad \text{or} \quad = D_p N_p - C_{Lp} \Delta p_p, \tag{2}$$

$$T_{p,act} = D_p \Delta p_p / \eta_{mp} \quad \text{or} \quad = D_p \Delta p_p + T_{fp}, \tag{3}$$

$$\eta_{vp} = \frac{Q_{po,ideal}}{Q_{po,ideal}} = \frac{Q_{po,ideal} - Q_{p,leak}}{Q_{po,ideal}}, \text{ and} \tag{4}$$

$$\eta_{mp} = \frac{T_{p,ideal}}{T_{p,act}} = \frac{T_{p,ideal}}{T_{p,ideal} + T_{p,\,friction}}. \tag{5}$$

However, the above-listed performance equations do not include the fluid properties that have a significant effect on the performance. The steady-state performance of hydraulic pumps and motors is primarily a function of friction, fluid density, viscosity, compressibility, and pressure-driven flow losses. Many models have already been developed through numerical analysis, experimental data, physical modeling, and analytical analysis. Some of the common parameters employed in these models are listed in Table 1, all of which have been used in characterizing the steady-state performance of pumps and motors.

Table 1: Terms for Empirical Flow and Torque Models [3, 12, 13, 14, 15, 16, 17, 18, 19, 20, 21, 22, 23].

Pressure-driven laminar flow loss	
$V_i\left(\Delta p/2\pi\mu\right)$	Wilson, 1950
$V_i\left(\Delta p/2\pi\mu\right)\left(A+B\,\omega/\omega_{\max}\right)\left(\Delta p/p_{\text{case}}\right)$	Dorey, 1988
$V_{Max}\left(\Delta p/\mu\right)$	Bavendiek, 1987
$\Delta p/\mu\omega$	Manring, 2005
$\Delta p/\mu$	Jeong, 2007
p_2/μ	Manring, 2016
$\alpha^2 p/\nu$	Johnson, 2017
Pressure-driven turbulent flow loss	
$V_i^{2/3}\sqrt{2\Delta p/\rho}$	Schlösser, 1961
$\sqrt{\Delta p/\mu\omega}$	Manring, 2005
$\sqrt{\Delta p/\rho}$	Jeong, 2007
$\rho\,\omega^3/\Delta p$	Jeong, 2007
$\sqrt{p_2}$	Manring, 2016
Compressibility loss	
$(A-B\varepsilon)\dfrac{V_{\text{i}}\Delta p}{\beta}$	Olsson, 1973
$\Delta p\omega V_{\text{i}}\varepsilon$	Zarotti & Nevegna, 1981

Table 1: Terms for Empirical Flow and Torque Models [3, 12, 13, 14, 15, 16, 17, 18, 19, 20, 21, 22, 23] (Continued).

Compressibility loss	
$\left(V_r + \frac{1+\varepsilon}{2}\right)\frac{\Delta p \omega V_i}{\beta}$	Dorey, 1988
$\omega\left(\Delta p/\beta\right)$	Jeong, 2007
$\left(1-p_2/\beta\right)V_{\mathrm{i}}\omega\varepsilon$	Manring, 2016
Viscous friction	
$\mu\omega V_{\mathrm{i}}$	Wilson, 1950
$\mu\omega/\Delta p$	Manring, 2005
$\mu\omega$	Jeong, 2007
Turbulent friction	
$\frac{\rho V_{\mathrm{i}}^{5/3}}{4\pi}\omega^2$	Schlösser, 1961
$\frac{\rho V_{\mathrm{i}}^{5/3}}{4\pi}\omega^2\varepsilon^3$	Thomas, 1961
Turbulent friction	
$\mu\omega^2$	Ivantysyan & Ivantysynova, 2003
$\rho\omega^2$	Jeong, 2007
Coulomb or boundary friction	
$V_i\left(\Delta p/2\pi\right)$	Wilson, 1950
$\frac{V_{\mathrm{i}}\mid p_1+\varepsilon' p_2\mid}{1+\left(\omega/\omega_{\mathrm{o}}\right)^{\alpha}}$	Hibi & Ichikawa, 1977
$\sqrt{\mu\omega/\Delta p}$	Manring, 2005
Δp^2	Jeong, 2007
$\sqrt{\frac{(\mu\omega/\Delta p)}{A+(\mu\omega/\Delta p)}}$	Michael, 2016

In an axial piston pump, the main leakage flow gaps are situated at the cylinder barrel and valve plate, slipper and swash plates and the piston, and the cylinder bore interfaces. The flow loss can be classified -- laminar flow loss occurs because of gaps between slippers and swash plate, pistons and cylinder block, and cylinder block and valve plate. the turbulent flow loss occurs because of orifice metering effects and cross-port leakage, as well as the flow loss occurs because of the volumetric reduction under compression, the flow loss because of the sliding motion, and the constant flow loss, mainly because of fixtures and sealing, and it is independent of operating conditions. Jeong's analytical model [16] is accurate and simple and incorporates the key physical features of hydraulic fluids. This model could be adapted for use in a variable displacement pump, with fluids of varying density and bulk modulus.

The friction losses associated with the hydraulic pump depend on the tribology of the surfaces moving relative to each other, and they depend on the operational parameters such as speed, pressure, or displacement [15]. Torque loss results from mechanical friction are proportional to operating pressure, and viscous friction is proportional to operating speed and viscosity of the fluid and also on the Stribeck number (a high Reynolds number). There is also a constant torque loss, mainly because of fixtures and sealing, and it is independent of operating conditions. The viscous friction is dominant at the high-speed operating range, and boundary friction is dominant at the low-speed range or starting speed. In some motors, the boundary friction is dominant at the high-speed range [14].

Chapter 3: Physical and Thermal Properties of the Hydraulic Fluids

3.1 Introduction

Hydraulic fluid viscosity, density, and bulk modulus have a major impact upon the efficiency, friction, and dynamic response of fluid power systems. These properties vary with pressure and temperature. The viscosity of the fluid decreases by nearly 50% for every 10°C increase in temperature. Temperature-driven changes in viscosity have been shown to affect leakage flow losses in pumps and friction losses in motors [24, 25]. While temperature has the most significant impact on viscosity, the pressure is also a factor. The viscosity of an organic liquid roughly doubles for every 50 MPa increase in pressure [26]. The high-pressure viscosity of the fluid is particularly important in elastohydrodynamic gear lube and rolling contact bearing lubrication [27]. It is also believed to have an impact on line-losses in fluid power equipment [28]. Pressure not only impacts the viscosity of the fluid, but it also affects fluid volume. A 50 MPa increase in pressure can decrease the volume of fluid by 2 to 4%. Fluids of high bulk modulus have been found to exhibit remarkably low flow losses [29]. Hence high-fidelity models of hydraulic pumps and motors must include the effects of temperature and pressure on fluid viscosity, density, and bulk modulus. As described below, models have been developed to approximate the effects of pressure and temperature on hydraulic fluid viscosity, density, and bulk modulus properties. The procedures that were used to develop the model coefficients may be found in Bair and Michael [26]. The associated MATLAB code is provided in the Appendices A and B. Within the code, Equations (9), (10), and (11) are used to model bulk modulus, Equations (18) and (19) are used to model kinematic viscosity and Equation (20) is used to model density. Note that the viscosity-pressure-temperature models described in Equations (14) and (15) are only applicable to EHD lubrication where contact pressures exceed 150 MPa.

3.2 Bulk Modulus

While there is no principle of conservation of volume, conservation of mass has been used to define the effects of pressure and temperature on fluid volume [15]. Thus,

$$\begin{aligned} &\frac{dV}{V} = -\beta_p dp + \beta_T dT, \\ &V = V_R\left[1-\beta_p\left(p-p_R\right)+\beta_T\left(T-T_R\right)\right], \end{aligned} \tag{6}$$

$$\begin{aligned} &\frac{d\rho}{\rho} = \beta_p dp - \beta_T dT, \\ &\rho = \rho_R\left[1+\beta_p\left(p-p_R\right)-\beta_T\left(T-T_R\right)\right]. \end{aligned} \tag{7}$$

Hence, the volume V and density ρ of the fluid at any temperature T and pressure p can, respectively, be given by Equations (6) and (7). Here, ρ_R is the reference density of the fluid at a reference temperature T_R, β_p is the isothermal coefficient of compressibility which describes the reduction of the volume and increase of the density while pressure rises, β_T is the isobaric thermal coefficient of volume expansion or thermal expansion coefficient which describes the increase of the volume and reduction of the density while temperature rises. That is,

$$\beta_p = \frac{1}{V}\left(\frac{\partial V}{\partial p}\right)_T = -\frac{1}{\rho}\left(\frac{\partial \rho}{\partial p}\right)_T \text{ and } \beta_T = \frac{1}{V}\left(\frac{\partial V}{\partial T}\right)_p = -\frac{1}{\rho}\left(\frac{\partial \rho}{\partial T}\right)_p.$$

The reciprocal of the compressibility coefficient β_p is defined as the bulk modulus, as shown in Equation (8):

$$K = \frac{1}{\beta_p} = -V\frac{dp}{dV}. \tag{8}$$

The fluid can be compressed isothermally or adiabatically. It is essential to distinguish between the isothermal (at a constant temperature) bulk modulus K_{iso} and the adiabatic (without any heat transfer) bulk modulus K_A for precise calculation and analysis. The adiabatic bulk modulus is used in the process where pressure changes occur rapidly, and

no exchange of heat with the surroundings takes place. Lacking experimental data, it may be approximated as $K_A \approx 1.15K_{\text{iso}}$ [15].

In the models presented herein, experimental data are used to model the pressure and temperature dependence of viscosity, density, and bulk modulus. The bulk modulus *K* of hydraulic fluid was modeled using the temperature-modified Tait equation of state [26, 27, 29] as:

$$K = \left\{1 - \frac{1}{1+K_0'}\ln\left[1+\frac{p}{K_0}\left(1+K_0'\right)\right]\right\}\left[K_0 + p\left(1+K_0'\right)\right]. \tag{9}$$

Here, K_0' is the pressure rate of change of isothermal bulk modulus *K* at p = 0 Pa or ambient pressure and K_0 is the isothermal bulk modulus at p = 0 Pa. As suggested by Fakhreddine and Zoller, it can be expressed [26, 27] as

$$K_0 = K_{00}\exp\left(-\beta_K T\right), \tag{10}$$

where K_{00} is the isothermal bulk modulus K_0 at zero absolute temperature and β_K is the thermal expansion coefficient in K^{-1}. The bulk modulus model represented by Equations (9) and (10) has been already validated using experimental data by Mettakadapa, Scott, and Michael [29]. This model is often held to be the most accurate, and it is even accurate for extrapolating to very high pressures [26, 29].

The influence of entrapped air in the fluid on bulk modulus can also be considered, as described by Ivantysyn and Ivantysynova [15]:

$$\frac{K^*}{K} = \frac{1+\dfrac{V_{air}}{V_F}}{1+\left(\dfrac{p_R}{p}\dfrac{V_{air}}{V_F}\right)\dfrac{K}{p}}, \tag{11}$$

where K^* is the bulk modulus of the fluid-air mixture, K is the bulk modulus of the fluid without any entrapped air which can be determined by combining Equations (9) and (10), V_{air} and V_F, respectively, are the volume of air and fluid in the fluid-air mixture, p_R is the reference pressure equal to atmospheric pressure, and p is the pressure of the fluid at any instance.

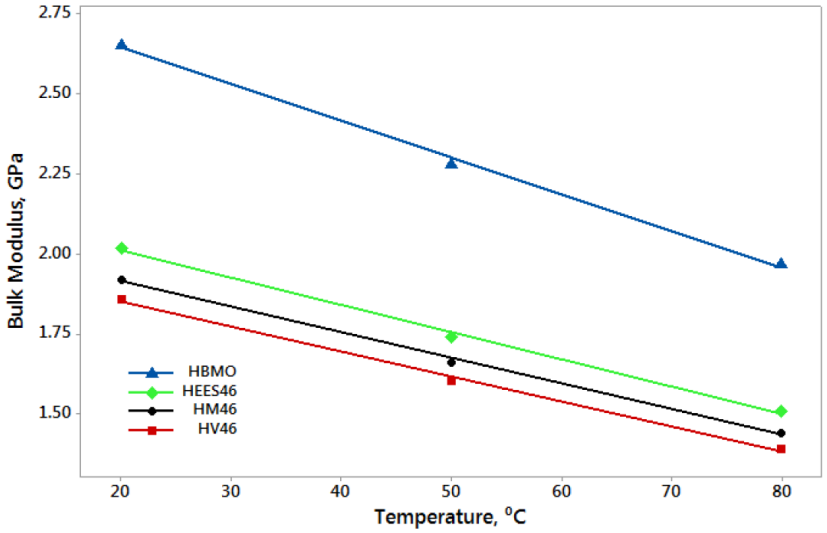

Figure 4: Bulk Modulus at 25 MPa and 20, 50 and 80º C [29].

3.3 Viscosity

Dynamic viscosity is a critical factor in modeling leakage flow, film thickness, and bearing load capacity in hydraulic pumps and motors [15]. Leakage flow has been found to correlate with the dynamic viscosity at ambient pressures. Film thickness and load capacity in rolling contact bearings have been found to correlate with the dynamic viscosity at high pressure. Figure 5 compares the experimentally found dynamic viscosity and the modeled viscosity using Equation (14). As shown in Figure 5, the viscosity of a typical hydraulic fluid increases exponentially at pressures above 150 MPa. Hence, two viscosity models are presented below to model absolute viscosity separately for hydrodynamic and elastohydrodynamic lubrication regime. They include the high-

pressure or piezoviscosity model of Bair and Michael [26] for bearing calculations, and Walther's [30] ambient pressure viscosity model for leakage flow and viscous friction modeling.

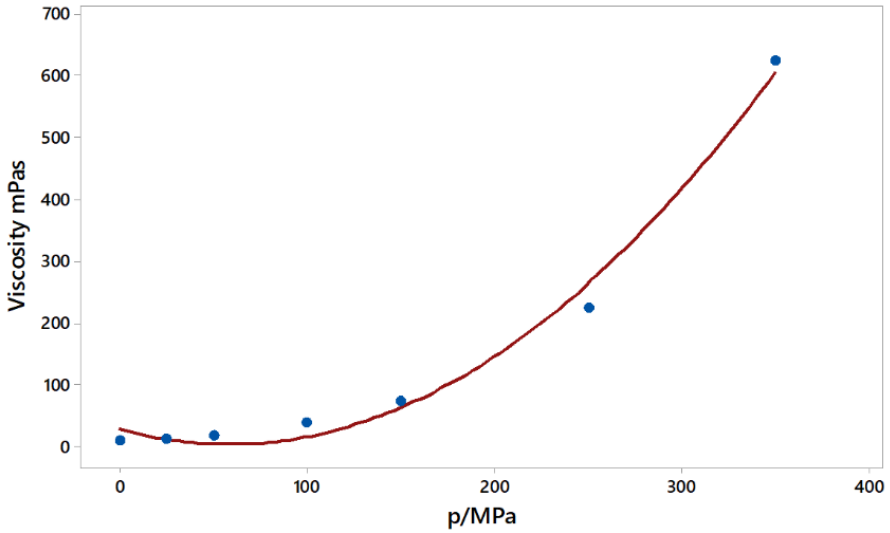

Figure 5: Viscosity for Conventional AW 46 Hydraulic Fluid at 80°C.

The pressure and temperature characteristics of fluid viscosity, μ, may be expressed by Equation (12) or Equation (13). Equation (12) is the well-known Barus equation [4]. Thus,

$$\mu = \mu_R \exp(\alpha_p p), \text{ and} \tag{12}$$

$$\mu = \mu_R \exp\left[\alpha_p p - k_T \left(T - T_R\right)\right]. \tag{13}$$

Here, $\mu_R = \mu\left(T_R, p = 0\right)$ is the reference dynamic viscosity of the fluid and $\alpha_p = \partial \ln \mu / \partial p$ is the viscosity-pressure coefficient. The effect of temperature may be incorporated by using Equation (13), where $k_T = -\partial \ln \mu / \partial T$ is a viscosity temperature coefficient.

In the MATLAB model presented herein, the pressure and temperature dependent absolute dynamic viscosity μ of the hydraulic fluid, for pressure above 150 MPa, is modeled using Equation (14) [26] as:

$$\mu = \mu_\infty \exp\left(\frac{B_F \phi_\infty}{\phi - \phi_\infty}\right). \tag{14}$$

Here, μ_∞ is the constant, B_F is analogous to the fragility parameters, ϕ_∞ is the scaling parameter for unbounded viscosity, and ϕ is the dimensionless scaling parameter, which is defined as

$$\phi = \left(\frac{T}{T_R}\right)\left(\frac{V}{V_R}\right)^\gamma. \tag{15}$$

In Equation (15), γ is the thermodynamic interaction parameter, V and V_R are the volume of the fluid at any temperature T and $\mathrm{T_R}$ and pressure p and $p = 0$, respectively. The relative volume V/V_R can be evaluated by the Murnaghan equation [26, 27] if the volume of the fluid at p = 0 Pa is V_0, as:

$$\frac{V}{V_0} = 1 - \frac{1}{1+K_0'}\ln\left[1 + \frac{p}{K_0}\left(1+K_0'\right)\right] \text{ and} \tag{16}$$

$$\frac{V_0}{V_R} = 1 + a_V\left(T - T_R\right). \tag{17}$$

The temperature-modified Tait and Murnaghan equations provide a means to model elastohydrodynamic effects in fluid power components and extend the accuracy of fluid power system models to higher pressure [26, 27].

3.3.1 Kinematic Viscosity

From the previous investigation, it was found that Walther's equation accurately relates the fluid viscosity for the pressure below 150 MPa as compared to the temperature-modified Tait and Murnaghan equations [26, 27]. The dynamic viscosity of the fluid of pressure below 150 MPa was accurately modeled by multiplying the density ρ of the fluid to the kinematic viscosity equation given by Walther's equation [30] at any temperature T:

$$\begin{aligned} \mu &= \upsilon \times \rho, \\ \mu &= \left[10^{10^{(B - A\log_{10} T)}} - 0.7 \right] \times \rho. \end{aligned} \tag{18}$$

Here, A and B are the constant which can be found using the ASTM D341 standard or which can be determined if kinematic viscosity of the fluid at two temperatures are known, as

$$\begin{aligned} A &= \frac{\log_{10}^{(\nu_{100°C}+0.7)} - \log_{10}^{(\nu_{40°C}+0.7)}}{\log_{10}^{(40+273.15)} - \log_{10}^{(100+273.15)}}, \text{ and} \\ B &= \log_{10}^{(\nu_{100°C}+0.7)} + A\log_{10}^{(100+273.15)}. \end{aligned} \tag{19}$$

3.4 Density

The density of the fluid was determined using Equation (7) as

$$\rho = \rho_R \left[1 + (1/K)(p - p_R) - a_V (T - T_R) \right]. \tag{20}$$

In the petroleum industry, an API (American Petroleum Institute) unit, which is a derivative of the standard specific gravity, is used. The API scale is expressed in degrees, which in some cases are more convenient to use than specific gravity readings. The API specific gravity is defined as [30, 31]:

$$\text{Degree API} = (141.5/SG) - 131.5. \tag{21}$$

Here, SG is the specific gravity at 15.6 °C (60 °F). The specific gravity of the fluid using API gravity at any temperature T in °F can be given [30, 31] by

$$SG = \frac{141.5}{\text{API} + 131.5} + \left(4 \times 10^{-4} \text{°F}^{-1}\right)(60\text{°F} - T). \tag{22}$$

3.5 Thermal Properties

The most critical thermal properties of lubricants are specific heat, thermal conductivity, and thermal diffusivity. These three parameters are essential in assessing heating effects in lubrication -- for example, the cooling properties of the oil, the operating temperature of the surfaces, and so on. They are also crucial in bearing design.

Specific heat c_p of mineral oil varies linearly with temperature and increases with increasing polarity or hydrogen bonding of the molecules. The specific heat of oil is usually half that of water. It can be expressed in terms of specific gravity SG at 15.6 °C and fluid temperature T [30, 31] as

$$c_p = \frac{1.63 + 0.0034T}{\sqrt{SG}}. \tag{23}$$

Here, the specific heat c_p of the fluid is in kJ/kg.K, and the temperature T is in °C.

Similarly, the thermal conductivity of mineral oil also varies linearly with temperature and is affected by the polarity and hydrogen bonding of the molecules. It can also be roughly estimated in terms of specific gravity SG at 15.6 °C and fluid temperature T [30, 31] as

$$k = \frac{0.12}{SG}\left(1 - 1.667 \times 10^{-4} T\right). \tag{24}$$

Here, the thermal conductivity k of the fluid is in W/m.K, and the temperature T is in °C.

Chapter 4: Mathematical Modeling of Axial Piston Pump

4.1 Pump Kinematics

The kinematics of the axial piston pump was described using the orthogonal coordinate system by Ivantysn and Ivantysynova [15], as shown in Figure 6. If the cylinder block rotates at a constant angular velocity ω along the z-axis, the piston executes a compounded movement, which consists of linear motion in the direction of z-axis and a rotation around the z-axis. The swash plate rotates around the x-axis, and the pistons are arranged parallel to both the z-axis and shaft axis.

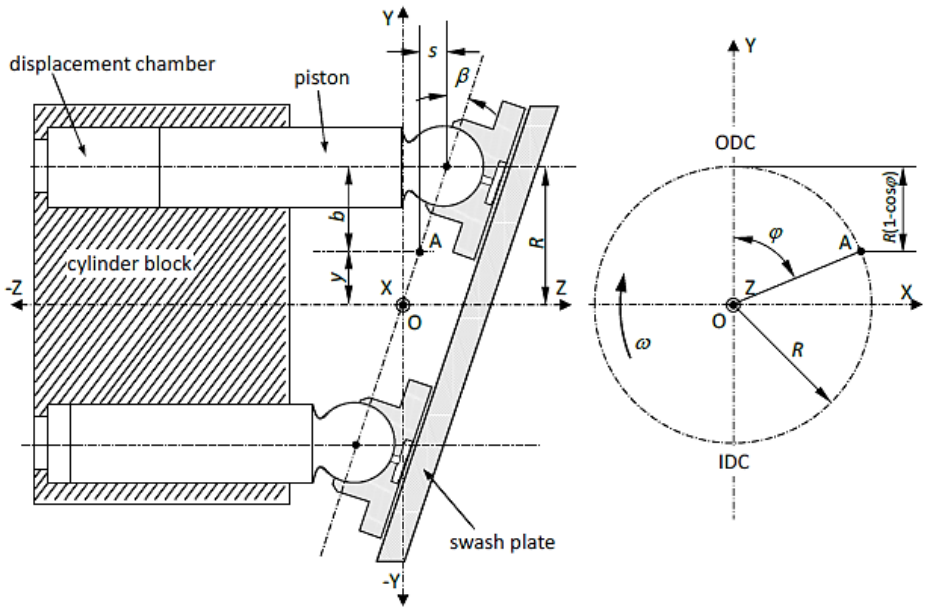

Figure 6: Schematic of an Axial Piston Pump to Explain the Kinematics [15]

Figure 6 shows the main components of the rotating group with the rectangular coordinate system. The outer dead center (ODC) of the piston -- the point on the piston pitch radius R at which the piston is displaced with the maximum distance from the bottom of the cylinder -- chosen as the initial position (i.e., angular position $\varphi = 0°$) for

the derivation of kinematic parameters. If β is the swashplate inclination angle and φ is the angular position of the piston, then the piston displacement s_k can be given [15] by

$$\begin{aligned} s_k &= -z \\ &= -b\tan\beta \\ &= -(R-y)\tan\beta \\ &= -(R-R\cos\varphi)\tan\beta \\ &= -R\tan\beta(1-\cos\varphi). \end{aligned} \tag{25}$$

By taking the derivative of piston displacement s_k with respect to angular position and equating the result to zero, it was determined that the maximum value of the piston displacement s_k could be achieved with a rotation of the cylinder block by an angle $\varphi = 180°$ -- that is, at the inner dead center (IDC). This maximum value of the piston displacement s_k for a swash plate angle β is defined as the piston stroke H_k [15]. Thus,

$$H_k = 2R\tan\beta. \tag{26}$$

The maximum value of stroke is achieved with the maximum swashplate angle, i.e.,

$$H_{k,\max} = 2R\tan\beta_{\max}.$$

The relative piston velocity in the z-direction can be given in terms of both the piston displacement and stroke [15] as

$$\begin{aligned} v_k &= \frac{ds_k}{dt} = \frac{ds_k}{d\varphi}\cdot\frac{d\varphi}{dt} = \frac{ds_k}{d\varphi}\cdot\omega \\ &= -\omega R\tan\beta\sin\varphi = -\frac{1}{2}\omega H_k\sin\varphi. \end{aligned} \tag{27}$$

Similarly, the piston acceleration can be given [15] as

$$\begin{aligned} a_k &= \frac{dv_k}{dt} = \frac{dv_k}{d\varphi}\cdot\frac{d\varphi}{dt} = \frac{dv_k}{d\varphi}\cdot\omega \\ &= -\omega^2 R\tan\beta\cos\varphi = -\frac{1}{2}\omega^2 H_k\cos\varphi. \end{aligned} \tag{28}$$

The circumferential velocity v_u and radial acceleration a_u of the piston caused by the rotation of the cylinder block can be expressed [15], respectively, as

$$v_u = R\omega \tag{29}$$

and

$$a_u = R\omega^2. \tag{30}$$

4.2 Volumetric Flow Rate

4.2.1 Theoretical Flow Rate and Ripple

The idealized discharge-flow of the pump is determined by considering a pump that does not leak while displacing incompressible fluid. If V_g is the geometric displacement volume and N is the rotational speed, the geometric flow rate can be given [15] by

$$Q_g = N \times V_g. \tag{31}$$

The geometric displacement volume of an axial piston pump can be expressed [15] as

$$\begin{aligned} V_g &= zA_k H_k \\ &= z\left(\frac{\pi d_k^2}{4}\right) 2R \tan\beta. \end{aligned} \tag{32}$$

Here, z is the total number of pistons in the pump, A_k is the area of a single piston, and d_k is the diameter of a piston. The maximum geometric displacement volume of an axial piston pump can be determined if the maximum swash plate angle of that pump is known or vice versa using Equation (32), i.e.,

$$V_{g,\max} = z\left(\frac{\pi d_k^2}{4}\right) 2R \tan\beta_{\max} = z\left(\frac{\pi d_k^2}{4}\right) H_{k,\max}.$$

Hence, the mean geometric flow rate of the pump over a time interval can be given by

$$Q_g = N \times z\left(\frac{\pi d_k^2}{4}\right) 2R \tan\beta. \tag{33}$$

The instantaneous volumetric flow rate Q_a of the pump can be given by summing the instantaneous volumetric flows of the individual piston which are in the delivery stroke. Thus,

$$Q_a = \sum_{i=1}^{k} Q_{ai}. \tag{34}$$

Here, k is the number of the pistons which are in the delivery stroke. In the case of an even number of pistons, the number of pistons positioned over the discharge port is half of the total number of pistons in the pump and the same as the number of pistons positioned over the suction port. However, in the case of an odd number of pistons, the number of pistons positioned over the discharge port is repeatedly fluctuating, and it depends upon the rotational position of the pump itself. This can be mathematically expressed [15] as

$$k = \begin{cases} \dfrac{z}{2} & \text{if } z \text{ is even number} \\ \dfrac{z \pm 1}{2} & \text{if } z \text{ is odd number} \end{cases}. \tag{35}$$

The idealized instantaneous volumetric flow of the individual piston is equal to the time rate of change of the instantaneous volume of the piston chamber. This change in the volume of the displacement chamber V_i with respect to time can be expressed [15] as

$$\begin{aligned} Q_{ai} &= -\frac{dV_i}{dt} = -v_{ki} A_k \\ &= \omega A_k R \tan\beta \sin\varphi_i = \frac{1}{2}\omega A_k H_k \sin\varphi_i. \end{aligned} \tag{36}$$

The instantaneous volume of the piston chamber V_i is continuously changing due to the linear motion of the piston in the cylinder block. The displacement chamber volume V_i at any instance if the flow out of the piston chamber is considered to be positive may be expressed [15] as

$$\begin{aligned} V_i &= V_0 - V_{sweep} \\ &= V_0 - s_k A_k \\ &= V_0 - R\tan\beta\left(1-\cos\varphi\right) A_k. \end{aligned} \tag{37}$$

Here, V_{sweep} is the volume sweep by the piston when it travels a distance of s_k, V_0 is the volume of the fluid in the displacement chamber when the piston is at outer dead center

(ODC) or the nominal volume of a piston chamber as if the swash plate angle is at maximum. When the piston is at ODC $(\varphi = 0°)$, the volume of the displacement chamber is the maximum achievable volume for a swash plate angle. On the other hand, when the piston is at IDC $(\varphi = 180°)$, the volume of the displacement chamber is the smallest achievable volume.

The volume of the displacement chamber when the piston is at the outer dead center (ODC) can be expressed in terms of the dead volume V_D in the displacement chamber as

$$\begin{aligned} V_0 &= V_D + H_{k,\max} A_k \\ &= V_D + \left(2R \tan \beta_{\max}\right) A_k . \end{aligned} \tag{38}$$

Since the pistons are spaced evenly by pitch angle $\Delta\varphi = 2\pi/z$ in a circular array about the centerline of the pump shaft, the circular position of the i^{th} piston may be expressed as

$$\begin{aligned} \varphi_i &= \varphi_1 + (i-1)\Delta\varphi \\ &= \varphi_1 + (i-1)\frac{2\pi}{z}. \end{aligned} \tag{39}$$

By combining Equations (34), (35), (36), and (39), the idealized discharge-flow ripple of the pump in case of both an even and odd total number of pistons in the pump can be expressed [15] as

$$Q_a = \begin{cases} \omega A_k R \tan\beta \sum_{i=1}^{z/2} \sin\left[\varphi + (i-1)\frac{2\pi}{z}\right] & \text{if } z \text{ is even number} \\ \omega A_k R \tan\beta \sum_{i=1}^{(z\pm1)/2} \sin\left[\varphi + (i-1)\frac{2\pi}{z}\right] & \text{if } z \text{ is odd number} \end{cases} . \tag{40}$$

4.2.2 Instantaneous Displacement Chamber Pressure

When a piston is at the outer dead center (ODC) point, the displacement chamber is filled up with fluid, the velocity of the piston is just zero, and the orifice area of high pressure (HP) and low pressure (LP) ports are zero. That is, the piston chamber is closed, except for the leakage path between the piston and its cylinder. At ODC, the piston reverses its direction of movement, and the fluid in the displacement chamber is thereby compressed due to the decrease of its volume. See Figure 7. First, through a small opening to the outlet, the fluid flows from the displacement chamber. Just before reaching the IDC, the displacement chamber is mostly emptied, except for the dead volume. At IDC, the piston again reverses its linear direction of movement, and the fluid in the displacement chamber starts to fill due to the increase of its volume through the opening to the inlet (suction port). The direction of the flow in the model can be governed by the pressure gradient. The opening to the discharge and suction port is governed by the valve plate geometry and must be modeled carefully to model the displacement chamber pressure precisely.

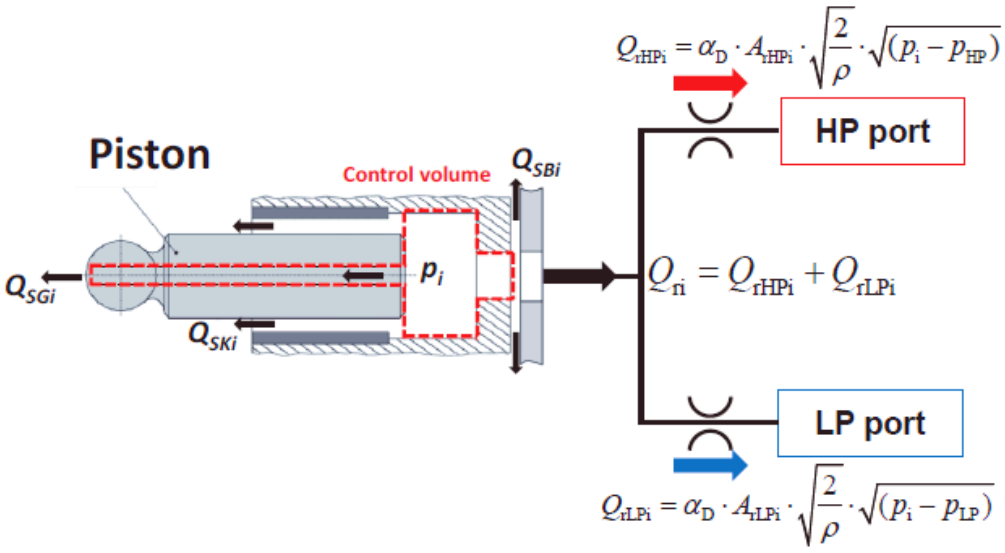

Figure 7: Control Volume of Displacement Chamber [32].

By applying the law of conservation of mass to the control volume in the displacement chamber shown in Figures 7 and 8, a mathematical model is derived for the transient pressure behavior in the displacement chamber. Thus,

$$\frac{dp_i}{dt} = \frac{K}{V_i}\left(Q_{ri} + Q_{leaki} - \frac{dV_i}{dt} \right). \tag{41}$$

Here, p_i is the transient pressure of the fluid in i^{th} displacement chamber, K is the bulk modulus of the fluid, V_i is the instantaneous volume of i^{th} displacement chamber, Q_{ri} is the sum of the flow rate leaving from and entering in i^{th} displacement chamber through discharge and suction ports, respectively. Therefore,

$$Q_{ri} = Q_{rHPi} + Q_{rLPi}. \tag{42}$$

Q_{leaki} is the sum of the external leakage flow through three different lubricating paths of the i^{th} displacement chamber.

$$Q_{leaki} = Q_{SKi} + Q_{SBi} + Q_{SGi}. \tag{43}$$

Generally, all the lubricating gaps varie with operating conditions and fluid during the operating period because of expansion and contraction of components and varying load carrying capacity of fluid film. However, for this analysis, all the lubricating gaps were assumed to be constant for simplifying the analysis.

The flow from the displacement chamber through the valve plate openings to the pressure ports (i.e., discharge and suction port) can be modeled as turbulent flow through the orifice. Therefore,

$$Q_{rLPi} = \alpha_D A_{rLPi} \sqrt{\frac{2}{\rho}\left| p_i - p_{LP} \right|} sign\left(p_i - p_{LP} \right) \tag{44}$$

and

$$Q_{rHPi} = \alpha_D A_{rHPi} \sqrt{\frac{2}{\rho}\left| p_i - p_{HP} \right|} sign\left(p_i - p_{HP} \right). \tag{45}$$

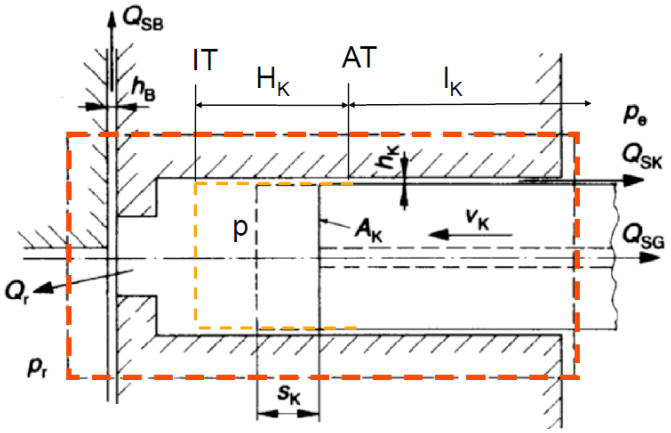

Figure 8: Piston States in a Displacement Chamber [15].

The leakage flow through the gap between the piston and its cylinder bore can be given [15] by

$$Q_{SKi} = \frac{\pi d_k h_k^3}{12\mu l_k}\left(p_i - p_e\right) - \frac{\pi d_k}{2} h_k v_{ki}. \tag{46}$$

Here, p_e is the pressure of fluid in the case of the pump, d_k is the diameter of the piston, h_k is the gap height or clearance between piston and its bore, v_{ki} is the velocity of the piston, μ is the dynamic viscosity, and l_k is the gap length of the piston which is the length in contact with cylinder, as shown in Figure 8. This length varies the displacement or stroke of the piston and can be given [15] as

$$l_k = l_A + s_{ki},$$

where l_A is the initial gap length that is the length of the piston in contact with the bore when the piston is at the inner dead center. Equation (46), therefore, can be rewritten as

$$Q_{SKi} = \frac{\pi d_k h_k^3}{12\mu\left(l_A + s_{ki}\right)}\left(p_i - p_e\right) - \frac{\pi d_k}{2} h_k v_{ki}. \tag{47}$$

Usually, the gap height h_k varies along the length of the piston as a function of rotational angle, but here contact and zero eccentricity between the piston and its bore were assumed.

The leakage flow through the gap between the slipper pad and swash plate can be given [15] by

$$Q_{SGi} = \frac{\pi h_G^3 d_d^4}{\mu\left(6d_d^4 \ln\frac{R_G}{r_G} + 128 h_G^3 l_d\right)}\left(p_i - p_e\right). \tag{48}$$

Here, h_G is the gap height between the slipper pad and the swash plate, which also varies and increases with increasing slipper surface. The gap height h_G is assumed to be constant. To continue with an explanation of the variables in Equation (48), d_d is the diameter of the capillary opening in the piston. This capillary opening is essential in lubricating the contact surface between the slipper pad and the piston. In addition, l_d is the total length of the piston, and R_G and r_G are the outer and inner radius of slipper land pad, respectively. This is illustrated in Figure 9.

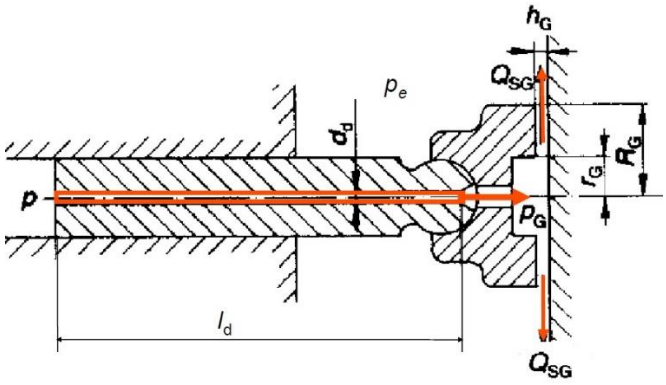

Figure 9: Leakage through Slipper Pad [15].

The leakage flow through the gap between the cylinder block and valve plate can be given [15] by

$$Q_{SBi} = \frac{h_B^3}{12\mu}\left(p_i - p_e\right)\int_\lambda \frac{1}{l}\, d\lambda. \tag{49}$$

Here, h_B is the gap height between the cylinder block and the valve plate, as shown in Figure 8. This gap height depends on the operating parameters, and it varies with the

rotational angle of the cylinder block. However, in this project, it was considered constant.

By substituting Equations (36), (37), (38), (42), and (43) into Equation (41), the ordinary differential equation that governs the transient pressure in the displacement chamber is obtained as

$$\begin{aligned}\frac{dp_i}{dt} &= \frac{K}{V_0 - s_{ki}A_k}\left(Q_{ri} + Q_{SKi} + Q_{SBi} + Q_{SGi} - v_{ki}A_k\right) \\ &= \frac{K}{V_D + \left(2R\tan\beta_{\max}\right)A_k - s_{ki}A_k}\left(Q_{ri} + Q_{SKi} + Q_{SBi} + Q_{SGi} - v_{ki}A_k\right).\end{aligned} \tag{50}$$

The instantaneous pressure profile in a displacement chamber can be accurately determined by solving this first-order ordinary differential equation using numerical methods such as ode45 and fourth-order Runge-Kutta (rk4).

4.2.2.1 Variable Orifice Area

The flow discharge and suction flow rates Q_{rHPi} and Q_{rHPi} described by Equations (45) and (46) strongly depend on the respective orifice areas (instantaneous valve plate area openings to the discharge and suction ports) A_{rHPi} and A_{rLPi} to the piston bore or kidney port. The area varies with the position angle φ of the kidney port relative to the initial position (i.e., angular position $\varphi = 0°$). A geometrical calculation for A_{rHP} is carried out for different angular segments when the kidney port locates on the discharge side from the ODC to the IDC ($0 < \varphi \leq 180$). The graphical representation of the areas variation with respect to phase angle φ is illustrated in Figure 10.

The discharge area A_{rHPi} can be modeled at seven angular segments. $[0 \quad \beta_1]$ is the angular segment during which the kidney port is completely closed, β_1 is the angle at which the silencing groove area starts to open, β_2 is the angle at which the major slot of the valve plate of the discharge side starts to open to the kidney port, β_3 is the angle at which the major slot opens to an area equal to the area of a circle formed by the kidney port with a radius equal to the kidney port radius r_{kp}, and β_4 is the angle at which the kidney port starts to open completely and it remain completely open until the angular position equals β_5. For the angular segment $[\beta_6 \quad \beta_7]$, the kidney ports open to an area less than the area of the circle formed by the radius of the kidney port. These angular segments are illustrated in Figure 10(b). The discharge side orifice area A_{rHPi} can be analytically found [12, 33] as

$$A_{rHP} = \begin{cases} 0 & 0 \leq \varphi \leq \beta_1 \\ 0.5 \times d_{sg} w_{sg} \left(\varphi / \varphi_f\right)^2 & \beta_1 \leq \varphi \leq \beta_2 \\ r_{kp}^2 (2\theta_1 - \sin(2\theta_1)) & \beta_2 \leq \varphi \leq \beta_3 \\ \pi r_{kp}^2 + 2r_{kp}(\varphi - \beta_2)R & \beta_3 \leq \varphi \leq \beta_4 \\ 2r_{kp} l_{kp} + \pi r_{kp}^2 & \beta_4 \leq \varphi \leq \beta_5 \\ 2r_{kp}[l_{kp} - (\varphi - \beta_4)R] + \pi r_{kp}^2 & \beta_5 \leq \varphi \leq \beta_6 \\ r_{kp}^2 (2\theta_2 - \sin(2\theta_2)) & \beta_6 \leq \varphi \leq \beta_7 \end{cases}, \quad (51)$$

where θ_1 and θ_2 in Equation (51), can be given [33] by

$$\theta_1 = \cos^{-1}\left(\frac{2r_{kp} - (\varphi - \beta_2)R}{2r_{kp}}\right) \text{ and } \theta_2 = \cos^{-1}\left(\frac{(\varphi - \beta_6)R}{2r_{kp}}\right). \quad (52)$$

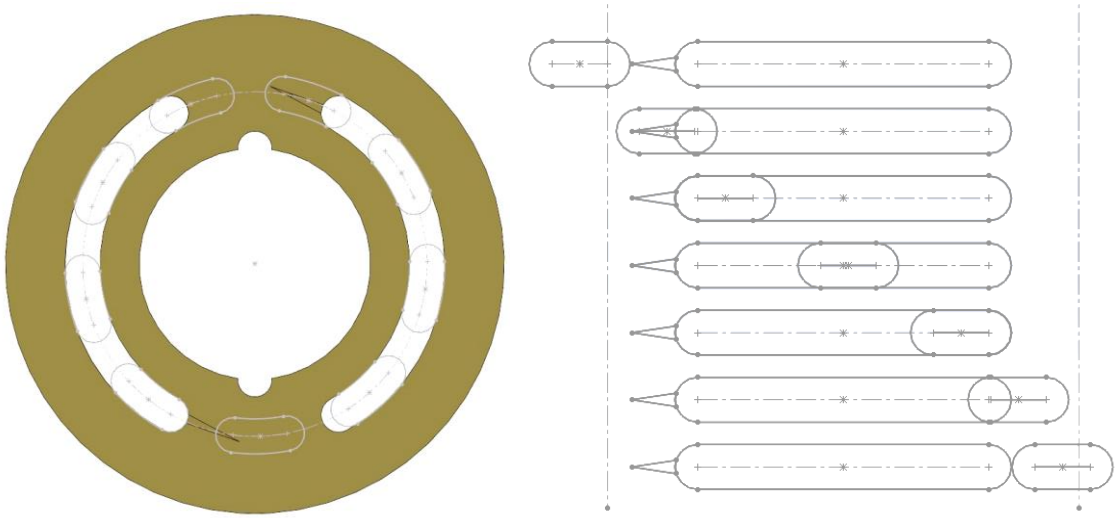

(a) **(b)**

Figure 10: Geometry of Valve Plate with Nine Kidney Ports.

Since the valve plate geometry of the suction side is the same as the discharge side, as shown in Figure 10, then the same calculation for A_{rLP} can be carried out for different angular segments when the kidney port is located on the discharge side from the IDC to the ODC $(180 < \varphi \leq 360)$.

It is important to precisely determine the transition slots/silencing grooves areas because they help in reducing the sudden pressure spike in the displacement chamber when each piston moves from intake slot to the discharge slot or vice versa. There are mainly three designs of the transition slots that are commonly used in the pump's design. The constant area transition slot design minimizes the required discharge area of the transition slot, the linearly varying transition slot design utilizes the shortest transition

slot length, and the quadratically varying transition slot design has no principal advantage [12, 34]. Some valve plate deigns also feature a damping hole to reduce the pressure spike and to lubricate the contact surface between the valve plate and the pump housing.

4.2.3 Overall Flow Rate of the Pump

The pump has z displacement chambers and the overall effect of the pump can be given by simulating each displacement chamber and summing the effect of each displacement chamber. For instance, the pump suction flow rate Q_{rLP} and discharge flow rate Q_{rHP} were given by summing the suction and discharge flow rate, respectively, of each displacement chamber which were phased out by the phase angle of $2\pi/z$. Thus,

$$Q_{rLP} = \sum_{i=1}^{z} Q_{rLPi} \tag{53}$$

and

$$Q_{rHP} = \sum_{i=1}^{z} Q_{rHPi}. \tag{54}$$

Similarly, the pump external leakage flow was evaluated by summing the leakage through each displacement chamber as

$$Q_{leak} = \sum_{i=1}^{z} Q_{leaki} = \sum_{i=1}^{z} \left(Q_{SKi} + Q_{SBi} + Q_{SGi} \right). \tag{55}$$

4.3 Torque Input on the Shaft and Swash Plate

4.3.1 Piston Dynamic Loading

The major external forces on the pistons act on the piston due to operating conditions and the geometry of piston. These forces include the displacement chamber pressure force, the axial inertia force, the viscous friction forces, the centrifugal force, and the reaction forces of the swashplate. Figure 11 shows a sectioned view of a single piston inside the cylinder block and all major acting forces on it in a Cartesian coordinate system.

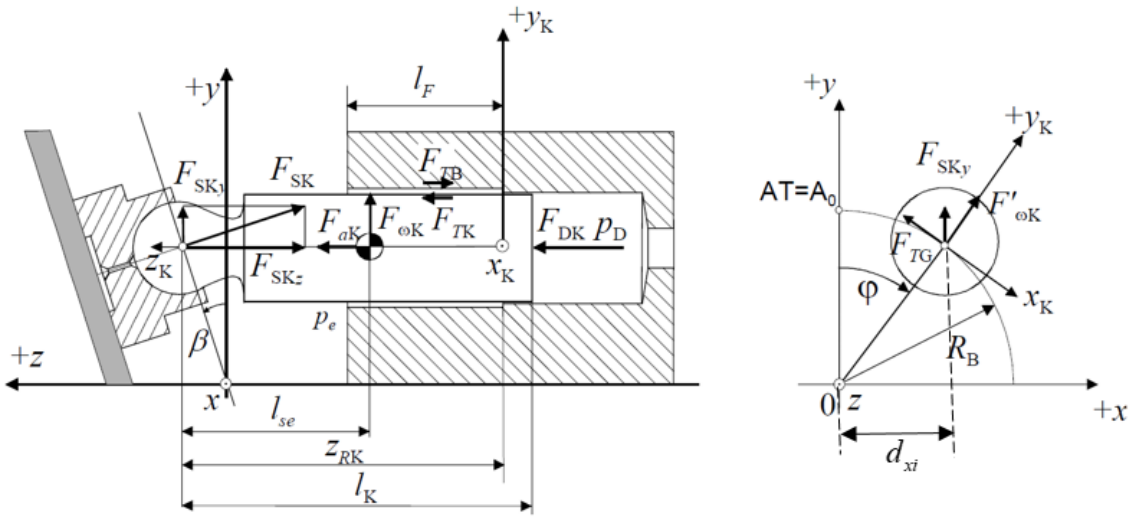

Figure 11: External Forces Acting on the Piston [34].

Three axial forces acting on the piston (along the *z*-axis) are the displacement chamber pressure force F_{DK}, the axial inertia force F_{aKz} due to the acceleration of the piston, and the viscous friction forces F_{TK} due to fluid film between the cylinder and the piston which depends on velocity distribution and fluid viscosity [34]. Therefore, the sum of the axial force F_{AKz} acting on the piston can be expressed [34] as

$$F_{AKz} = F_{DK} + F_{aKz} + F_{TK}. \tag{56}$$

Among these three axial forces, the displacement chamber pressure force F_{DK} is the largest load acting on the piston. The displacement chamber pressure force and axial inertia forces, respectively, can be given [34] by

$$F_{DK} = \frac{\pi d_K^2}{4}\left(p_i - p_e\right) \tag{57}$$

and

$$F_{aKz} = -m_K a_K = m_K \omega^2 R \tan\beta \cos\varphi. \tag{58}$$

Here, p_i is the i^{th} displacement chamber pressure and p_e is the case pressure.

The axial force F_{AKz} is transferred to the swashplate through the slipped pad in the direction orthogonal to the swash plate. This results in a large transverse force F_{SKy} on the piston which is carried by the fluid film between the piston and the bore. It can be given [34] by

$$F_{SKy} = F_{AKz} \tan\beta. \tag{59}$$

Similarly, the swash plate reaction force F_{SK} acting on the piston, perpendicular to the plane of the swash plate, can be expressed [34] as

$$F_{SK} = -\frac{F_{AKz}}{\cos\beta}. \tag{60}$$

Because of the rotation of the piston along with the drive shaft, a centrifugal force $F_{\omega K}$ acts on the piston and the slipper, which can be given [34] by

$$F_{\omega K} = \left(m_K + m_G\right)\omega^2 R. \tag{61}$$

Here, m_K and m_G, respectively, are the mass of the piston and the slipper pad, ω is the rotational frequency of the drive shaft, and R is the pitch circle diameter.

A minor external viscous friction occurs on the slipper pad due to the sliding of the slipper pad on the swash plate act. This force also depends on the film thickness between the slipper pad and swash plate and the viscosity of the film. For the constant film thickness, it can be expressed [34] as,

$$F_{TG} = \mu \frac{\omega R}{h_G} \pi \left(R_G^2 - r_G^2 \right). \tag{62}$$

The parameters in Equation (62) are very well illustrated in Figure 9.

Hence, all the force acting on the piston can be expressed in two components of external forces [34] as

$$\begin{aligned} F_{Kx} &= -F_{SKy} \sin\varphi + F_{TG} \\ &= -F_{AKz} \tan\beta \sin\varphi + \mu \frac{\omega R}{h_G} \pi \left(R_G^2 - r_G^2 \right) \end{aligned} \tag{63}$$

and

$$\begin{aligned} F_{Ky} &= F_{SKy} \cos\varphi + F_{\omega K} \\ &= F_{AKz} \tan\beta \cos\varphi + \left(m_K + m_G \right) \omega^2 R. \end{aligned} \tag{64}$$

These forces results in the following external moments or torque [34] about the origin, shown in Figure 11:

$$\begin{aligned} M_{Kx} &= -z_{RK} F_{SKy} \cos\varphi - \left(z_{RK} - l_{SK} \right) F_{\omega K} \\ &= -z_{RK} F_{AKz} \tan\beta \cos\varphi - \left(z_{RK} - l_{SK} \right) \left(m_K + m_G \right) \omega^2 R \end{aligned} \tag{65}$$

and

$$\begin{aligned} M_{Ky} &= z_{RK} F_{Kx} \\ &= z_{RK} \left(-F_{SKy} \sin\varphi + F_{TG} \right) \\ &= z_{RK} \left(-F_{AKz} \tan\beta \sin\varphi + \mu \frac{\omega R}{h_G} \pi \left(R_G^2 - r_G^2 \right) \right). \end{aligned} \tag{66}$$

Here, M_{Kx} is the external moment on the piston about the *x*-axis and M_{Ky} is the external moment on the piston about the *y*-axis. It must be noted that the origin shown in Figure 11 is local to the piston. These forces and moments must be completely sustained by the fluid film load carrying capacity and develop adequate force and moment to counterbalance these external forces and moments by hydrodynamic pressure [15, 34].

4.3.2 Instantaneous Torque on the Shaft

The torque exerted by a single piston on the drive shaft of the pump is the moment exerted about the center of the cylinder block by a single piston. It can be expressed as

$$T_{zi} = d_{xi} \times \left(F_{SKiy} + F_{TGi} \sin \varphi_i + F_{TCi} \right). \tag{67}$$

Here, F_{SKiy} is the vertical component of the swash plate reaction force F_{SKi}, F_{TGi} is the viscous friction on slipper pad, F_{TCi} is the viscous friction on the kidney port which is sliding on the valve plate, and d_{xi} is the horizontal distance of the i^{th} piston away from the y-axis, as shown in Figure 11. Therefore,

$$d_{xi} = R \sin \varphi_i. \tag{68}$$

Substituting Equations (56), (59), and (68) into Equation (67), Equation (69) is obtained:

$$T_{zi} = R \sin \varphi_i \left[\left(F_{DKi} + F_{aKiz} + F_{TKi} \right) \tan \beta + F_{TGi} \sin \varphi_i + F_{TCi} \right]. \tag{69}$$

Now, substituting the external forces from Equations (57), (58), and (62) into Equation (69), Equation (71) is obtained:

$$T_{zi} = R \sin \varphi_i \left[\left(A_k \left(p_i - p_e \right) - m_K a_{Ki} + F_{TKi} \right) \tan \beta + \mu \omega R \left(\frac{\pi \left(R_G^2 - r_G^2 \right)}{h_G} \sin \varphi_i + \frac{A_D}{h_B} \right) \right]. \tag{70}$$

The viscous friction F_{TKi} between the cylinder and piston is approximated by viscous damping, that is, $v_k C_k$. The similar approach for determining the instantaneous torque exerted by a single piston on the drive shaft is taken by Manring [35]. However, that study only considered ideal forces, not viscous friction. Later, Manring [36] proposed a method for determining the viscous friction between the cylinder and piston.

4.3.3 Overall Torque on the Shaft of the Pump

The net instantaneous or overall torque exerted on the pump shaft can be given by Equation (69):

$$T = \sum_{i=1}^{z} R \sin\varphi_i \left[\left(F_{DKi} + F_{aKiz} + F_{TKi} \right) \tan\beta + F_{TGi} \sin\varphi_i + F_{TCi} \right]. \tag{71}$$

By integrating Equation (69) from 0 to 2π, the average torque exerted on the pump shaft can be given as

$$T_{avg} = \frac{z}{2\pi} \int_0^{2\pi} \left\{ R \sin\varphi_i \left[\left(F_{DKi} + F_{aKiz} + F_{TKi} \right) \tan\beta + F_{TGi} \sin\varphi_i + F_{TCi} \right] \right\} d\varphi_i. \tag{72}$$

The damping coefficient, which is a lumped parameter that describes energy dissipation effects in dynamic systems, can be calculated [12], for the actuators and pistons as

$$C = \frac{\mu A}{h} = \frac{\mu}{h} \left(\pi D L \right). \tag{73}$$

Here, μ is the dynamic viscosity of a fluid, A is the surface area in contact at the plate, L is the length of the specimen in contact, and h is the fluid film thickness or clearance that exists between the two plates.

4.4 MATLAB Simulink Models

The complete function block diagram, which captures the relationship between components and key states of the pump, is shown in Figure 12. This is an integrated model of which consists of four main models – the phase angle model, the piston configuration model, the swivel torque model, and the torque on the shaft model.

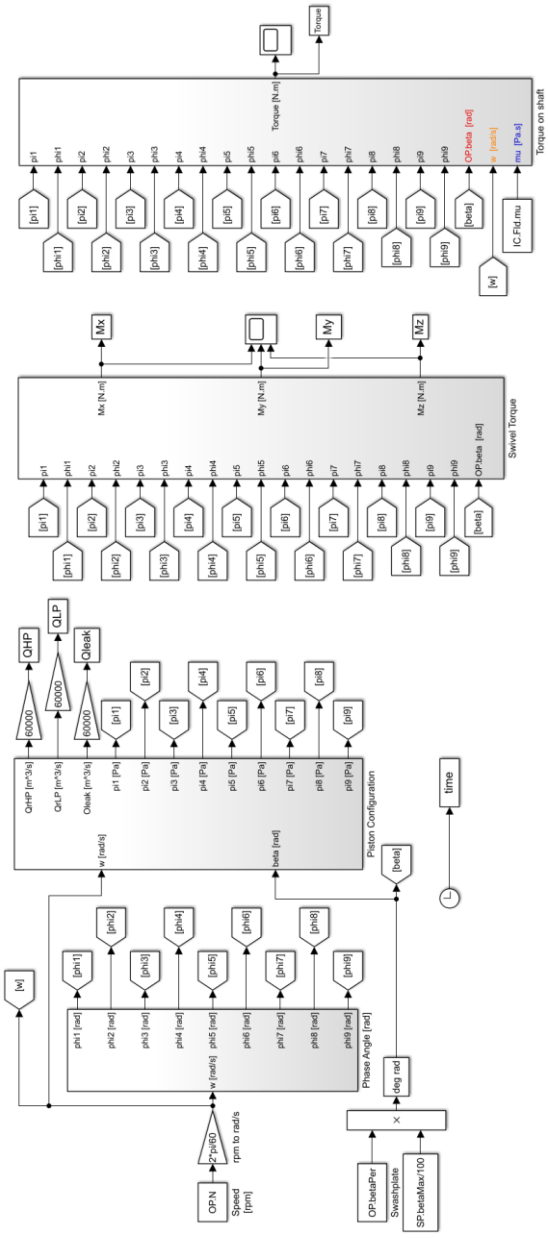

Figure 12: Integrated Model.

The phase angle model is simply the phase out of each piston by the pitch angle, $\Delta\varphi$. It is shown in Figure 13.

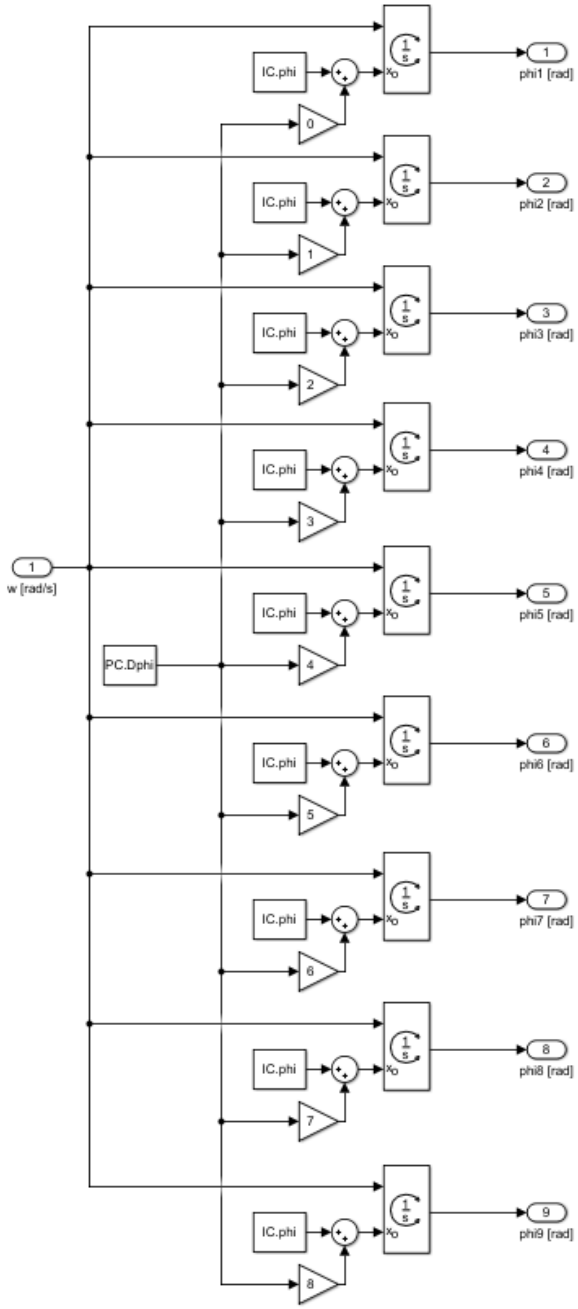

Figure 13: Phase Angle Model.

The phase angle subsystem block can be simply understood as

$$\varphi\left(t+\Delta t\right)=\varphi\left(t\right)+\varphi t. \tag{74}$$

The piston configuration subsystem block, shown in Figure 14, consists of nine pistons which are phase out. This model takes the various volumetric flows from each piston and summs them. It is based on Equations (53), (54), and (55).

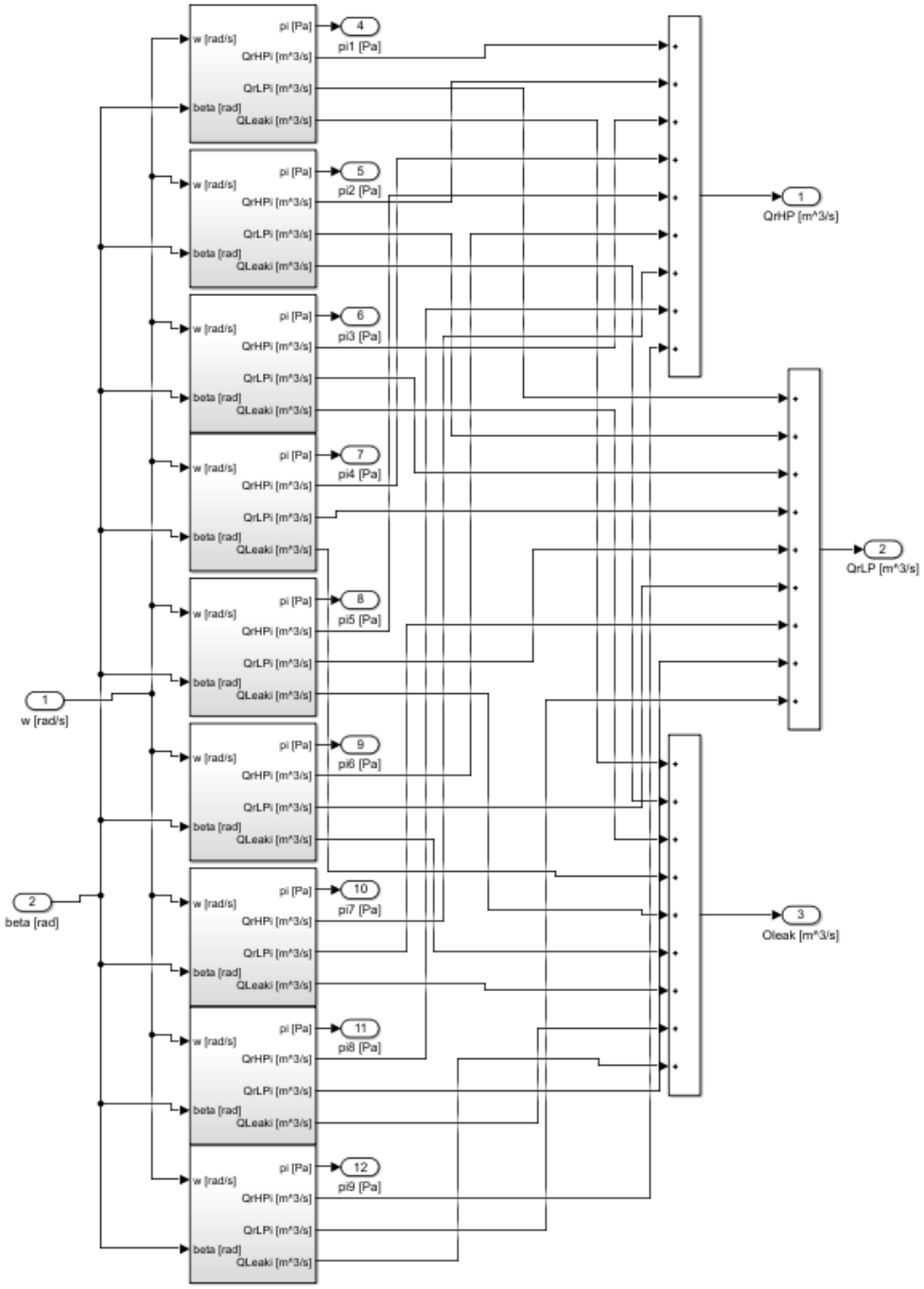

Figure 14: Piston Configuration Model (Overall Flow).

Figure 15 shows the instantaneous displacement chamber pressure model which determines the instantaneous pressure in a single displacement chamber. This model consists of subsystem models – the fluid properties, the discharge or suction area, the piston kinematics, and flow rates. It is based on Equation (50).

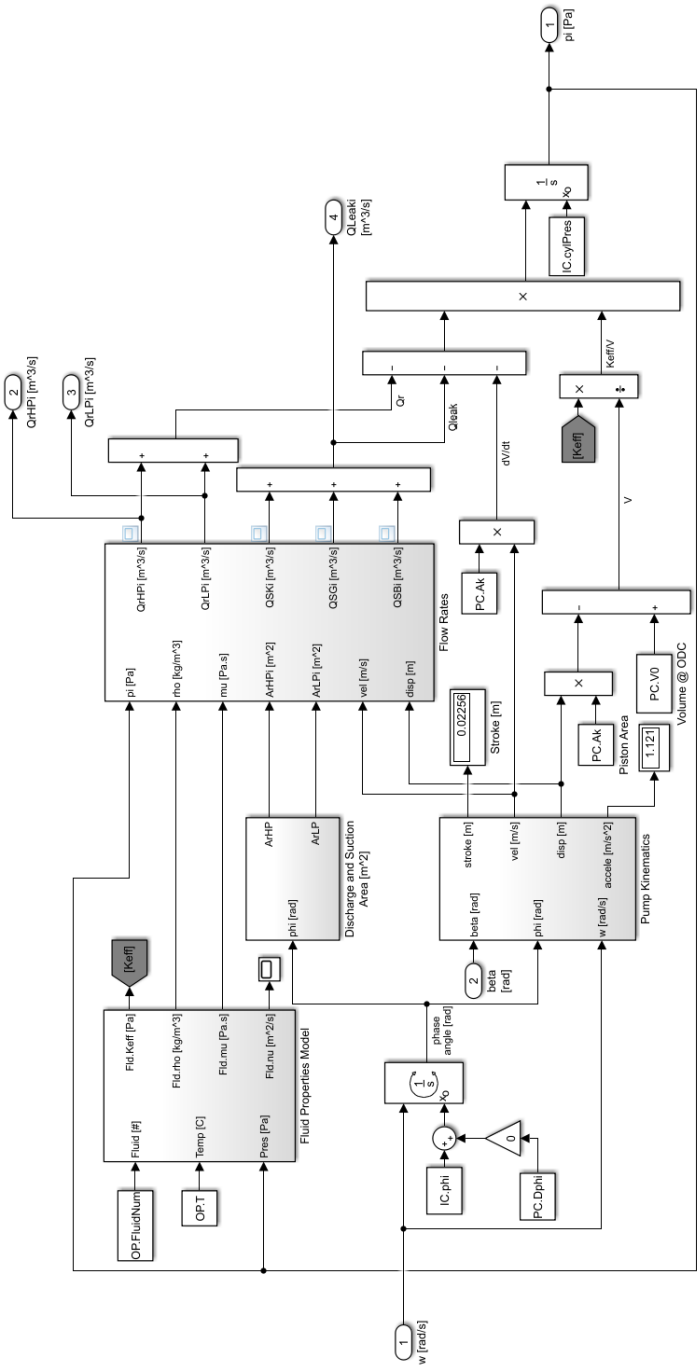

Figure 15: Instantaneous Displacement Chamber Pressure (Piston) Model.

The fluid properties subsystem block, shown in Figure 16, determines the instantaneous bulk modulus, effective bulk modulus, density, kinematic viscosity, specific heat, and thermal conductivity of the fluid based on fluid pressure and temperature.

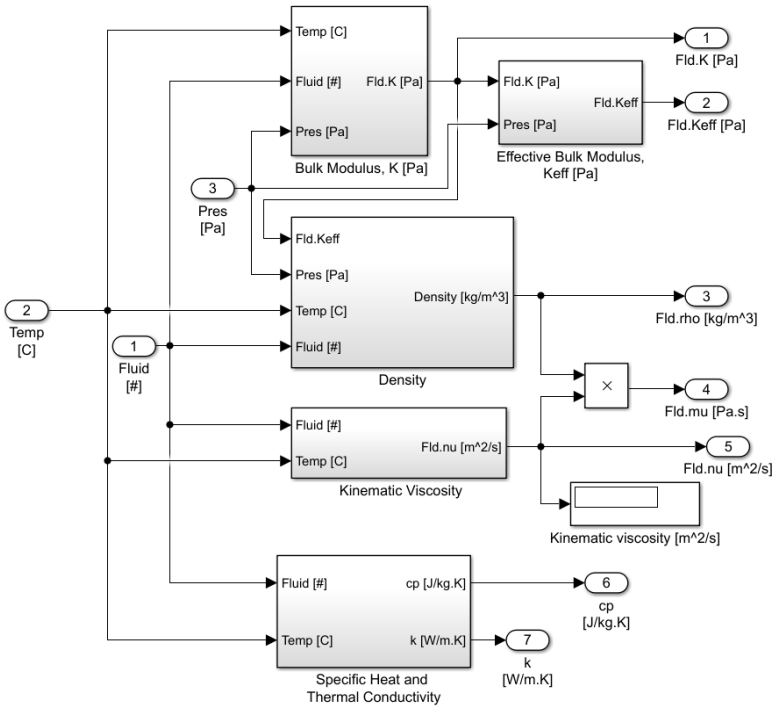

Figure 16: Fluid Properties Model.

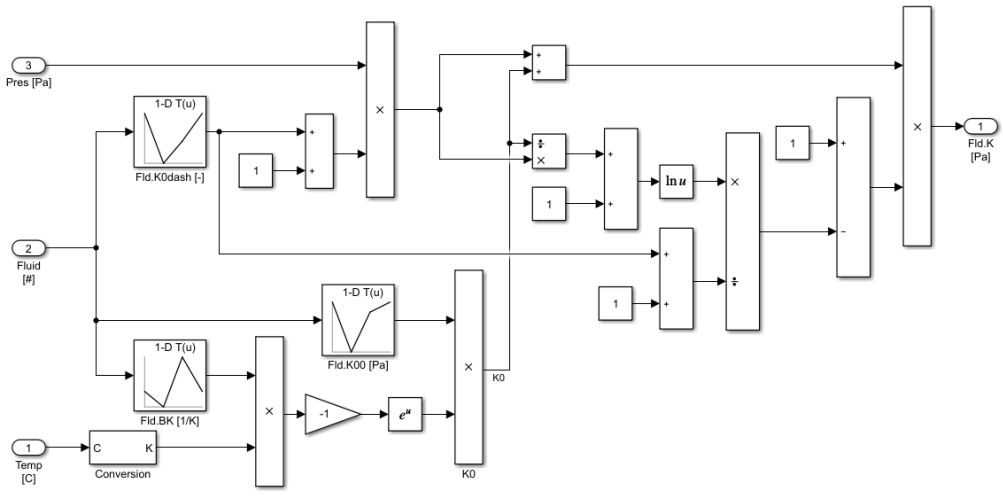

Figure 17: Bulk Modulus Model.

The bulk modulus, effective bulk modulus, density, kinematic viscosity, dynamic viscosity, specific heat, and thermal conductivity models are shown, respectively, in Figures 17 through 21. These models, respectively, are based on Equations (9), (11), (20), (18), (23), and (24).

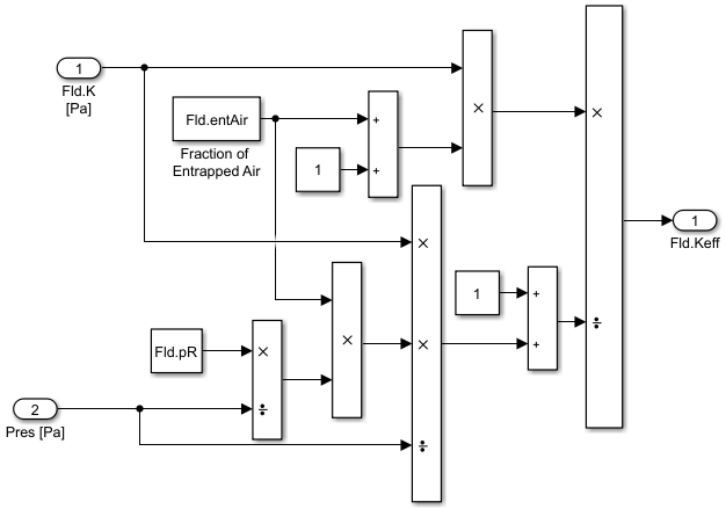

Figure 18: Effective Bulk Modulus Model.

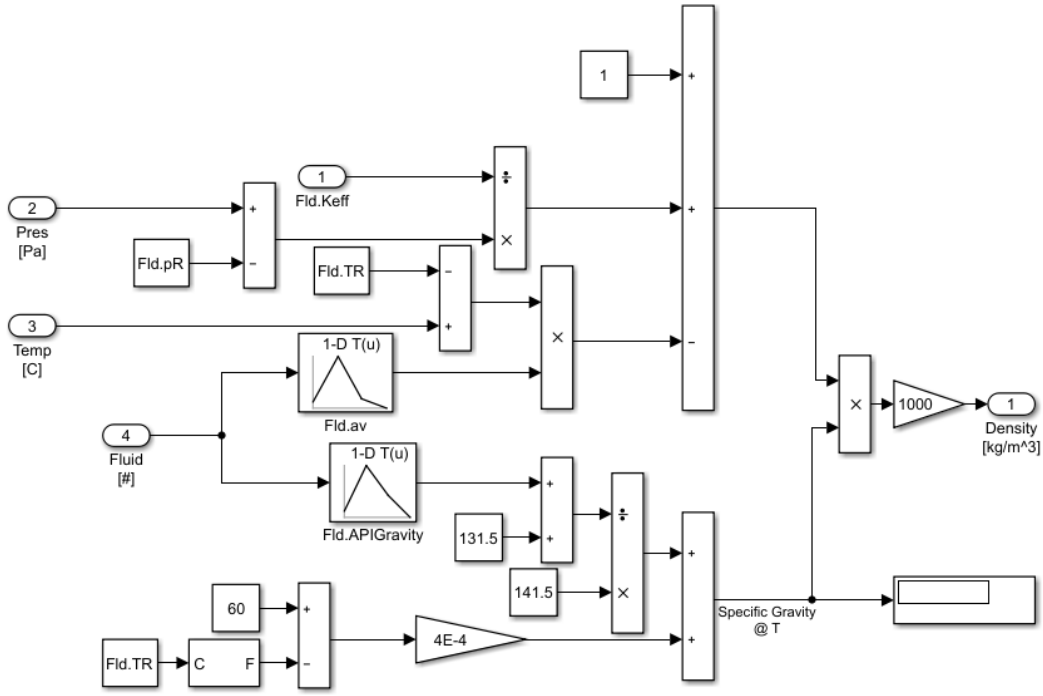

Figure 19: Density Model.

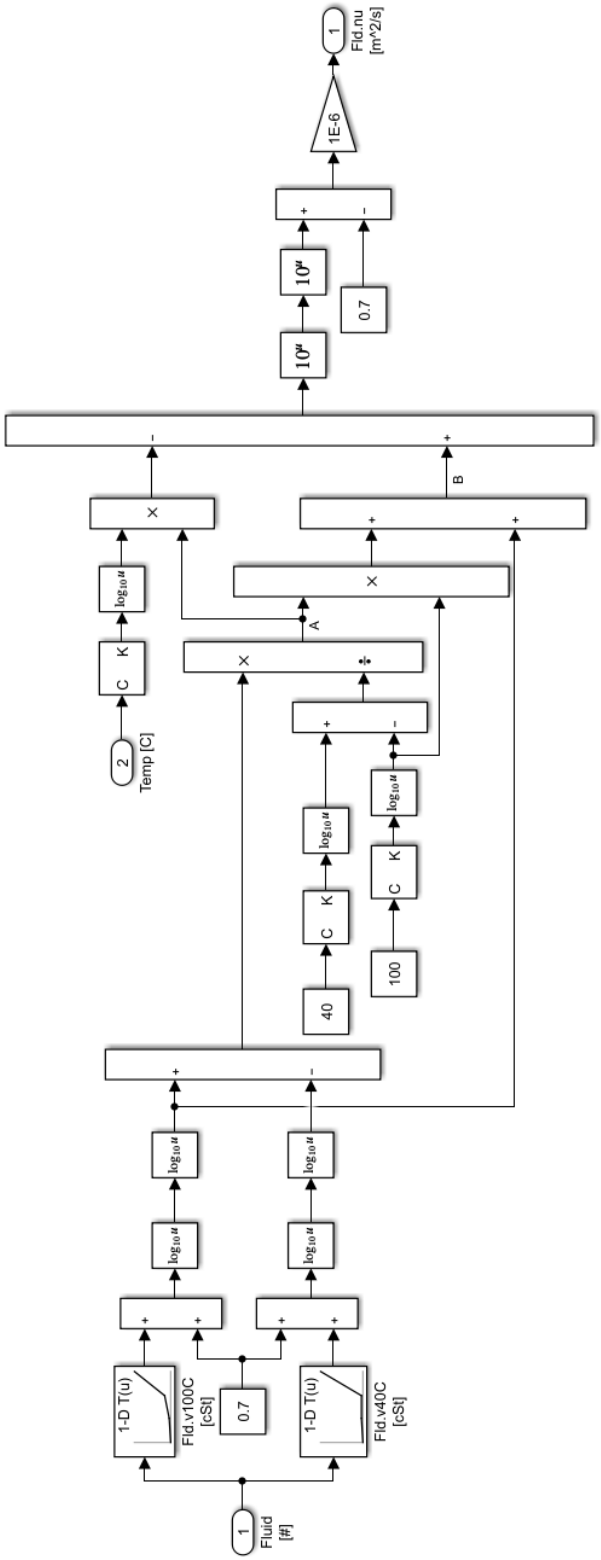

Figure 20: Kinematic Viscosity Model.

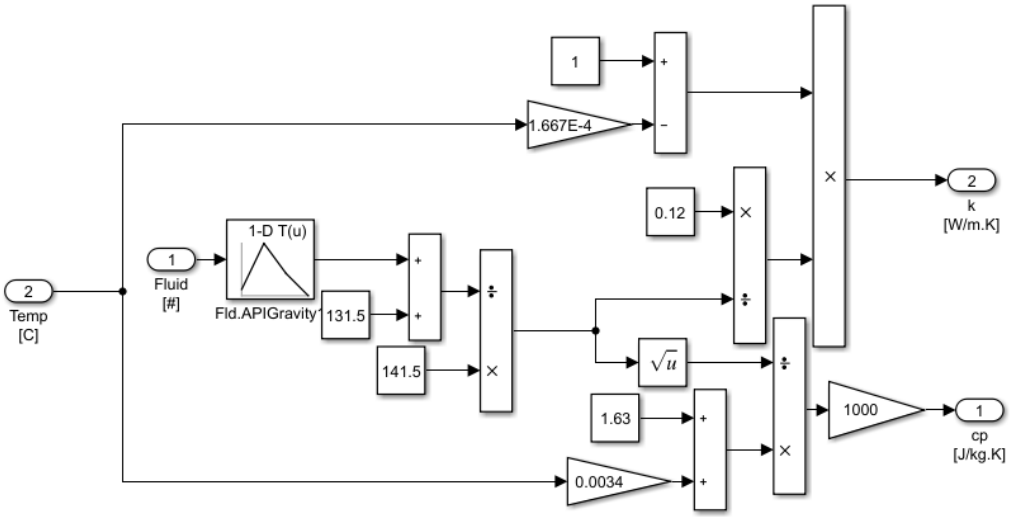

Figure 21: Specific Heat and Thermal Conductivity Model.

The pump kinematics model which is based on Equations (25) to (28), is shown in Figure 22.

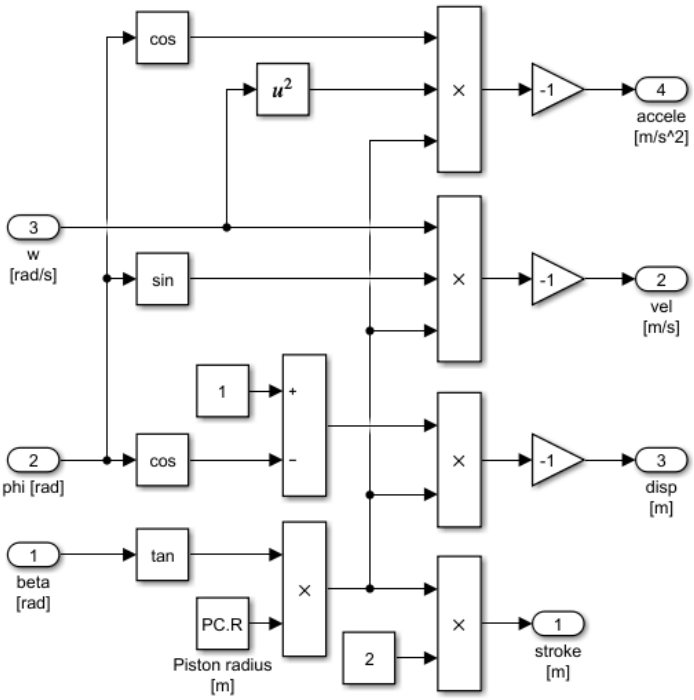

Figure 22: Pump Kinematics Model.

Figures (23) and (24) shows the models which determine the discharge and suction orifice instantaneous area. This model employs an *if-else* condition to separately model for the suction orifice area and the discharge orifice area. It is based on Equations (52) and (53).

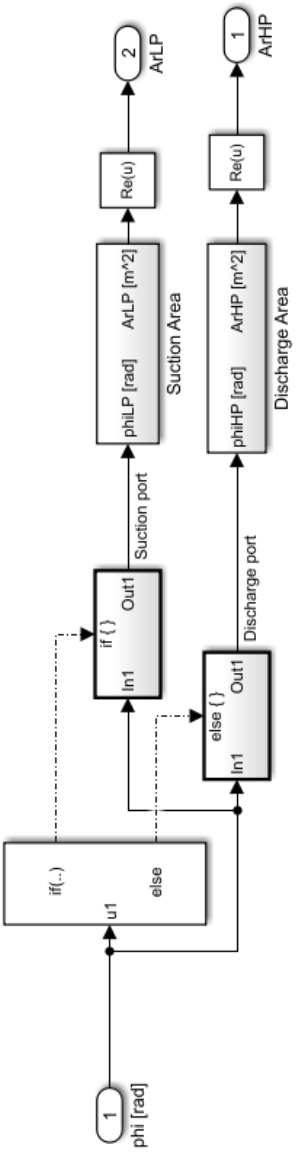

Figure 23: Discharge and Suction Area Model.

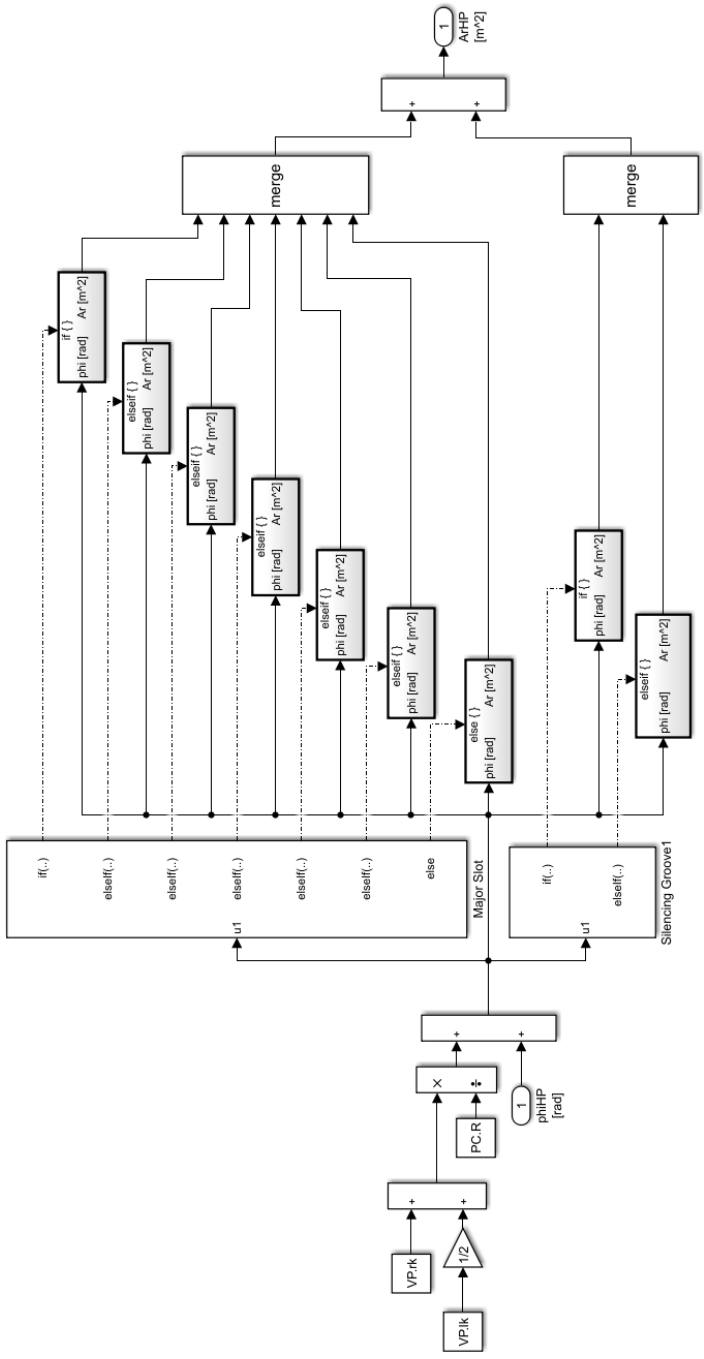

Figure 24: Discharge Area Model.

The discharge, suctions, and various leakage flows were modeled, respectively, using Equations (44), (45), and (47) through (49), and these flows shown in Figure 25.

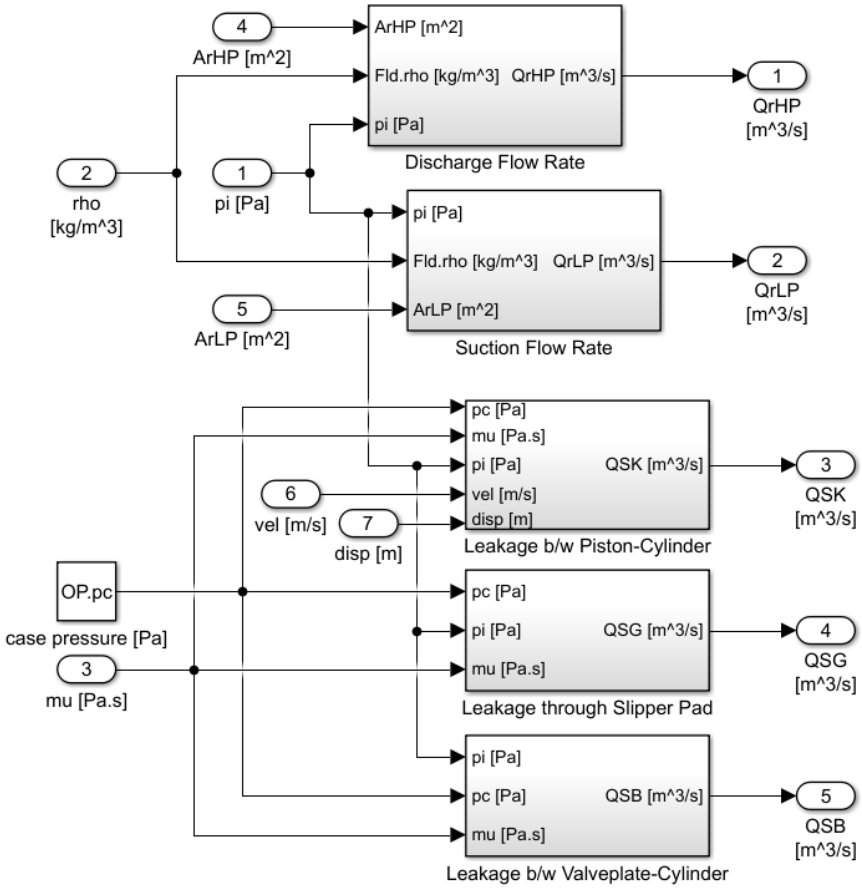

Figure 25: Flow Rates Model.

The swivel torque model and its subsystem block are shown in Figures 26 and 27, respectively.

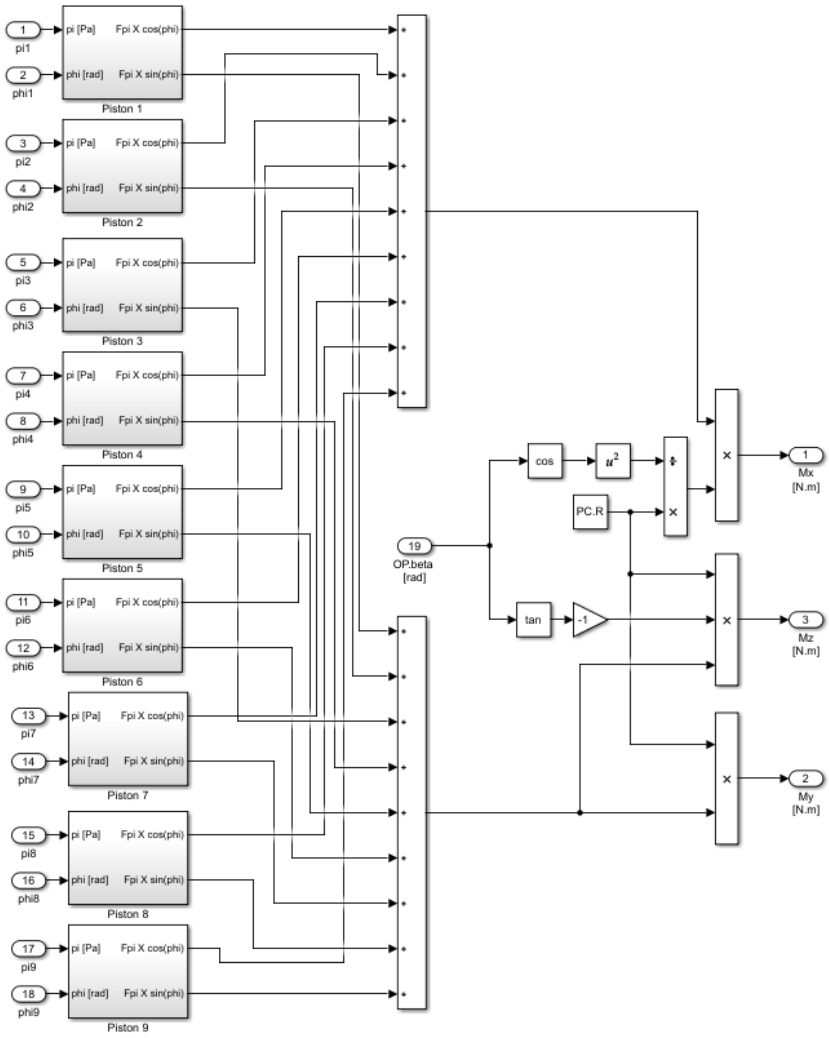

Figure 26: Swivel Torque Model.

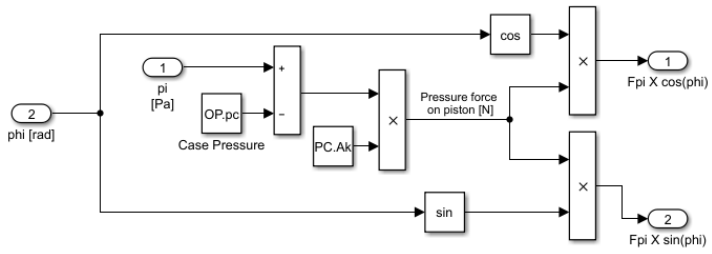

Figure 27: Piston Subsystem Block of Swivel Torque Model.

The torque on the shaft of the pump is determined by the torque on the shaft model which is shown in Figure 28. It contains nine piston subsystem blocks, which determine the torque applied by a single piston on the drive shaft of the pump.

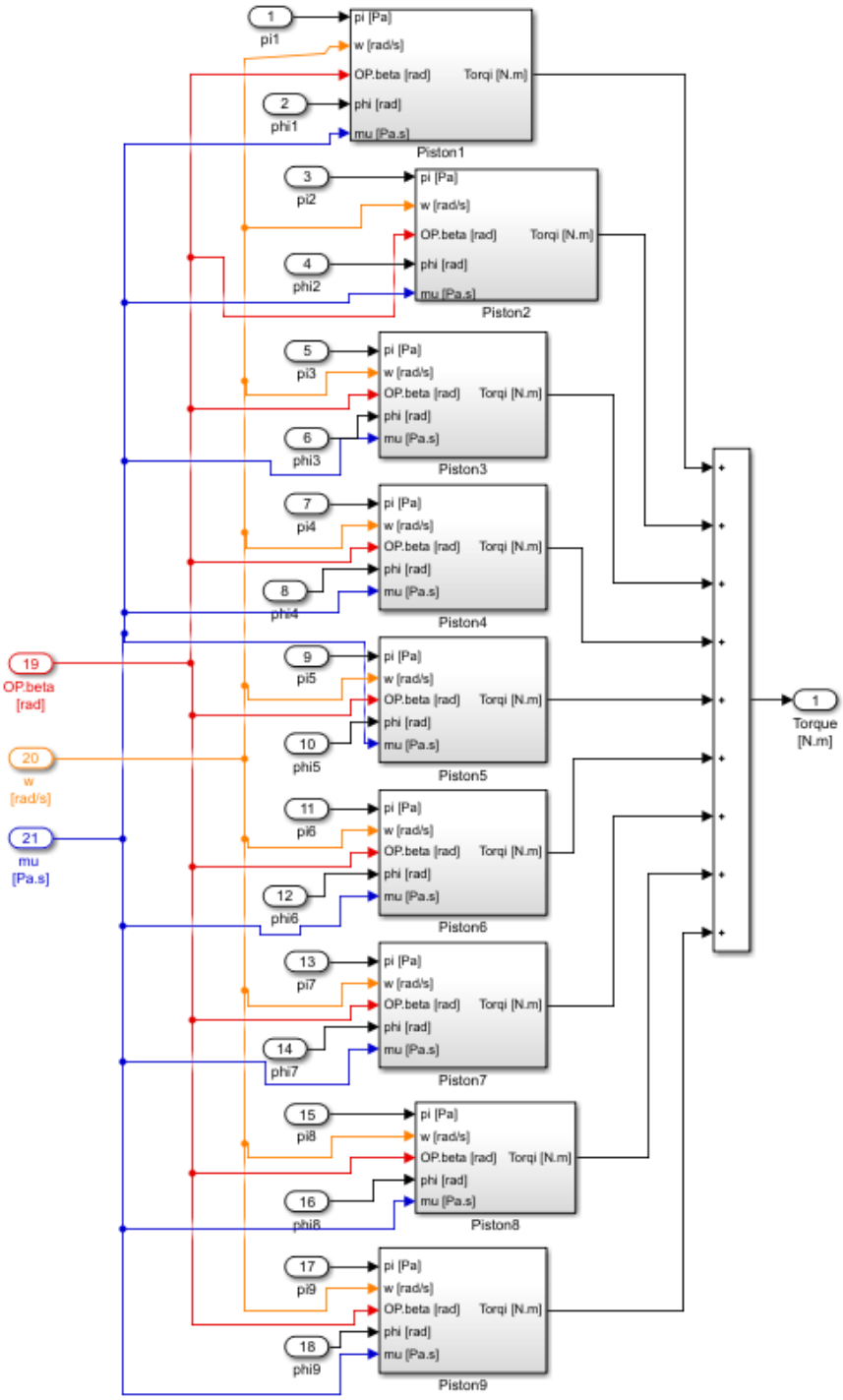

Figure 28: Torque on the Shaft Model.

The instantaneous torque exerted by a single piston on the drive shaft by the subsystem block is shown in Figure 29.

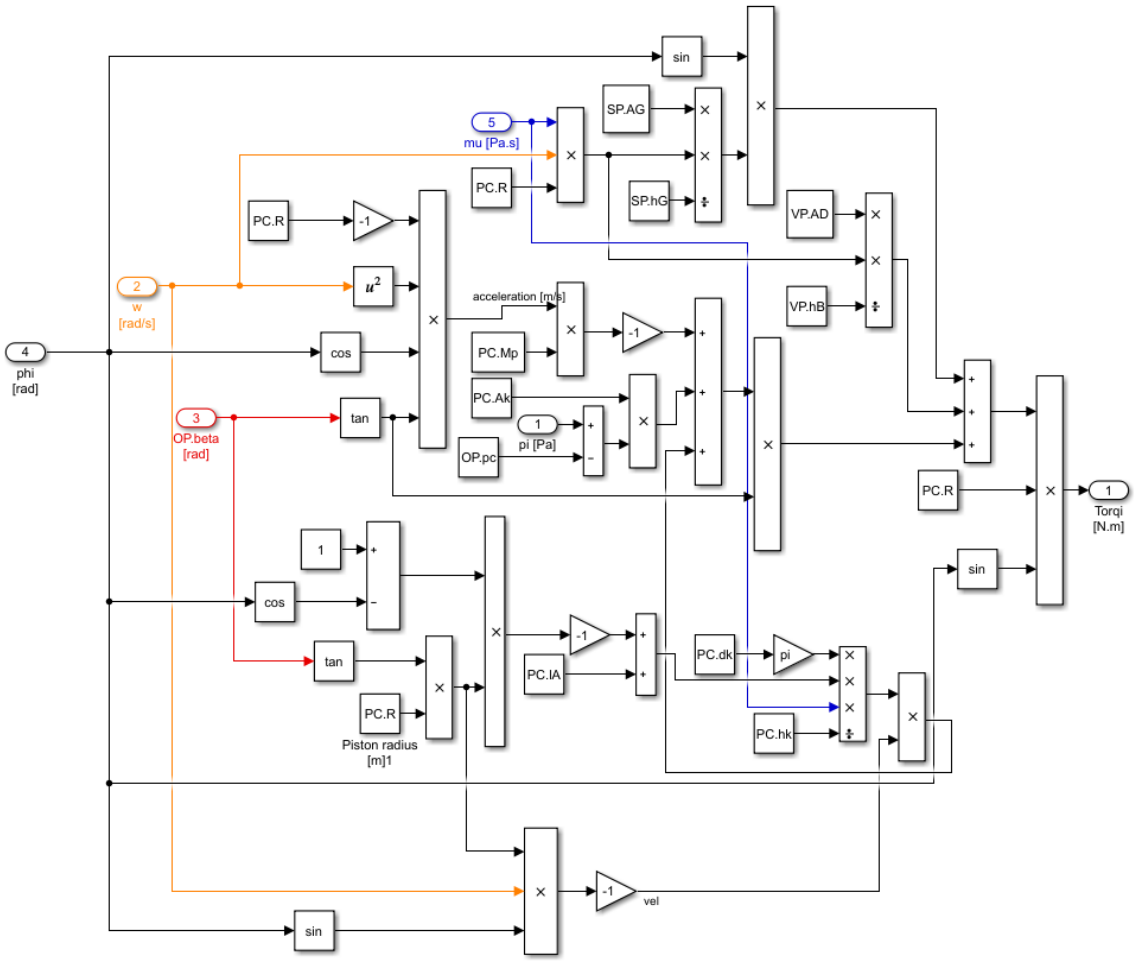

Figure 29: Instantaneous Torque on the Shaft by a Single Piston.

Parameters used in the model were either obtained from the specification sheets or by measuring actual components of the axial pump assembly, and parameters which are listed in Table 2. The swashplate was molded in Solidworks CAD software, and the exact mass of the swashplate was entered to determine the mass moment of inertia of the swashplate about the axis of rotation, as shown in Figure 30.

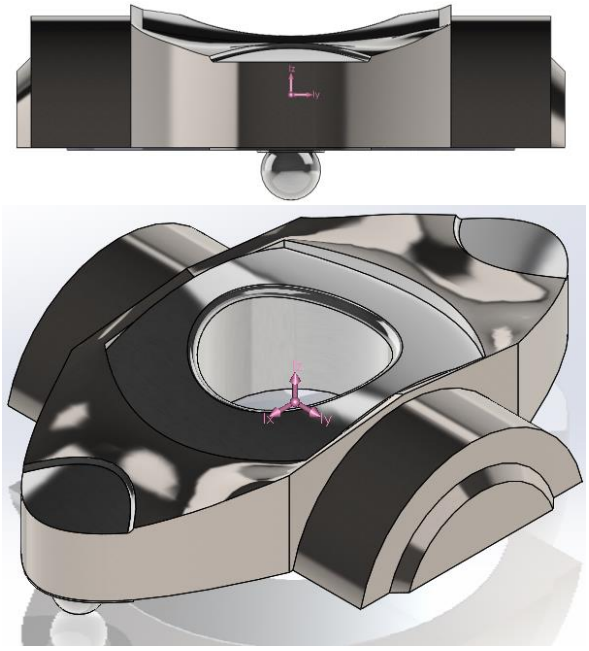

Mass properties of swashplate
Configuration: Default
Coordinate system: -- default --

Mass (user-overridden) = 1307.400 grams

Volume = 230478.476 cubic millimeters

Surface area = 35472.357 square millimeters

Center of mass: (millimeters)
X = 0.033
Y = 11.119
Z = 0.000

Principal axes of inertia and principal moments of inertia: (grams * square millimeters)
Taken at the center of mass.
Ix = (0.000, 0.000, 1.000) Px = 1163607.306
Iy = (1.000, 0.001, 0.000) Py = 1757164.726
Iz = (-0.001, 1.000, 0.000) Pz = 2786639.025

Moments of inertia: (grams * square millimeters)
Taken at the center of mass and aligned with the output coordinate system.

Lxx = 1757165.322	Lxy = 783.694	Lxz = 0.068
Lyx = 783.694	Lyy = 2786638.428	Lyz = -0.097
Lzx = 0.068	Lzy = -0.097	Lzz = 1163607.306

Moments of inertia: (grams * square millimeters)
Taken at the output coordinate system.

Ixx = 1918814.610	Ixy = 1256.634	Ixz = 0.068
Iyx = 1256.634	Iyy = 2786639.812	Iyz = -0.186
Izx = 0.068	Izy = -0.186	Izz = 1325257.976

Figure 30: Swashplate Mass Moment of Inertia.

Table 2: Parameters Used in Modeling.

Symbol	Description	Value [unit]
A_G	area of slipper pad in contact with swash plate	2.5125E-4 m
A_k	area of a piston	2.2698E-4 m^2
D_l	diameter of the large actuator	24.60E-3 m
D_s	diameter of the small actuator	4.95E-3 m
d_k	diameter of a single piston	17.00E-3 m
H_{max}	maximum stroke of the pump	22.564E-3 m
h_G	gap between slipper pad and swash plate	15.00E-6 m
h_k	clearance between piston and bore	8.00E-6 m
I	swashplate mass moment of inertia	2786638.43E-9 $kg \cdot m^2$
k	bias-spring constant	46312.18 N/m
L	distance from the actuator to the swashplate pivot	65.80E-3 m
l_A	length of the piston/cylinder interface at IDC	37.50E-3 m
l_T	total length of a piston	37.50E-3 m
M_l	mass of the large actuator	134.301 g
M_s	mass of the small actuator	79.028 g
m_k	mass of a single piston with slipper pad	67.558E-3 kg
R	pitch circle radius	33.50E-3 m
R_G	outer radius of slipper pad	10.70E-3 m
r_G	inner radius of slipper pad	5.90E-3 m
$V_{g\,max}$	maximum geometric displacement of the pump	46.0945 cc/rev
z	total number of pistons	9
β_{max}	Maximum swashplate angle	18.61°
$\Delta\varphi$	piston pitch or phase angle	40°

Chapter 5: Experimental Methodology

An open-loop axial piston pump of 45 cc/rev with precision electronic displacement control was employed in this study. The power to drive the pump was supplied by a variable frequency drive and a 75 hp inverter type electric motor. The electric motor was instrumented with a torque transducer and rotary encoder, as shown in Figure 31. Rotational frequency, inlet oil temperature, swash plate angle, and pump outlet pressure were controlled via automation. System pressure was regulated by a pilot operated cartridge valve. The pump outlet flow rate was measured using a gear-type positive displacement flow meter positioned upstream of the pressure control valve. The ISO VG 46 fluid was cooled and filtered in the return line. Also, the fluid temperature at the pump inlet was controlled by exchanging the heat with water in a heat exchanger that is controlled by set-point temperature. The system was operated under steady-state conditions for 45 seconds and data for each test point were collected over the final 15 seconds.

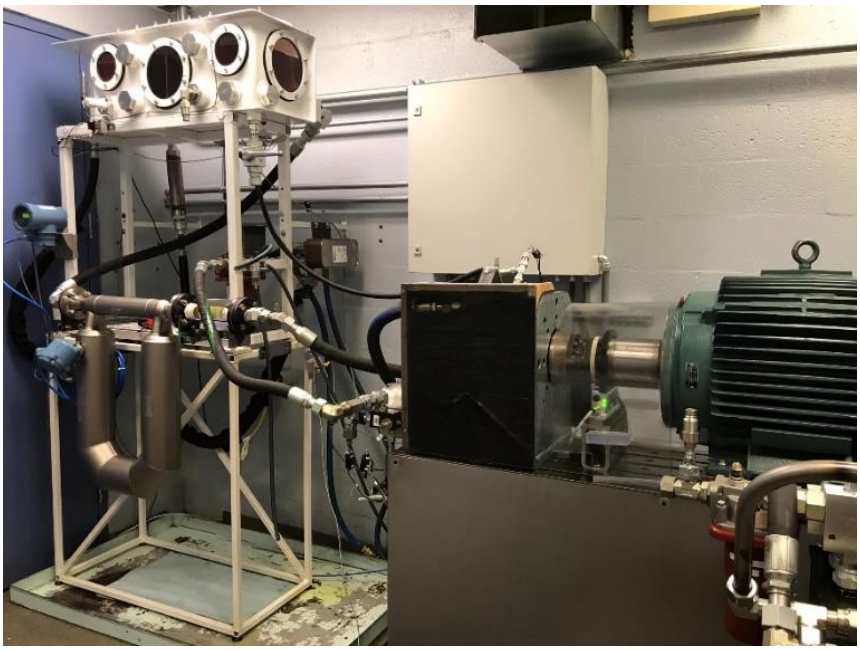

Figure 31: Hydraulic Test Rig at the Fluid Power Institute, MSOE.

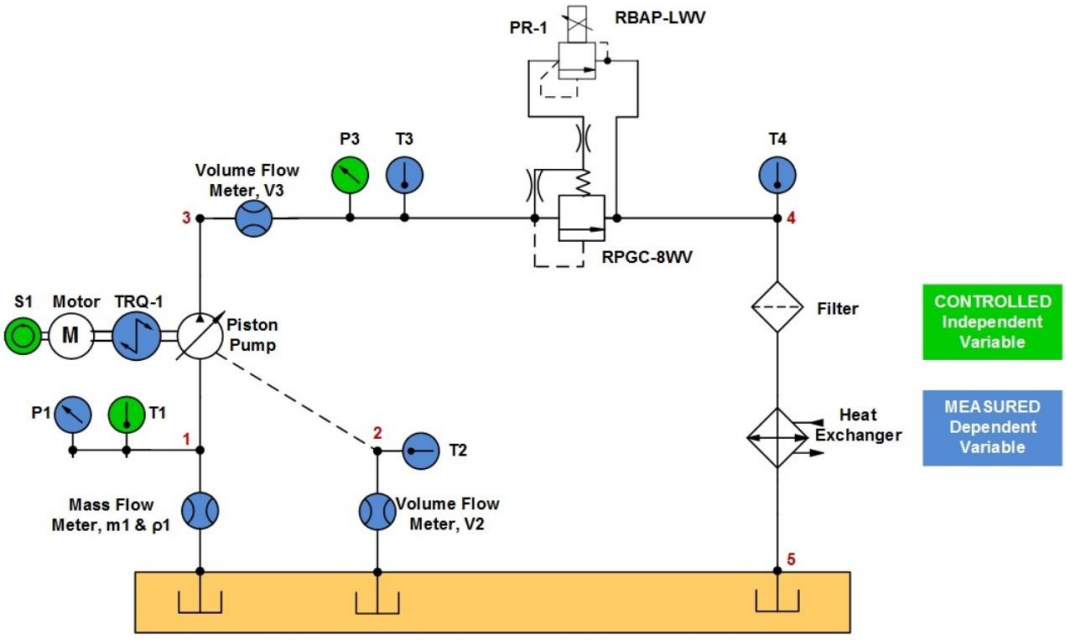

Figure 32: Hydraulic Circuit Schematic of the Test Rig.

The detailed circuit diagram of the test rig is shown in Figure 32. The green color indicates the parameters that are controlled, whereas the blue indicates the measured dependent variables. This stand was automated by PLC programming, and hence, it had a very good repeatability characteristic. The instruments that were used for the data acquisition are listed in Table 3.

Table 3: Instruments and Sensors Used in the Test Stand.

Parameter	Sensor	Max Rating	Error
Shaft speed	BEI Encoder HS35F	6000 rpm	±0.05%
Torque input	HBM T40B	500 N-m	±0.03%
Air mass flow rate	Aalborg GFC 37	20 L/min	±1.5%
Inlet mass flow rate and Density	Micro Motion CMF200M341N2BAE2ZZ	87,100 kg/hr	±0.05%
Outlet volumetric flow	Max Machinery G240	240 lpm	±0.3%
Case volumetric flow	Max Machinery G045	45 lpm	±0.3%
Pressure inlet	GEMS	7 bars	±0.25%
Pressure outlet	GP50	350 bars	±0.5%
Temperature	OMEGA Type J	220 ^{0}C	±1.1^{0}C

Full factorial testing was conducted at six pressures (1000-3500 psi), four rotational speeds (1000-2200 rpm), and four displacements (25-100%). As shown in Figure 33, each point in the full factorial set (∗) forms the vertex of the right angle and is therefore *orthogonal*. The orthogonal test plan consisted of 100 data points. The factorial value was 96. To set the size to 100, four high speed, high-pressure data points were added to the test plan. For developing high fidelity empirical flow and torque models for the pump, the Latin Hypercube Sampling design of experiment was chosen. To be consistent with the full factorial, 96 data points were sampled using the Latin hypercube algorithm. All 96 LHS data points (o) were non-orthogonal. Four high speed, high-pressure data points were also added to the LHS test plan to ensure that boundary conditions were included in the dataset. Thus, both sample sets contained 100 data points.

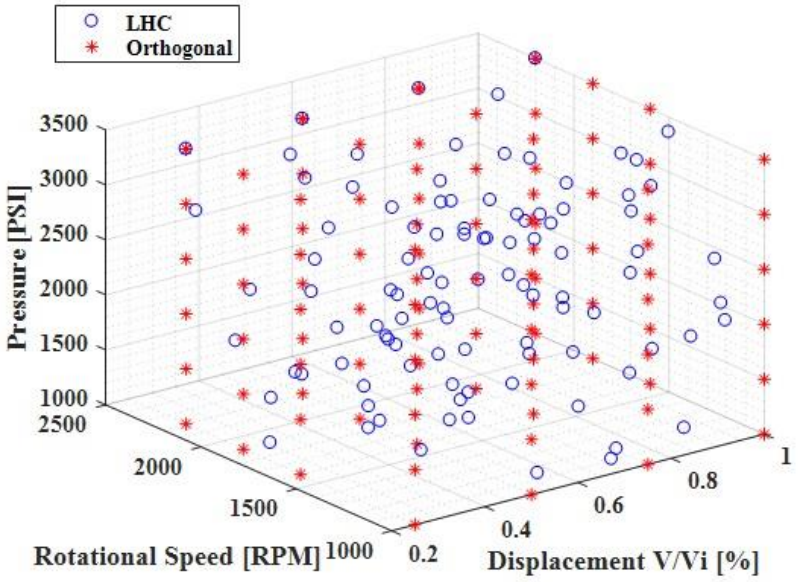

Figure 33: Orthogonal and Latin Hypercube-Based Design of Experiments.

Four fluids that differ in their physical properties were chosen from base oil groups II and III. The description of the fluid and their properties are listed in Table 4. The properties include the viscosity index, API gravity, and other properties that are necessary to model the temperature and pressure effects using the proposed models in Chapter 3. The testing of these fluids was mainly done for the pump inlet temperature controlled to 50°C. However, the temperature was fluctuating $\pm 8°C$. Only for fluid PP10D, which is an SAE10 type fluid, was tested at both 50°C and 80°C.

Table 4: Descriptions of Hydraulic Oils and their Properties.

Parameter		**Fluid I**	**Fluid II**	**Fluid III**	**Fluid IV**
Fluid ID		PP10D	PP11D	PP12D	PP13D
Description/Group		SAE10/GrII	HM46/GrIII	HV46/GrII	SAE15W40/GrII
Viscosity Index		137	141	164	140
API Gravity @ 15.6ºC		31.7	39	34.2	30.7
Kinematic Viscosity, mm^2/sec	@ 40ºC	41.8	43.37	45.6	112.7
	@ 100ºC	7.24	7.53	8.45	15.14
Parameters for the Tait Equation of State, $T_R = 20\ ^oC$					
K_0'		11.331	10.427	10.823	11.331
K_{00}, GPa		8.898	8.032	8.718	8.898
β_K, K^{-1}		0.005744	0.005716	0.005808	0.005744
a_v, $^oC^{-1}$		0.0006345	0.0007221	0.000640	0.0006217
Parameters for the Thermodynamic Scaling of Viscosity					
γ		3.528	3.403	3.751	3.528
μ_∞ / mPa·s		0.1452	0.1143	0.3108	0.1452
φ_∞		0.3595	0.2429	0.2820	0.3595
B_F		11.882	17.521	16.760	11.882
Reference Parameters					
Temperature, T_R, ^oC		20	20	20	20
Pressure, p_R, MPa		0	0	0	0

To calculate the theoretical flow rate, it was necessary to measure the rotational frequency of the pump and determine the volume of fluid displaced per revolution. The electronic control on the pump records the swashplate angle in terms of percentage of displacement to the maximum displacement of the pump. Therefore, first, it was necessary to determine the maximum swash plate angle using experimental data so that the recorded displacement in percentage could be accurately converted into displacement (cc/rev). The Toet method was employed to determine the pump displacement using collected steady-state test data, in compliance with the modified version of ISO 4409. For this purpose, a low-pressure $(\leq 500 \text{ psi})$ set of data for the PP13D fluid was collected.

The Toet method features a two-step process to determine pump displacement [37]. In the first step of the process, the ratio of pump outlet flow rated to rotational frequency is plotted for each of several test pressures, as shown in Figure 34.

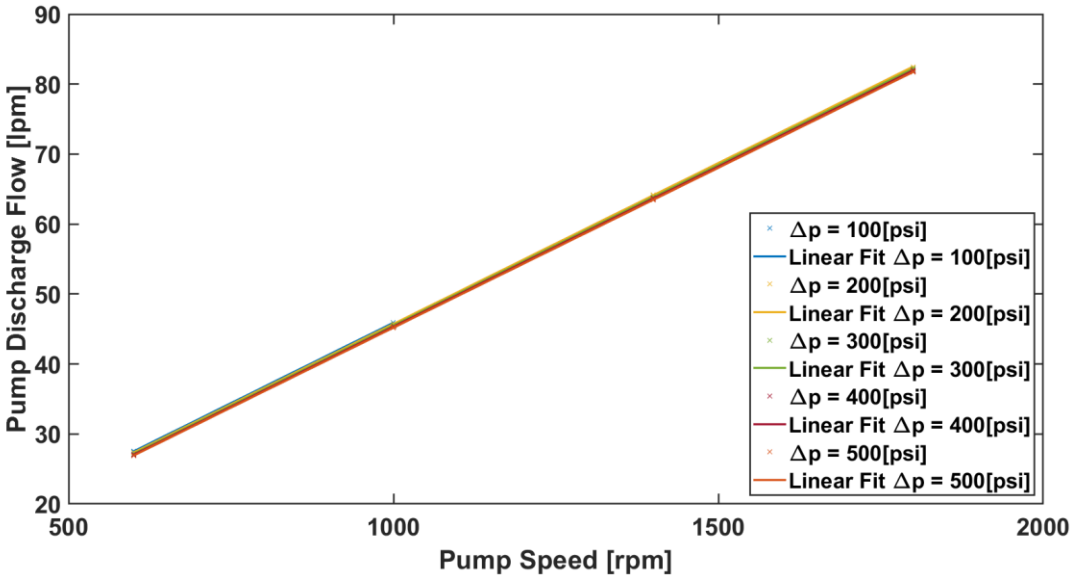

Figure 34: First Step of the Toet Method.

In the second step of the Toet method, $\partial Q_{out}/\partial N$ is plotted as a function of pressure. The zero intercept from a linear fit of the data equals the derived displacement. Hence, the derived displacement is 46.0945 cc/rev as shown in Figure 35. The MATLAB function used to determine the maximum displacement using the Toet Method is featured in Appendix D.

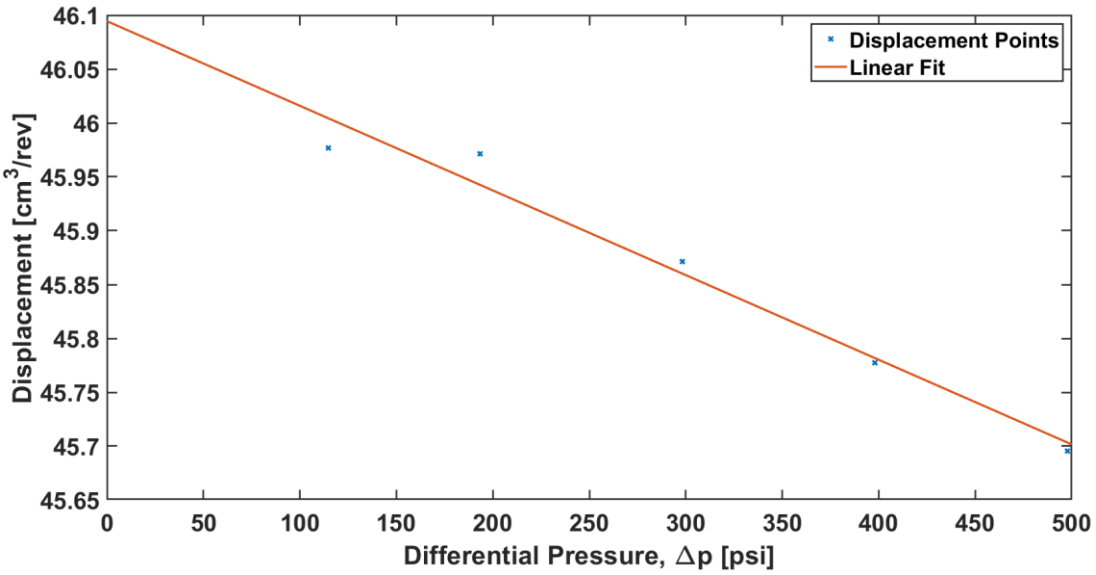

Figure 35: Second Step of the Toet Method.

Chapter 6: Results and Discussion

6.1 Empirical Modeling

Four criteria were used for assessing the model quality:

- Mean standard error (S): The mean standard error expresses the model error in the units of the dependent variable.
- Correlation coefficient (R^2): The correlation coefficient expresses the proportion of the variation in the dependent variable that is predictable from the independent variables.
- Akaike's Information Criteria (AIC), and Variance Inflation Factor (VIF): These criteria screen models that exhibit multicollinearity. This is undesirable because multicollinearity results in models that over-fit data. Models that over-fit data can generate high residuals when applied to new datasets [39]. AIC specifically estimates the quality of each model, relative to each of the other models.

It must be noted that models with higher R^2 and lower S, AIC, and VIF fit better. The best subset regression analysis was conducted using the physics-based flow loss expressions listed in Table 1. The MATLAB functions for the best subset regression and the multiple linear regression analysis were written to select the best combination of terms, and determine their coefficients, respectively. These MATLAB functions and the corresponding script are included in Appendices E, and F.

6.1.1 Pump Discharge Flow Model

Models consisting of four, five, and six terms (excluding the constant) were evaluated for discharge flow; however, for the final results, the best four-term models based on model quality criteria were selected. As can be seen in Table 5, the addition of this term reduced the standard error of the model by 5.0E-3 liters per minute but increased the collinearity between terms. The reduction in standard error on increasing an extra term was not significant enough. Therefore, only four-term models were

considered. Table 5 shows the four- and five-term discharge flow models obtained from the MATLAB program and their mean standard error, R-squared, maximum VIF, and AIC values. The count in Table 5 just counts the number of the model. This program evaluates any number of terms and models to give the best possible model.

Table 5: Pump Discharge Flow Models.

Number of Variables	Rsquared	StdError	MaxofVIF	count	Model	AIC
5	0.99974	0.42117	3.80257	47085	-2.3461e-05*(P/(mu*N))-0.0016851*(sqrt(P2))-1.1226*(N*P/K)+0.44741*((1-P2/K)*D*N)+7.1341e-07*(P*(D^2)/mu)+2.2406	-93
5	0.99974	0.42275	3.83289	46953	-2.4239e-05*(P/(mu*N))-1.1169*(N*P/K)+0.4473*((1-P2/K)*D*N)-2.23e-07*(P)+7.2359e-07*(P*(D^2)/mu)-0.81283	-95
5	0.99974	0.42462	3.79705	24882	+0.44458*(N*D)-1.3717e-05*(P/(mu*N))-0.0018242*(sqrt(P2))-1.2074*(N*P/K)+5.0065e-07*(P*(D^2)/mu)+2.7704	-261
5	0.99974	0.42542	6.31646	52811	-0.19869*((rho/P)*N^3)-0.0018242*(sqrt(P2))-1.0496*(N*P/K)+0.44928*((1-P2/K)*D*N)+5.3081e-07*(P*(D^2)/mu)+2.4423	-53
4	0.99973	0.42610	3.47040	3217	+0.44543*(N*D)-0.001855*(sqrt(P2))-1.1998*(N*P/K)+4.1059e-07*(P*(D^2)/mu)+2.7266	-860
5	0.99974	0.42618	4.14119	47289	-1.5892e-05*(P/(mu*N))-0.001596*(sqrt(P/rho))-1.0798*(N*P/K)+0.44731*((1-P2/K)*D*N)+7.2324e-07*(P*(D^2)/mu)+2.3378	-89
5	0.99974	0.42651	5.32509	19342	-7.0292e-08*(P/mu)-0.0017503*(sqrt(P2))-1.0645*(N*P/K)+0.44825*((1-P2/K)*D*N)+6.2308e-07*(P*(D^2)/mu)+2.2504	-544
5	0.99974	0.42651	5.32509	46803	-7.0292e-08*((P/mu)*Dmax)-0.0017503*(sqrt(P2))-1.0645*(N*P/K)+0.44825*((1-P2/K)*D*N)+6.2308e-07*(P*(D^2)/mu)+2.2504	-100
5	0.99974	0.42651	5.32509	48905	-7.0292e-08*((P/mu))-0.0017503*(sqrt(P2))-1.0645*(N*P/K)+0.44825*((1-P2/K)*D*N)+6.2308e-07*(P*(D^2)/mu)+2.2504	-84
5	0.99974	0.42652	5.32509	50270	-6.9731e-08*(P2/mu)-0.0017503*(sqrt(P2))-1.0648*(N*P/K)+0.44826*((1-P2/K)*D*N)+6.2269e-07*(P*(D^2)/mu)+2.2502	-74
5	0.99974	0.42652	6.31527	26492	+0.44556*(N*D)-0.063668*((rho/P)*N^3)-0.0018828*(sqrt(P2))-1.1807*(N*P/K)+4.0121e-07*(P*(D^2)/mu)+2.8159	-175
5	0.99974	0.42654	4.04400	26207	+0.44571*(N*D)+0.00079122*(sqrt(P/(mu*N)))-0.0018633*(sqrt(P2))-1.2*(N*P/K)+3.8213e-07*(P*(D^2)/mu)+2.679	-187
5	0.99974	0.42669	5.35458	25701	+0.44555*(N*D)+1.3038e-08*(P2/mu)-0.0018526*(sqrt(P2))-1.2081*(N*P/K)+3.9882e-07*(P*(D^2)/mu)+2.7107	-210
5	0.99974	0.42669	5.35459	12072	+1.265e-08*(P/mu)+0.44554*(N*D)-0.0018527*(sqrt(P2))-1.2078*(N*P/K)+3.9919e-07*(P*(D^2)/mu)+2.7112	-608
5	0.99974	0.42669	5.35459	24322	+0.44554*(N*D)+1.265e-08*((P/mu)*Dmax)-0.0018527*(sqrt(P2))-1.2078*(N*P/K)+3.9919e-07*(P*(D^2)/mu)+2.7112	-281
5	0.99974	0.42669	5.35459	25337	+0.44554*(N*D)+1.265e-08*((P/mu))-0.0018527*(sqrt(P2))-1.2078*(N*P/K)+3.9919e-07*(P*(D^2)/mu)+2.7112	-236
4	0.99973	0.42671	3.47978	10487	-0.0017375*(sqrt(P2))-1.1091*(N*P/K)+0.44887*((1-P2/K)*D*N)+5.6001e-07*(P*(D^2)/mu)+2.1645	-759

The four-term model is physically interpreted as

$$Q = \beta_o + \beta_1 \omega V_i + \beta_2 \sqrt{p_2} + \beta_3 \frac{\omega \Delta p}{K} + \beta_4 \frac{\Delta p V_i^2}{\mu}. \tag{75}$$

Equation (75) includes a constant (β_0) and coefficients for theoretical displacement (β_1), turbulent flow losses (β_2), compressibility (β_3), and displacement angle squared (β_4). The displacement angle squared (ε^2) coefficient has a positive value and therefore is not a viscous flow loss term.

As shown in Figure 36, the four-term and five-term models yielded a linear agreement with measured pump flow rates. Figure 36 shows that the additional parameter had a minimal impact on the correlation with measured values. The maximum flow rate was approximately 100 lpm. The mean standard error (S) for both flow models was approximately 0.43 lpm, as shown in Table 5. Hence, the mean standard error was 0.43% of the maximum flow rate. Caution must be used when comparing the percent mean standard error (0.43%) and the combination of error values (0.59%), because the

mean standard error, S, is a global average, while $\partial\eta_V$ varies proportionally with the measured flow rate. Nonetheless, it can be concluded that the models describe the pump flow behavior at a level of precision commensurate with the measurement accuracy.

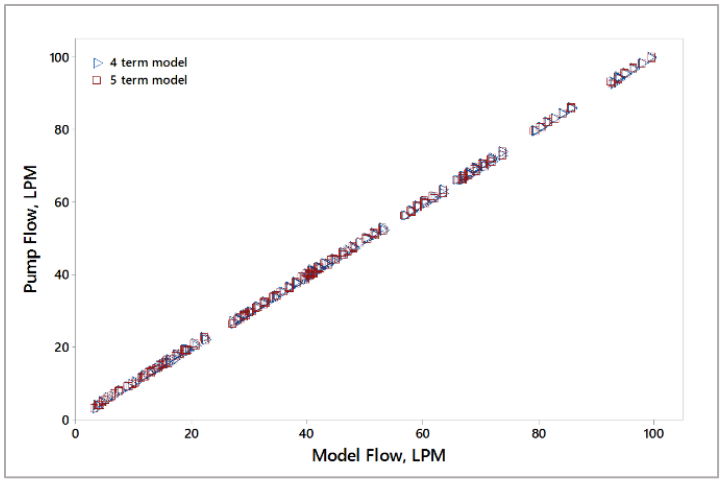

Figure 36: Comparison of the Four- and Five-Term Models.

6.1.2 Pump Torque Model

The approach that was taken to determine the pump flow model was also considered to obtain the pump torque model. Table 6 shows the three- and four-term torque models obtained from the MATLAB program and their mean standard error, R-squared, maximum VIF, and AIC values. The steady-state multiple regression torque T_p, a model for the axial piston pump, was developed based on these operating parameters using experimental data:

$$T_p = T_{const} + T_{visc} + T_{mech} + T_{stri}, \tag{76}$$

$$T_p = \beta_o + \beta_1 \mu N + \beta_2 V_i \frac{\Delta p}{2\pi} + \beta_3 \sqrt{\frac{\mu N}{\Delta p}}. \tag{77}$$

Here, torque loss, T_{mech}, results from mechanical friction proportional to operating pressure, T_{visc} is viscous friction, which is proportional to operating speed and viscosity

of fluid, T_{stri} is the fluid shearing and the mixed film friction, which is proportional to the Stribeck number (high-Reynolds number) coefficient, and T_{const} is the constant torque loss, mainly because of fixtures and sealing, and it is independent of operating conditions. In addition, β_0, β_1, β_2, and β_3 are all empirical constants.

Table 6: Pump Torque Models.

Number of Variables	Rsquared	StdError	MaxofVIF	count	Model	AIC
4	0.99933	1.19400	4.72418	219	-159824.5738*(rho*(Vth^5/3)(N^2)/(4*pi))+0.00010926*(rho*(N^2))+6.5376*(Vth*P/(2*pi))-150.9298*(sqrt(mu*N/P))+7.2982	-942.2186538
4	0.99932	1.20084	4.71693	229	-123699.694*(rho*(Vth^5/3)(N^2)/(4*pi))+3.1956e-06*(mu*(N^2))+6.5349*(Vth*P/(2*pi))-173.6634*(sqrt(mu*N/P))+7.6354	-911.0340372
4	0.99932	1.20101	6.36372	440	+26.5158*(mu*N*Vth)+0.0010043*(mu*N)+6.4565*(Vth*P/(2*pi))-261.0543*(sqrt(mu*N/P))+7.2496	-710.723922
4	0.99932	1.20309	6.34621	394	+26.8607*(mu*N*Vth)+9.943e-05*(rho*(N^2))+6.443*(Vth*P/(2*pi))-235.1545*(sqrt(mu*N/P))+9.1565	-762.4086146
4	0.99932	1.20354	6.35511	404	+26.6401*(mu*N*Vth)+2.9667e-06*(mu*(N^2))+6.4513*(Vth*P/(2*pi))-247.6633*(sqrt(mu*N/P))+9.2345	-735.7320648
4	0.99932	1.20375	4.69762	279	+0.0010609*(mu*N)-83611.6903*(rho*(Vth^5/3)(N^2)/(4*pi))+6.5272*(Vth*P/(2*pi))-198.0884*(sqrt(mu*N/P))+5.8171	-863.9208229
4	0.99932	1.20475	4.18329	217	-194768.397*(rho*(Vth^5/3)(N^2)/(4*pi))+0.00010655*(rho*(N^2))+6.5548*(Vth*P/(2*pi))-3141.7137*(mu*N/P)+5.6428	-953.1782435
4	0.99932	1.20475	4.18329	341	-3141.7137*(mu*N/P)-194768.397*(rho*(Vth^5/3)(N^2)/(4*pi))+0.00010655*(rho*(N^2))+6.5548*(Vth*P/(2*pi))+5.6428	-821.7766167
3	0.99931	1.20708	2.08975	101	+0.0010319*(mu*N)+6.4993*(Vth*P/(2*pi))-221.1382*(sqrt(mu*N/P))+6.4605	-1305.365738
4	0.99931	1.20842	3.47171	245	+0.0010522*(mu*N)+6.4963*(Vth*P/(2*pi))+17.3403*(Vth*(Po-20*Pi)/(1+(N/1.81)^2.35))-221.6541*(sqrt(mu*N/P))+6.3672	-882.1057726
3	0.99931	1.20935	1.88587	154	+0.00010218*(rho*(N^2))+6.486*(Vth*P/(2*pi))-193.9715*(sqrt(mu*N/P))+8.4097	-1085.347204
3	0.99931	1.20967	1.98321	137	+3.0486e-06*(mu*(N^2))+6.4942*(Vth*P/(2*pi))-207.1984*(sqrt(mu*N/P))+8.4963	-1134.388132
4	0.99931	1.21066	3.49846	180	+0.00010437*(rho*(N^2))+6.4825*(Vth*P/(2*pi))+18.7944*(Vth*(Po-20*Pi)/(1+(N/1.81)^2.35))-193.9726*(sqrt(mu*N/P))+8.3502	-1012.990937
4	0.99931	1.21109	3.26418	190	+3.0063e-06*(mu*(N^2))+6.4964*(Vth*P/(2*pi))-12.6091*(Vth*(Po-20*Pi)/(1+(N/1.81)^2.35))-207.0954*(sqrt(mu*N/P))+8.5355	-987.9827943
4	0.99930	1.21460	4.18375	346	-3600.7861*(mu*N/P)-163290.8265*(rho*(Vth^5/3)(N^2)/(4*pi))+3.0928e-06*(mu*(N^2))+6.5543*(Vth*P/(2*pi))+5.7387	-813.8555658
4	0.99930	1.21460	4.18375	227	-163290.8265*(rho*(Vth^5/3)(N^2)/(4*pi))+3.0928e-06*(mu*(N^2))+6.5543*(Vth*P/(2*pi))-3600.7861*(mu*N/P)+5.7387	-921.1611604
4	0.99929	1.22594	4.17292	373	-3984.8953*(mu*N/P)+0.0010097*(mu*N)-131845.8264*(rho*(Vth^5/3)(N^2)/(4*pi))+6.5513*(Vth*P/(2*pi))+3.7388	-798.4690534
4	0.99929	1.22594	4.17292	277	+0.0010097*(mu*N)-131845.8264*(rho*(Vth^5/3)(N^2)/(4*pi))+6.5513*(Vth*P/(2*pi))-3984.8953*(mu*N/P)+3.7388	-872.9099653
4	0.99929	1.22900	3.52044	311	-4320.0296*(mu*N/P)+0.00010382*(rho*(N^2))+6.482*(Vth*P/(2*pi))+63.2883*(Vth*(Po-20*Pi)/(1+(N/1.81)^2.35))+6.2782	-846.5267782

Hence, the model expressed in Equation (77) accurately reflects a broad range of operating speeds and pressures. A better empirical torque model can be obtained if the best subset regression analysis is combined with a nonlinear regression model, specifically for low speed, since the torque loss is not a linear function. Specifically modeling torque loss for hydraulic model, it is vital to consider nonlinear regression model because of the characteristic of torque loss at low speed.

6.2 Mathematical Modeling in MATLAB Simulink

The bulk modulus and viscosity models presented in this paper were previously validated experimentally but not the density model. Figure 37 presents the recorded density of the fluid at the pump inlet using a Coriolis flow meter and the density obtained through the presented density model. The model seems to exactly replicate the experimental data.

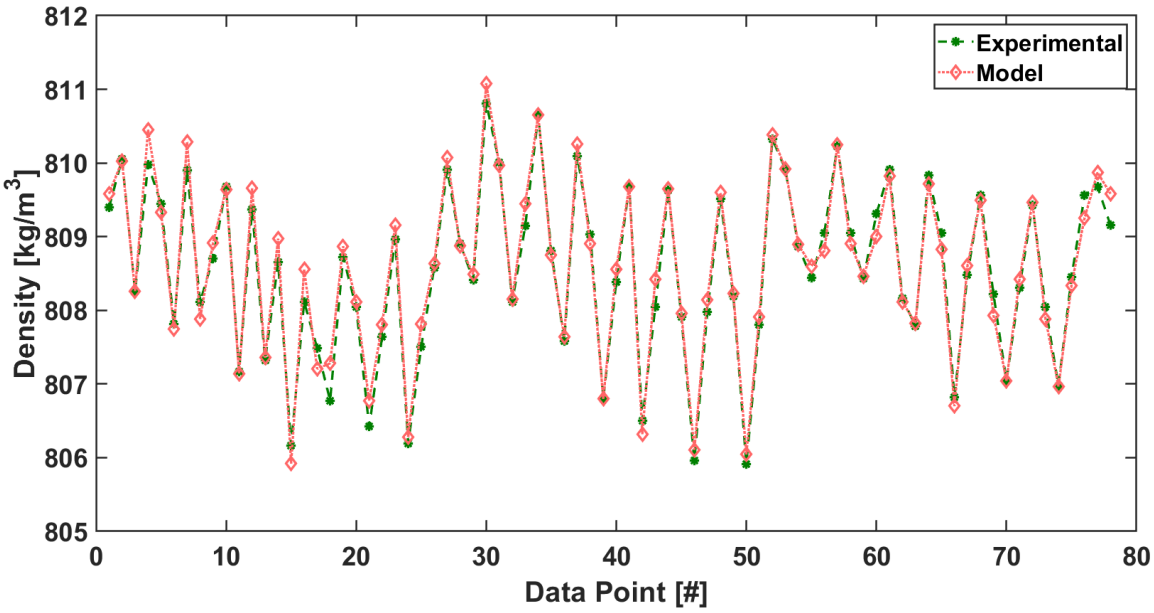

Figure 37: Density of the PP11D Fluid.

The statistical comparison of the density model was also made to quantify the error in the model. The linear regression model between modeled density and experimentally obtained density was conducted. The results of this analysis are shown in Table 7. The model has a coefficient of determination (R-squared) of 97.5% and a standard error of 0.189 kg/m^3. Hence, it can be concluded that the density model presented is quite accurate.

Table 7: Linear Regression Fit for Density.

```
mdl =
Linear regression model:
    y ~ 1 + x1

Estimated Coefficients:
                   Estimate       SE        tStat        pValue
                   ________    ________    ________    __________

    (Intercept)    -2.0564       14.778    -0.13915        0.8897
    x1              1.0026     0.018278      54.854    6.9976e-63


Number of observations: 78, Error degrees of freedom: 76
Root Mean Squared Error: 0.189
R-squared: 0.975,  Adjusted R-Squared 0.975
F-statistic vs. constant model: 3.01e+03, p-value = 7e-63
```

In the process of developing the integrated model, it was necessary to validate each submodel and to observe the behavior of the submodel. Figure 38 shows results from the pump kinematic model. Figure 38 shows the varying displacement, velocity, and acceleration of a single piston as a function of phase angle for maximum displacement and 13 rpm. From Figure 38, it can be stated that the piston has zero velocity at IDC and ODC, since the piston chance its direction of motion. Therefore, the piston has maximum acceleration at IDC and ODC. The sign and magnitude of the kinematics parameters depend on the chosen origin. As a result, the displacement of the piston is minimum at ODC and maximum at IDC. The displacement of the piston is always negative because the linear direction of motion was considered negative.

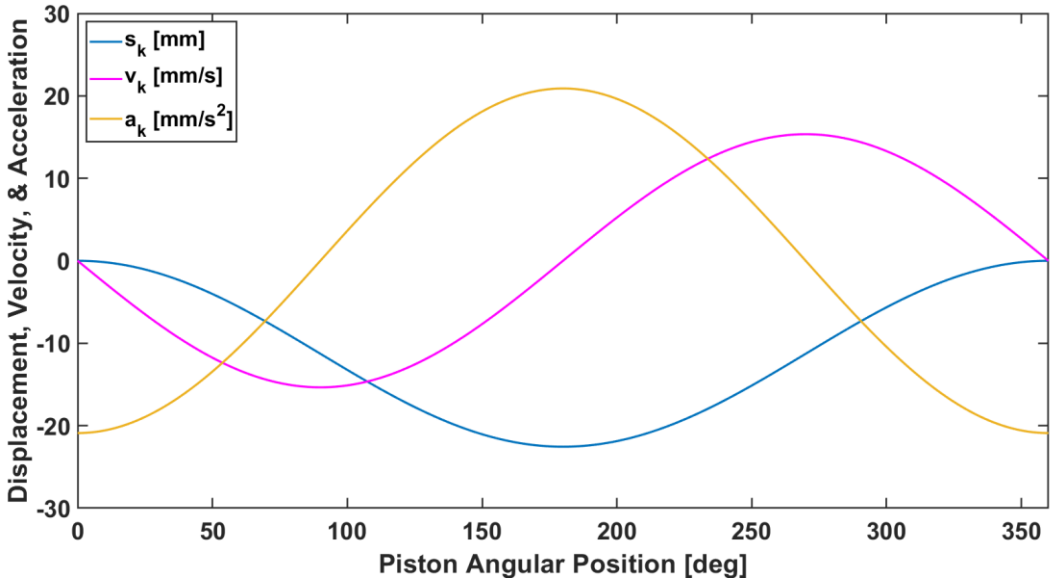

Figure 38: Pump Kinematics Parameters at Maximum Swash Plate Angle and 13 rpm.

Using the kinematic model, the ideal flow rate and ripple were plotted, which is shown in the Figure 39. The figure shows the discharge flow rate through nine pistons in a revolution and sum of these flow rates, which is defined as the ideal flow rate of the pump. The sinusoidal variation of the flow rate is known as the flow ripple. The flow ripple is undesirable in pumps because they cause enormous noise and vibration [38]. From the idealized results, it was observed that the pump design with an even number of pistons has higher flow ripple compared to the pump design with an odd number of pistons. Pump with an even number of pistons, sometimes features two pistons simultaneously located at IDC and ODC (i.e., neither displacing nor intaking fluid) , whereas this is not the case with a pump design consisting of an odd number of pistons.

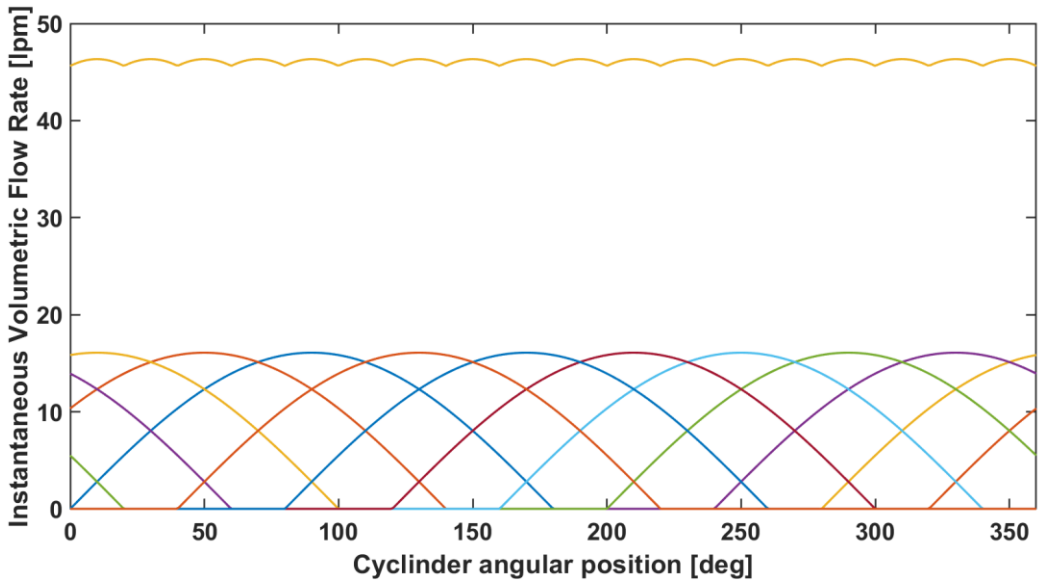

Figure 39: Theoretical Flow Ripple based on Kinematics.

The varying orifice areas of the high-pressure side (discharge side) and the low-pressure side (intake side) as a function of the phase angle are shown in Figure 40. These were plotted using the analytical formulas presented in this paper. The small opening of the valve plate to the kidney port just after ODC (0°) and IDC (180°) is due to the transition slot geometry. Then, the major slot linearly starts to open to the kidney part and at approximately 36°, the kidney port completely opens to the major slot. It stays opens and then linearly starts to close. The same process repeats for the suction side as a result of the symmetrical geometric of the valve plate.

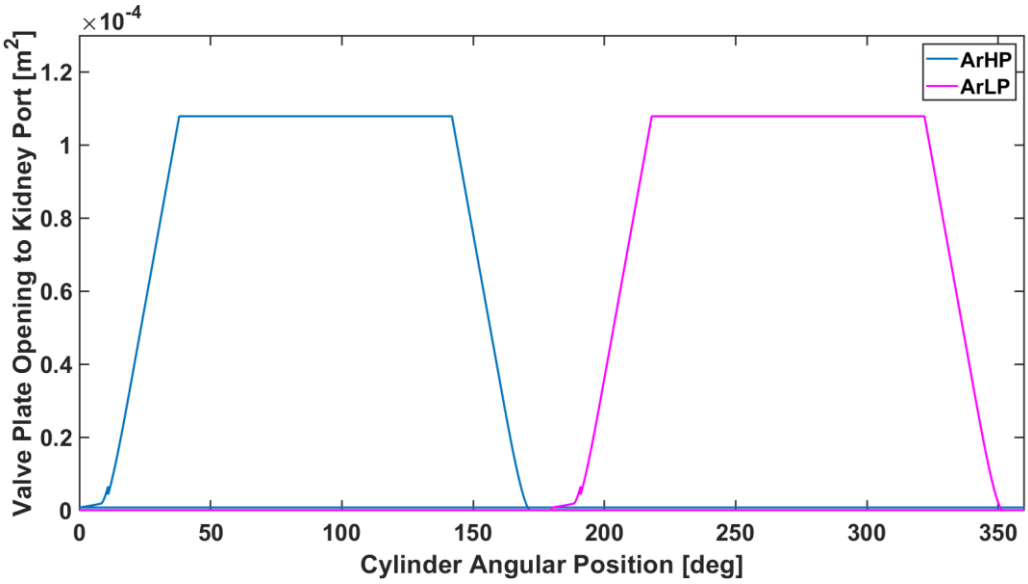

Figure 40: Instantaneous Discharge or Suction Area of the Valve Plate Opening.

Figure 41 shows pressure in a displacement chamber for a revolution of a time for the speed of 1000 rev/min, system pressure of 2000 psi, and maximum pump displacement. Figure 41 simultaneously shows the high-pressure side orifice area as a function of time. From the figure, it can be observed that the sudden spikes in pressure occur when the piston travels from the intake port to the discharge port or vice versa. When the piston moves from the discharge port to the intake port, a negative pressure spike of around 30 psi was observed, whereas when the piston moves from the intake port to the discharge port, a positive pressure spike was observed of around 78 psi. These spikes in the displacement chambers significantly depend on the geometry of the transition slot and on the operating parameters of the pump.

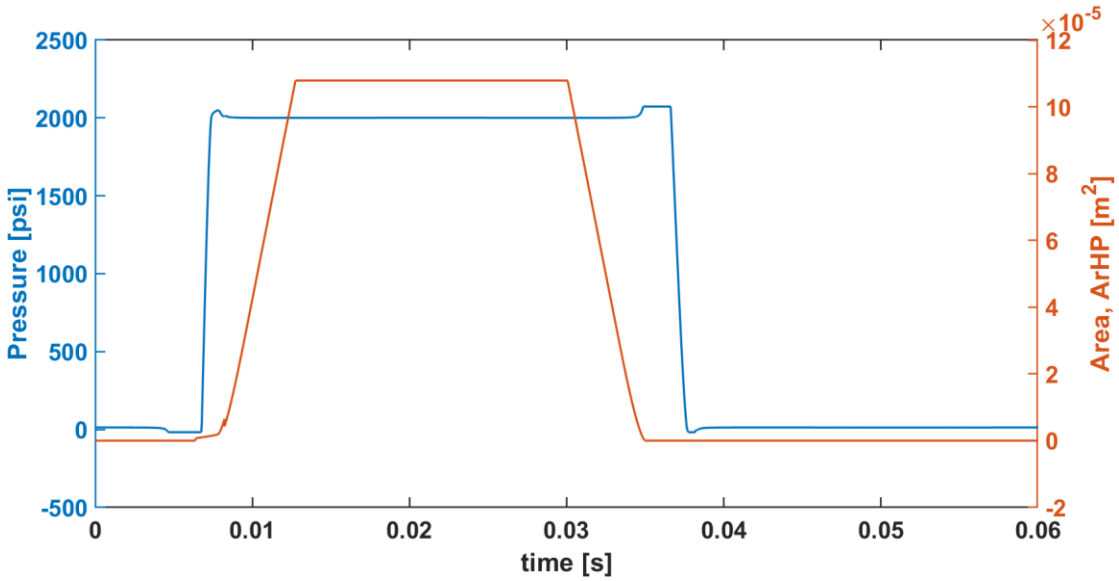

Figure 41: Displacement Chamber Pressure.

The instantaneous pump discharge flow was obtained by summing the flow rates of each of the nine pistons and it is shown in Figure 42. The flow ripple varies between 36.7 lpm and 44.3 lpm for the pump speed of 1000 rpm and displacement of 46.09 cc/rev, and a system pressure of 2000 psi. Figure 42 also shows the mean value of the modeled flow ripple and the mean pump discharge recorded experimentally. The difference in the pump discharge flow between the modeled flow and the recorded flow is about 3%. This difference in discharge flow is seen to decrease for higher pump speeds.

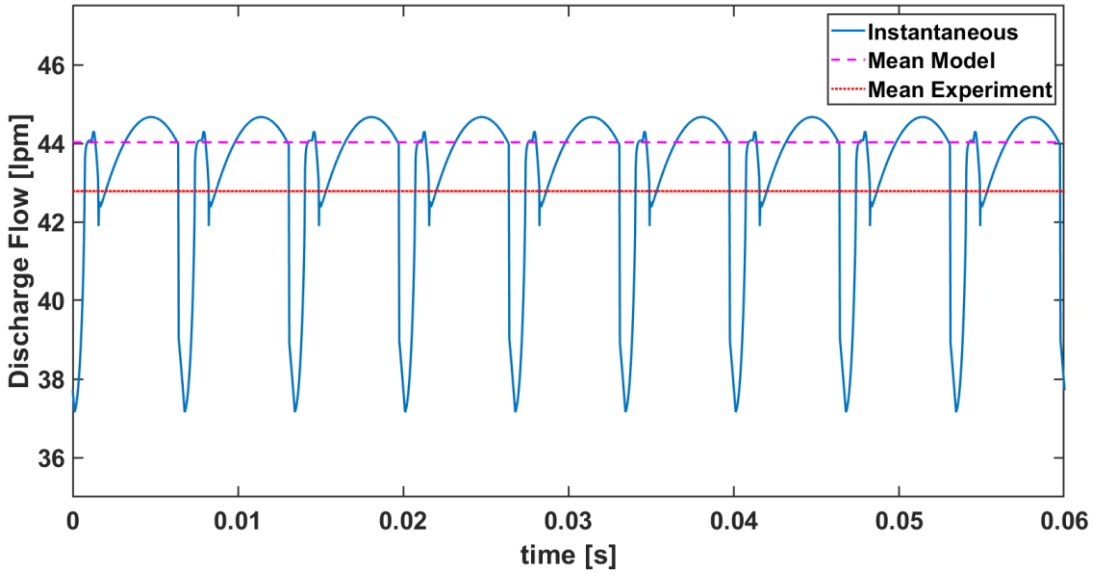

Figure 42: Pump Discharge Flow at 1000 rpm and 2000 psi for 100% Displacement.

Similarly, the leakage flow through each piston was summed to determine the overall pump leakage, which is shown in Figure 43. Figure 43 shows the instantaneous leakage of the pump through three lubricating paths in a revolution of the cylinder block. The mean value of leakage of the model is almost 50% lower than the recorded leakage flow of the pump. This result might be due to not considering other leakage paths, such as the leakage from the ball and socket joint between piston and slipper pad.

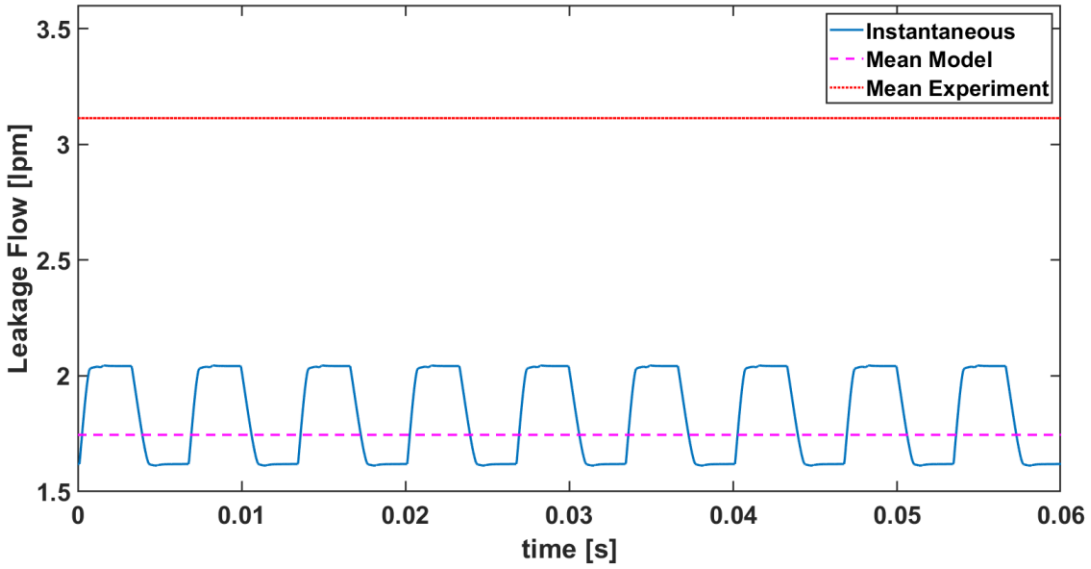

Figure 43: Pump Leakage Flow at 1000 rpm and 2000 psi for 100% Displacement.

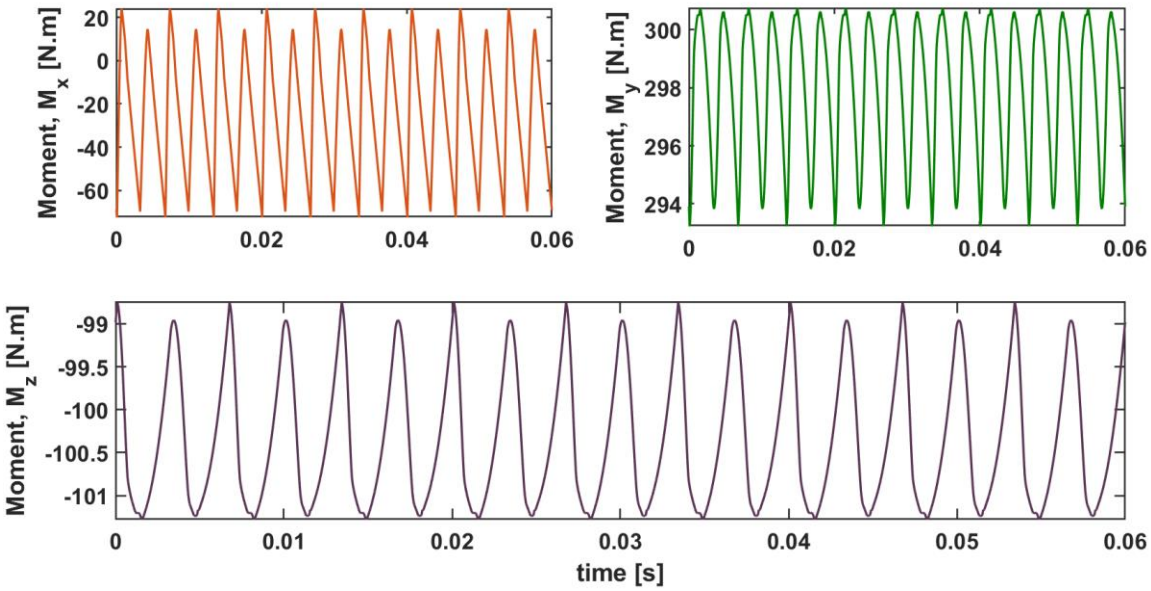

Figure 44: Moment on Swash Plate at 1000 rpm and 2000 psi for 100% Displacement.

Moment applied on the swash plate by the displacement chamber pressure force is shown in Figure 44. The moment on the swash plate about the *x*-axis is the moment that is compensated by the actuators to control the swash plate angle. The moment on the swash plate about the *z*-axis is the moment that is applied on the drive shaft of the pump.

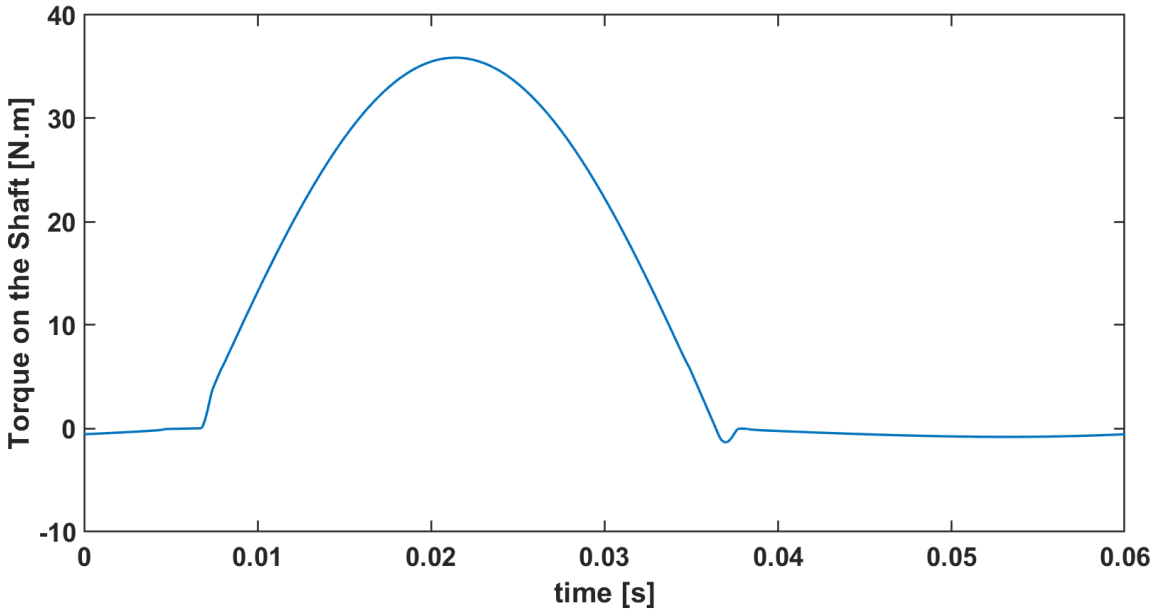

Figure 45: Torque by a Piston at 1000 rpm and 2000 psi for 100% Displacement.

Figure 45 shows the torque applied by a single piston on the drive shaft of the piston at rotational speed of 1000 rev/min and pump outlet pressure of 2000 psi for maximum displacement of the pump. The torque applied by a single piston increases as the piston moves from the ODC to the IDC and then decreases as the piston moves from the IDC to the ODC. This is due to the variation in the displacement chamber's pressure because the pressure force is the most significant force on the piston. By summing the torque applied simultaneously by all pistons, the overall torque on the drive shaft was determined, which is shown in Figure 46. It can be observed that the torque from the developed model is considerably different in compared to the experimental torque on the shaft. This result might be due to not accurately modeling the viscous friction between

the piston and cylinder and also not considering the churning losses. Also, the gap geometry has a significant impact on the viscous friction and its effects.

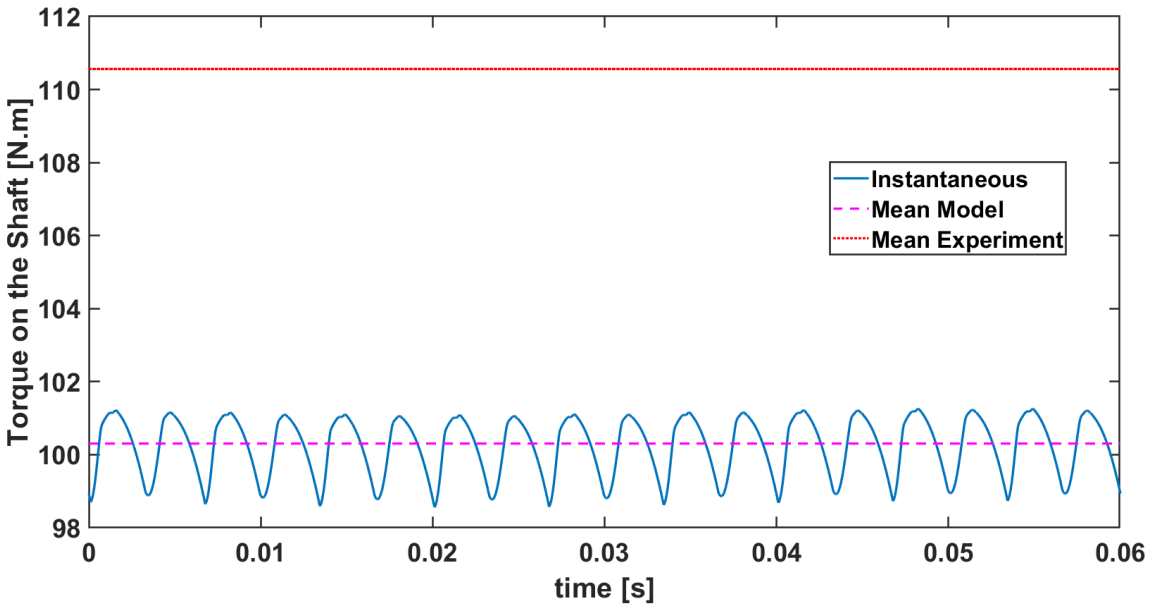

Figure 46: Torque on the Shaft at 1000 rpm and 2000 psi for 100% Displacement.

The mean discharge flow of the pump obtained experimentally and the mean discharge flow from the Simulink model are plotted for four-speed, six-pressure and maximum displacement, and are shown in Figure 47. Figure 47 indicates that the developed Simulink model very well replicates the actual pump discharge flow, especially at high speed and low pressure.

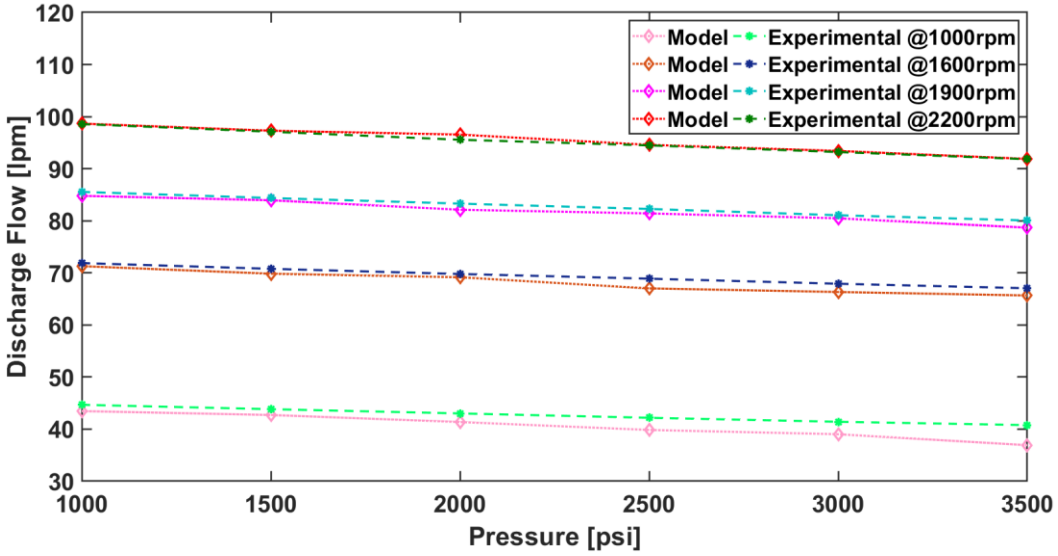

Figure 47: Steady State Discharge Flow for PP11D at 100% Displacement.

Figure 47 shows the results of discharge flow for PP11D. Since the flow model accurately replicated the actual discharge flow of the pump, the discharge flow was simulated for PP10D fluid to see if the model would work for other fluids, as shown in Figure 48.

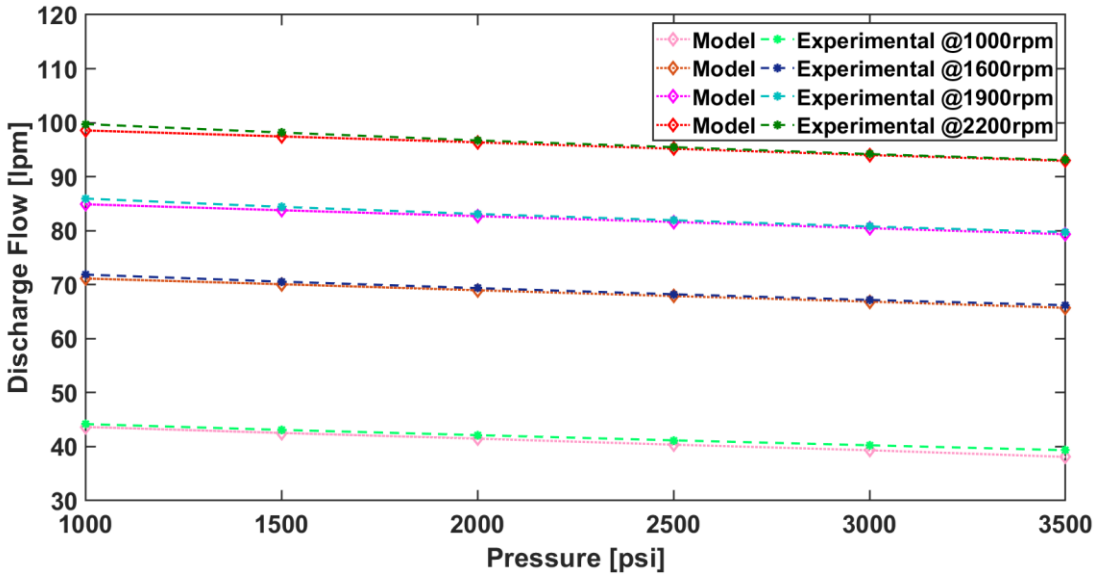

Figure 48: Steady State Discharge Flow for PP10D at 100% Displacement.

The predictions and measured pump output flow rate shows good agreement for both the PP10D and PP11D fluids. Examining at the torque model, it was concluded that the model could not predict the torque loss accurately because the viscous friction between the cylinder and the piston was not modeled precisely. Also, the churning losses need to be considered. To improve the accuracy of the torque model, it is necessary to develop a high-fidelity model for viscous friction and the variable gap geometry.

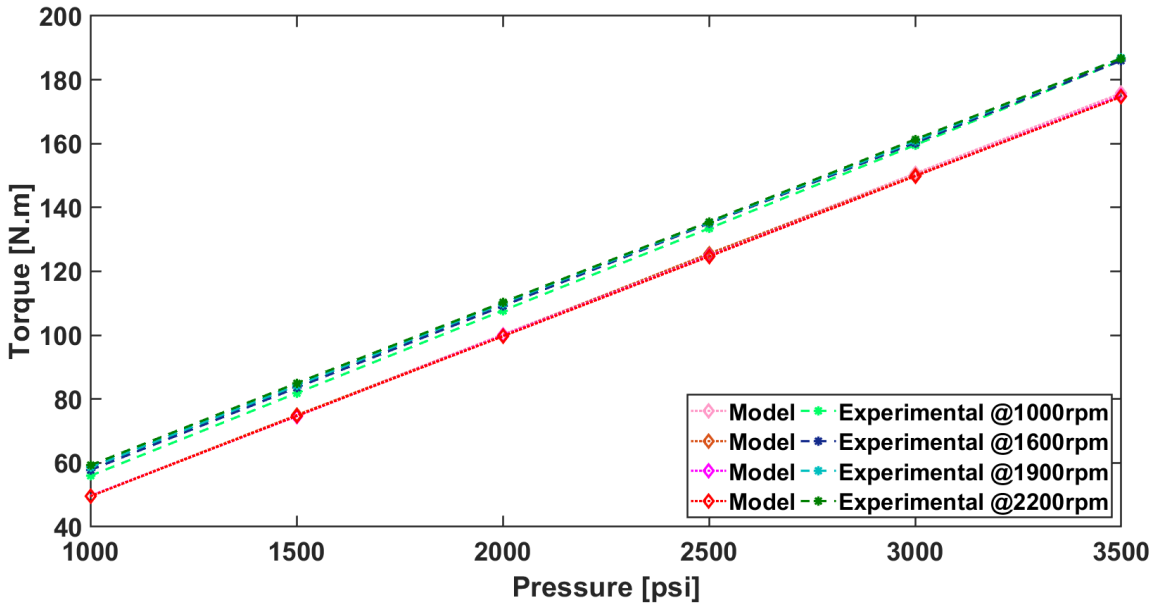

Figure 49: Steady State Shaft Torque at 100% Displacement.

Chapter 7: Summary

The goal of this project was to develop a steady-state input torque and output flow rate model of an axial piston swash plate pump that incorporates detailed model of the fluid properties that influence the efficiency of hydraulic machinery. The uniqueness of this project was the blending of fluid properties with the mechanical design of an axial piston pump. The academic significance of this project included the opportunity to greatly expand and enhance the author's knowledge of hydraulic pumps and their modeling. In addition, at present, the results obtained from the test rig at MSOE's Fluid Power Institute have been validated using an empirical model that was developed using regression analysis. If error is induced while conducting the experiment, the regression model would likely not be able to accurately predict an outcome, bit, in general, this Simulink model could be used to validate experimental results of any fluids for any axial piston pumps.

In the first phase, this project involved conducting research not just on the physical components, but also on the fluid properties that influence the efficiency of hydraulic machinery. An axial piston pump was taken apart to investigate and to acquire actual dimensions of each component of the pump for the purpose of creating a MATLAB Simulink model. After developing the pressure and temperature dependent bulk modulus, viscosity, and density model, empirical models for the axial piston swashplate pump flow and torque were developed using best subset regression analysis. These empirical models were developed by combining steady-state data based on the Latin Hypercube sampling design of experiment of multiple fluids. The project entailed the development and validation of a MATLAB Simulink model of the axial piston pump associated with the dynamometer with the goal of minimizing time efforts and costs for future tests. Empirical models based upon Latin Hypercube sampling design of experiment were shown to be very effective in predicting both discharge flow and torque input. MATLAB Simulink models which incorporated the fluid properties model were successful in predicting discharge flow and torque input. The torque input model was associated with a considerable error compared to the flow rate model since the viscous friction and the gap heights between tribological surfaces were approximated and

considered constant, respectively. A higher fidelity model for gap geometry and viscous friction would enhance the torque and flow models.

In the future, in order to improve the model developed in this project, it would be beneficial to accurately derive varying orifice area for the valve plate since the orifice area has major effect of the flow rates. This area consists of webs on the discharge side, which provide additional strength to the valve plate on the high-pressure side. The gap between parts moving relative to each other function as sliding bearings and fulfill a sealing function. Because of these functions, the gap geometry is not constant; it depends on the operating conditions such as speed, pressure, displacement, and fluid viscosity. It strongly influences the friction and volumetric flow losses [34]. Therefore, the varying gap height must be incorporated with the accurate viscous friction model, which would help in accurately predicting leakage flow and torque loss between tribological interference, including piston/cylinder, slipper/swash plate, and cylinder/valve plate. Elevated fluid temperature caused by energy dissipation occurs due to viscous friction between moving parts, which can significantly reduce the life of fluid by deteriorating it and can make a pump more susceptible to the wear. Moreover, it is vital to predict local changes in the viscosity due to change in the temperature of the fluid. The decrease in viscosity due to s rise in the temperature of fluid results in increases in leakage flow loss and decreases in load bearing capacity of fluid film [34]. Therefore, temperature cannot be neglected and must be modeled by including a thermal model so that exact leakage flow and torque loss can be predicted. These improvements would also help in clearly distinguishing fluids that differ in their physical and thermal properties. In addition, it is necessary to develop a dynamic model of the swash plate control to induce a fluctuating swash plate angle so that fluctuating displacement chamber pressure can be observed, and its effect on the volumetric flow and friction can also be recorded. The major goal for future research would be to proceed towards the development of a model that would not just be an aid in determining energy efficient hydraulic oil, but would also be capable of aiding in the comparison and evaluation of fluid additives that might result in higher efficiency.

References

[1] Ludema, Kenneth C. (1996). *Friction, Wear, Lubrication: A Textbook in Tribology*. CRC press.

[2] Love, L., Lanke, E., Alles, P. (2012). "Estimating the Impact (Energy, Emissions, and Economics) of the U.S. Fluid Power Industry," Oak Ridge National Laboratory: Report No.: ORNL/TM-2011/14.

[3] Burgess, K. (2014). *Modeling and Analysis of a Large-scale Hydraulic Dynamometer Using MATLAB® Simulink*. M.S. Milwaukee School of Engineering.

[4] Michael, Paul, Director of Reliability of Fluid Power Institute, Milwaukee School of Engineering. 15 September 2018. Conversation with the author, Milwaukee, WI.

[5] Michael, P. and Mettakadapa, S. (2016). "Bulk Modulus and Traction Effects in an Axial Piston Pump and a Radial Piston Motor," *Proceedings of the 10th International Fluid Power Conference,* March 8-10, Dresden, Germany, Vol. 2, 301-312.

[6] Garcia, JM. Johnson, J. and Michael P. (2015). "Toward the Development of a Pump Energy Rating System based upon Performance Indexes," *Proceedings of the Fluid Power Innovation Research Conference*, Chicago, IL.

[7] Khalil, M. (2016). *Introduction to Hydraulics for Industry Professionals*. Franksville, WI: CompuDraulic.

[8] Mandal, N., Saha, R., Mookherjee, S. and Sanyal, D. (2013). "Pressure Compensator Design for a Swash Plate Axial Piston Pump." *Journal of Dynamic Systems, Measurement, and Control*, 136(2), p.021001.

[9] Reese, I. (2018). *Fixed Variable Displacement Pumps | LunchBox Sessions*. [online] LunchBox Sessions. Available at: https://www.lunchboxsessions.com/materials/fixed-variable-displacement-pumps/fixed-variable-displacement-pumps-manual [Accessed 16 Nov. 2017].

[10] Zeiger, G. and Akers, A. (1985). "Torque on the Swashplate of an Axial Piston Pump." *Journal of Dynamic Systems, Measurement, and Control*, 107(3), p.220.

[11] International Organization for Standardization, "ISO 4409:2007(E) Hydraulic Fluid Power – Positive Displacement Pumps, Motors and Integral Transmissions – Methods of Testing and Presenting Basic Steady State Performance." Geneva.

[12] Manring, N. (2013). *Fluid Power Pumps and Motors*. New York: McGraw-Hill Education.

[13] Manring, N. (2016). “Mapping the Efficiency for a Hydrostatic Transmission.” *Journal of Dynamic Systems, Measurement, and Control*, 138(3), p.031004.

[14] Hibi, A. and Ichikawa, T. (1977). “Mathematical Model of the Torque Characteristics for Hydraulic Motors.” *Bulletin of JSME*, 20(143), pp.616-621.

[15] Ivantysn, J., and Ivantysynova, M. (2001). *Hydrostatic Pumps and Motor, Principles, Designs, Performance, Modeling, Analysis, Control and Testing.* New Delhi: Academic Books International.

[16] Jeong, H-S. (2007). “A Novel Performance Model Given by the Physical Dimensions of Hydraulic Axial Piston Motors: Model Derivation,” *Journal of Mechanical Science and Technology*, Vol. 21, No. 1, pp. 83-97.

[17] Johansen, P. (2014). *Tribodynamic Modeling of Digital Fluid Power Motors*. Ph.D. Aalborg University.

[18] Murrenhoff, H., Piepenstock, U. and Kohmäscher, T. (2008). “Analysing Losses in Hydrostatic Drives. “*Proceedings of the JFPS International Symposium on Fluid Power*, 2008(7-1), pp.103-108.

[19] Olsson, O. (1973). “Mathematical Efficiency Model,” Kompendium i Hydraulik, Institute of Technology, Linköping, Sweden.

[20] Rahmfeld, R. and Skirde, E. (2010). “Efficiency Measurement and Modeling - Essential for Optimizing Hydrostatic Systems”. *7th International Fluid Power Conference*, pp.1-14.

[21] Schlösser, W. (1961). “Mathematical Model for Displacement Pumps and Motors,” Hydraulic Power Transmission, April 1961, pp. 252-257 and 269 and May 1961, pp. 324-328.

[22] Wilson, W.E. (1950). *Positive Displacement Pumps and Fluid Motors*, Pitman Publishing, NY.

[23] Michael, P., Khalid, H., and Wanke, T. (2012), "An Investigation of External Gear Pump Efficiency and Stribeck Values," SAE Technical Paper 2012-01-2041, https://doi.org/10.4271/2012-01-2041.

[24] Michael, P. Cheekolu, M. Panwar, P. Devlin, M. Davidson, R., Johnson D. & A. Martini (2018) “Temporary and Permanent Viscosity Loss Correlated to Hydraulic System Performance,” *Tribology Transactions*, https://doi.org/10.1080/10402004.2018.1439210.

[25] Michael, P. Mettakadapa, S. and Shahahmadi, S. (2016), “An Adsorption Model for Hydraulic Motor Lubrication,” *ASME Journal of Tribology*, Vol. 138: pp 14503-1 to 14503-6.

[26] Bair, S. and Michael, P., 2010, “Modeling the Pressure and Temperature Dependence of Viscosity and Volume for Hydraulic Fluids,” *International Journal of Fluid Power*, 2, pp. 37-42.

[27] Bair, S., 2007. *High Pressure Rheology for Quantitative Elastohydrodynamics.* Tribology and Interface Engineering Series, Vol. 54. Elsevier.

[28] Manring N. (2005*). Hydraulic Control Systems*. New York: John Wiley and Sons.

[29] Mettakadapa, Shreya, Scott Bair, Shinji Aoki, Masahiro Kobessho, Laura Carter, Hideto Kamimura, and Paul W. Michael. (2015). "A Fluid Property Model for Piston Pump Case Drain and Pressure Compensator Flow Losses." In *ASME/BATH 2015 Symposium on Fluid Power and Motion Control*, pp. V001T01A009-V001T01A009. American Society of Mechanical Engineers.

[30] Stachowiak, G. and Batchelor, A. (2014). *Engineering Tribology*. 4th ed. Oxford: Butterworth-Heinemann.

[31] Seeton, C. (2006). Viscosity–Temperature Correlation for Liquids. *Tribology Letters*, 22(1), pp.67-78.

[32] Kim, T., Kalbfleisch, P., and Ivantysynova, M. (2014). The Effect of Cross Porting on Derived Displacement Volume. *International Journal of Fluid Power, 15*(2), pp.77-85.

[33] Guan, C., Jiao, Z., and He, S. (2014). Theoretical Study of Flow Ripple for an Aviation Axial-Piston Pump with Damping Holes in the Valve Plate. *Chinese Journal of Aeronautics*, *27*(1), pp.169-181.

[34] Wieczorek, U., and Ivatysynova, M. (2002). Computer Aided Optimization of Bearing and Sealing Gaps in Hydrostatic Machines - The Simulation Tool CASPAR. *International Journal of Fluid Power, 3*(1), pp.7-20.

[35] Manring, N. (1998). “The Torque on the Input Shaft of an Axial-Piston Swash-Plate Type Hydrostatic Pump.” *Journal of Dynamic Systems, Measurement, and Control*, 120(1), pp.57-62.

[36] Manring, N. (1999). “Friction Forces Within the Cylinder Bores of Swash-Plate Type Axial-Piston Pumps and Motors.” *Journal of Dynamic Systems, Measurement, and Control*, 121(3), pp.531-537.

[37] Toet, G. (1970). Die Bestimmung Des Theoretischen Hubvolumens Von Hydrostatischen Verdrängerpumpen und Motoren aus Volumetrischen Messungen. *Ölhydraulik und Pneumatik 14. Nr.* 5, pp.185-190.

[38] Manring, N. (2000). “The Discharge Flow Ripple of an Axial-Piston Swash-Plate Type Hydrostatic Pump.” *Journal of Dynamic Systems, Measurement, and Control*, 122(2), pp.263-268.

[39] Ulbrich, N. (2009). “Regression Model Optimization for Analysis of Experimental Data”. *Proceedings of the 47th AIAA Aerospace Science Meeting and Exhibition*, AIAA 2009-1344, Orlando, FL.

APPENDIX

Appendix A: MATLAB Function to Determine Fluid Properties Model

```
function [FldPro] = FldPropModel(Fld,T,p)
    % [FldPro] = FldPropModel(Fld,T,p)
    %
    % DESCRIPTION
    % This function to calculate Density, Bulk modulus, and viscosity of
    % the fluid at any instance.
    %
    % REQUIRED ARGUMENTS
    % T         : Temperature of the fluid at any instance [C]
    % p         : Pressure of the fluid at any instance [Pa]
    % Fld       : Fluid properties parameters of a specified fluid. This is
    %             in a structure format and contains the following parameters:
        % K0dash    : Pressure rate of change of isothermal bulk modulus at p = 0 [-]
        % K00       : K0 at zero absolute temperature [Pa]
        % BK        : Temperature coefficient of K0 {1/K]
        % av        : Thermal expansivity defined for volume linear with temperature
[1/C]
        % gamma     : Thermodynamic interaction parameter [-]
        % mu_inf    : Viscosity extrapolated to infinite temperature [Pa.S]
        % phi_inf   : scaling parameter for unbounded viscosity [-]
        % BF        : fragility parameter [-]
        % pR        : Reference pressure [Pa]
        % TR        : Reference temperature [C]
        % v40C      : Measured kinematic viscosity of the fluid at 40C [cSt]
        % v100C     : Measured kinematic viscosity of the fluid at 100C [cSt]
        % APIGravity: Inverse measure of a petroleum liquid's density relative to
        %             that of water (specific gravity) [-]
        % entAir    : Fraction of entrained air [Vair/Vfld]
    %
    % OPTIONAL ARGUMENTS
    % No optional argument.
    %
    % OUTPUT VARIABLES
    % K         : Bulk modulus of the fluid [Pa]
    % rho       : Density of the fluid [kg/m^3]
    % cp        : Specific heat of the fluid [J/kg.K]
    % k         : Thermal Conductivity of the fluid [W/m.K]
    % nu        : Kinematic viscosity of the fluid [m^2/s]
    % mu        : Dynamic viscosity of the fluid [Pa.s].
    %
    % REQUIRED FUNCTIONS (USER-DEFINED)
    % No required function

    %{
    Created      : 08/07/2018, Pawan Panwar, MSOE
    Last Modified: 10/19/2018, Pawan Panwar, MSOE
```

```
    CHANGE LOG
    ===============   10/19/2018   ===============
    -Formated as per the Guidelines.
    -Removed constant parameters from required argument.
    ================================================

    ===============   08/07/2018   ===============
    -Initial release.
    ================================================
    %}

% Calculation
% Bulk Modulus using the temperature modified Tait equation
K0 = Fld.K00*exp(-Fld.BK*convtemp(T,'C','K'));      % Isothermal bulk modulus K at p = 0
Pa [Pa]
Fld.K = ((1-(1/(1+Fld.K0dash))*log(1+p.*(1+Fld.K0dash)./K0)).*(K0+p*(1+Fld.K0dash))); %
Bulk modulus K at any p & T [Pa]
FldPro.Keff = Fld.K.*(1+Fld.entAir )./(1+((Fld.pR./p).*Fld.entAir.*Fld.K./p));   %
Considered entrapped air in the fluid [Pa]

% Density using the equation from Dr. Monika's Book
Fld.SG = (141.5/(Fld.APIGravity+131.5))+(60-convtemp(Fld.TR,'C','F'))*4E-4;% Specific
gravity at temperature T [-]
FldPro.rho = Fld.SG*(1+((p-Fld.pR)./Fld.K)-Fld.av*(T-Fld.TR))*1000;         % Density of
fluid [kg/m^3]

% Specific heat and Thermal Conductivity
SG1 = 141.5/(Fld.APIGravity+131.5);                    % Specific gravity at 15.6C or 60F
[-]
FldPro.cp = (1/sqrt(SG1))*(1.63+0.0034*T)*1000;        % Specific heat [J/kg.K]
FldPro.k = (0.12/SG1)*(1-T*1.667E-4);                  % Thermal Conductivity [W/m.K]

% Kinematic Viscosity using Walther's Equation
A = (log10(log10(Fld.v100C+0.7))-
(log10(log10(Fld.v40C+0.7))))/(log10((40+273.15)/(100+273.15)));
B = log10(log10(Fld.v100C+0.7)) + A*log10(100+273.15);
FldPro.nu = (10.^(10.^(B-A*log10(T+273.15)))-0.7)*1E-6;  % Kinematic viscosity [m^2/s]

% Dynamic Viscosity
if p<=150E6           % If pressure p<=150 MPa (Walther's equation) - Hydrodynamic Regime
    FldPro.mu = FldPro.nu.*FldPro.rho;                  % Dynamic viscosity [Pa.S]

else p>150E6        % At pressure p>150 MPa - Elastrohydrodynamic Regime
    %  Relative volume V0/VR using Murnaghan equation [-]
    VbyVR = (1+Fld.av*(T-Fld.TR)).*(1-(1/(1+Fld.K0dash)).*log(1+p*(1+Fld.K0dash)/K0))
    phi = (convtemp(T,'C','K')/convtemp(Fld.TR,'C','K'))*VbyVR^Fld.gamma;
    FldPro.mu = Fld.mu_inf*exp(Fld.BF*Fld.phi_inf/(phi-Fld.phi_inf));% Dynamic viscosity
[Pa.S]
end

end
```

Appendix B: MATLAB Function to Acquire Parameters of the Fluids

```
function [FldPar,Fld] = FluidParameters(FluidNum)
    % [FldPar,Fld] = FluidParameters(FluidNum)
    %
    % DESCRIPTION
    % Returns fixed parameters of all the fluids and of a specified fluid
    %
    % REQUIRED ARGUMENTS
    % FluidNum : Numerical value 1, 2, 3, 4, or 5 respectively for fluids
    %            GRP1, HVI, TMP, PAO, or PAG
    %
    % OPTIONAL ARGUMENTS
    % No optional argument.
    %
    % OUTPUT VARIABLES (in structure format)
    % FldPar   : Fluid properties parameters of all the fluids
    % Fld      : Fluid properties parameters of a specified fluid
    %
    % REQUIRED FUNCTIONS (USER-DEFINED)
    % No required function

    %{
    Created      : 08/07/2018, Pawan Panwar, MSOE
    Last Modified: 10/19/2018, Pawan Panwar, MSOE

    CHANGE LOG
    ===============   10/19/2018   ===============
    -Formated as per the Guidelines.
    ================================================

    ===============   08/07/2018   ===============
    -Initial release.
    ================================================
    %}

% Fluid Properties parameters (FldPar) respectively for fluids PP10D, PP11D, PP12D, and
PP13D
% Parameters for Bulk modulus and Relative volume calculations
FldPar.K0dash = [11.331 10.427 10.823 11.331]; % Pressure rate of change of isothermal
bulk modulus at p = 0 [-]
FldPar.K00 = [8.898 8.032 8.718 8.898]*1E9;    % K0 at zero absolute temperature [Pa]
FldPar.BK = [5.744 5.716 5.808 5.744]*1E-3;    % Temperature coefficient of K0 {1/K]
FldPar.av = [6.345 7.221 6.400 6.217]*1E-4;    % Thermal expansivity defined for volume
linear with temperature [1/K]

% Parameters for dynamic viscosity calculation using Tait Equation
FldPar.gamma = [3.528 3.403 3.751 3.528];      % thermodynamic interaction parameter [-]
FldPar.mu_inf = [1.452 1.143 3.108 1.452]*1E-4;% Viscosity extrapolated to infinite
temperature [Pa.S]
FldPar.phi_inf = [0.3595 0.2429 0.2820 0.3595];% scaling parameter for unbounded
viscosity [-]
```

```
FldPar.BF = [11.882 17.521 16.760 11.882];     % fragility parameter [-]

% Parameters for kinematic viscosity calculation using Walther Equation
FldPar.v40C = [41.8 43.37 45.6 112.7];         % Measured kinematic viscosity of the
fluid at 40C [cSt]
FldPar.v100C = [7.24 7.53 8.45 15.14];          % Measured kinematic viscosity of the
fluid at 100C [cSt]
FldPar.APIGravity = [31.7 39 34.2 30.7];        % Inverse measure of a petroleum liquid's
density relative to
                                              % that of water (specific gravity) [-]

% Selecting parameters of the specified fluid for the analysis
if FluidNum == 1
    Fld.K0dash = FldPar.K0dash(1); Fld.K00 = FldPar.K00(1); Fld.BK = FldPar.BK(1); Fld.av
= FldPar.av(1);
    Fld.gamma = FldPar.gamma(1); Fld.mu_inf = FldPar.mu_inf(1); Fld.phi_inf =
FldPar.phi_inf(1); Fld.BF = FldPar.BF(1);
    Fld.v40C = FldPar.v40C(1); Fld.v100C = FldPar.v100C(1); Fld.APIGravity =
FldPar.APIGravity(1);
elseif FluidNum == 2
    Fld.K0dash = FldPar.K0dash(2); Fld.K00 = FldPar.K00(2); Fld.BK = FldPar.BK(2); Fld.av
= FldPar.av(2);
    Fld.gamma = FldPar.gamma(2); Fld.mu_inf = FldPar.mu_inf(2); Fld.phi_inf =
FldPar.phi_inf(2); Fld.BF = FldPar.BF(2);
    Fld.v40C = FldPar.v40C(2); Fld.v100C = FldPar.v100C(2); Fld.APIGravity =
FldPar.APIGravity(2);
elseif FluidNum == 3
    Fld.K0dash = FldPar.K0dash(3); Fld.K00 = FldPar.K00(3); Fld.BK = FldPar.BK(3); Fld.av
= FldPar.av(3);
    Fld.gamma = FldPar.gamma(3); Fld.mu_inf = FldPar.mu_inf(3); Fld.phi_inf =
FldPar.phi_inf(3); Fld.BF = FldPar.BF(3);
    Fld.v40C = FldPar.v40C(3); Fld.v100C = FldPar.v100C(3); Fld.APIGravity =
FldPar.APIGravity(3);
elseif FluidNum == 4
    Fld.K0dash = FldPar.K0dash(4); Fld.K00 = FldPar.K00(4); Fld.BK = FldPar.BK(4); Fld.av
= FldPar.av(4);
    Fld.gamma = FldPar.gamma(4); Fld.mu_inf = FldPar.mu_inf(4); Fld.phi_inf =
FldPar.phi_inf(4); Fld.BF = FldPar.BF(4);
    Fld.v40C = FldPar.v40C(4); Fld.v100C = FldPar.v100C(4); Fld.APIGravity =
FldPar.APIGravity(4);
end

% Reference conditions
Fld.TR = 20;                                  % Reference temperature [C]
Fld.pR = 0;                                   % Reference pressure [Pa]
Fld.entAir = .005;                            % Fraction of entrained air [Vair/Vfld]

end
```

Appendix C: MATLAB Function to Determine Theoretical Flow Ripple

```
function [TheoFlow] = TheoreticalFlowModel(OP,SM,PC)
% Instantaneous flow rate of each pistons [m^3/s]
for j = 1:length(SM.phi)
    for i = 1:PC.z
        % Determining the angular position of each piston [rad]
        theta(j,i) = SM.phi(j)+(i-1)*PC.Dphi;
        if theta(j,i)>2*pi
            theta(j,i) = theta(j,i)-2*pi;
        end

        % Checking wheather the piston in discharge stroke or in suction stroke
        if theta(j,i)>0 & theta(j,i)<=pi
            % Theoretical flow ripple [lpm]
            TheoFlow.Qth(j,i) = 2*pi*OP.N*PC.Ak*PC.R*tan(OP.beta)*sin(theta(j,i))*1E3;
        else
            TheoFlow.Qth(j,i) = 0;
        end
    end
end

% To calculate overall instantaneous flow rate of the pump [lpm]
for j = 1:length(SM.phi)
    TheoFlow.Qtha(j,1) = sum(TheoFlow.Qth(j,:));
end

TheoFlow.Qamin = min(TheoFlow.Qtha);
TheoFlow.Qami = mean(TheoFlow.Qtha);
TheoFlow.Qamax = max(TheoFlow.Qtha);

if mod(PC.z,2) == 0
    TheoFlow.phiM = pi/PC.z;
else
    TheoFlow.phiM = pi/(2*PC.z);
end
TheoFlow.DQ = TheoFlow.phiM*tan(TheoFlow.phiM/2);
end
```

Appendix D: MATLAB Function for TOET Method

```
function [ExpVgmax] = ToetMethod()

% Description: This program give the actual maximum geometric displacement of the
% variable displacement machine. It employs Toet method proposed by Jason Nicholson and
% Jose M. Garcia- Bravo in revised ISO 8624 and ISO 4409

% Import the experimental data
[~, ~, raw, dates] = xlsread('C:\Users\panwarp\Google Drive\2. MS Engineering\GE 796-98
Capstone Project\Experiment Data\Final
Data\20170919_PP12D_Orthog_LowPSI.xlsx','LowPSI_Run1234','A2:V81','',@convertSpreadsheetE
xcelDates);
stringVectors = string(raw(:,2));
stringVectors(ismissing(stringVectors)) = '';
raw = raw(:,[3,4,5,6,7,8,9,10,11,12,13,14,15,16,17,18,19,20,21,22]);
dates = dates(:,1);

% Create output variable
data = reshape([raw{:}],size(raw));

% Analysis
displmentProxy = data(:,18);          % Fraction of dispalcement or swash plate angle [-]
N = data(:,4);                        % Pump input speed [rpm]
Dp = data(:,12)-(data(:,13)+14.7);    % Pressure drop across pump [psi]
Qd = data(:,7);                       % Pump discharge flow (output flow) [gpm]

% Clear temporary variables
clearvars data raw dates stringVectors;

% 1st Step of Toet Method: Speed versus Output flow
pressurelevelResolution = 100; % psi
DpLevels = unique(round(Dp/pressurelevelResolution)*pressurelevelResolution);
DISPLACEMENT_LEVEL = 1;

% Creating zero vectors to store values during analysis
displacement = zeros(length(DpLevels),1);
intercept = zeros(length(DpLevels),1);
pressureAverage = zeros(length(DpLevels),1);
pressureStandardDeviation = zeros(length(DpLevels),1);

% loop over the pressure levels and calculate the displacement for each
% pressure level.
figure1 = figure('Color',[1 1 1]); % Create figure
axes1 = axes('Parent',figure1,'Position',[0.130520833333333 0.149123633359333 0.775
0.798176836124235]);
hold(axes1,'on');
for i = 1:length(DpLevels)

    % Find points near the current pressure level
    pressureLevelCurrent = DpLevels(i);
    index = abs(Dp - pressureLevelCurrent) < pressurelevelResolution/2 & displmentProxy
```

```
== DISPLACEMENT_LEVEL;

    % calculate the average pressure and stardard deviation
    pressureAverage(i) = mean(Dp(index));
    pressureStandardDeviation(i) = std(Dp(index));

    % linear fit of speed vs. flow
    coefficients = [ones(sum(index),1) N(index)]\Qd(index);
    displacement(i) = coefficients(2);
    intercept(i) = coefficients(1);

    % Plot the points and the linear fit
    h= plot(N(index), 3.785411784*Qd(index),'x','DisplayName', sprintf('\\Deltap =
%g[psi]', pressureLevelCurrent));
    hold all;
    x = [min(N(index)); max(N(index))];
    y = 3.785411784*(x*displacement(i) + intercept(i));
    plot(x,y, 'Color', h.Color, 'DisplayName', sprintf('Linear Fit \\Deltap = %g[psi]',
pressureLevelCurrent),'LineWidth',2,'Parent',axes1)
end
xlabel('Pump Speed [rpm]','FontWeight','bold')
ylabel('Pump Discharge Flow [lpm]','FontWeight','bold')
set(axes1,'FontSize',22,'FontWeight','bold','LineWidth',1.5);
box(axes1,'on'); grid(axes1,'off');
legend('show','Location','southeast')

% 2nd Step of Toet Method: Differential pressure versus Displacement

% Linear fit of Differential pressure versus Displacement
coefficients = [ones(length(DpLevels),1) pressureAverage]\displacement;

% Theoretical displacement is the intercept
Vth = coefficients(1);                      % Theoretical displacement [gal/rev]
displacementDdp = coefficients(2);
ExpVgmax = coefficients(1)*3785.411784;     % Theoretical displacement [cc/rev]

% Show the plot of the points vs the vit
figure2 = figure('Color',[1 1 1]); % Create figure
axes2 = axes('Parent',figure2,'Position',[0.130520833333333 0.149123633359333 0.775
0.798176836124235]); hold(axes2,'on');

plot2 = plot(pressureAverage, displacement*3785.411784,'x','DisplayName', 'Displacement
Points','LineWidth',2,'Parent',axes2); xlimits = xlim();
x = [0 xlimits(2)];
y = (Vth+displacementDdp*x)*3785.411784; hold all;
plot2 = plot(x, y, 'DisplayName', 'Linear Fit','LineWidth',2,'Parent',axes2); grid on;
xlabel('Differential Pressure, \Deltap [psi]','FontWeight','bold')
ylabel('Displacement [cm^3/rev]','FontWeight','bold')
set(axes2,'FontSize',22,'FontWeight','bold','LineWidth',1.5);
box(axes2,'on'); grid(axes2,'off');
legend('show','Location','northeast')
```

Appendix E: MATLAB Script for Empirical Model of Flow and Torque

```
clear all; clc; close all; format shortG
% DESCRIPTION
% This is the main program which will call the program and sub program to
% conduct best subset and multiple linear regression analysis to determine
% best empirical flow and torque models for the pump in the Test Cell 2
% of a specified number of terms and other criteria.
%
% REQUIRED ARGUMENTS
% It required the excel worksheet that contains experimental data from
% the Test Cell 2 of the pump.
%
% OPTIONAL ARGUMENTS
% No optional argument.
%
% OUTPUT VARIABLES
% It will generate an excel worksheet to paste generated empirical
% models and their stats to give user to choose best model from them.
%
% REQUIRED FUNCTIONS (USER-DEFINED)
% FluidParameters.m
% FldPropModel.m
% BestSubsetReg.m

%{
    Created      : 08/07/2018, Pawan Panwar, MSOE
    Last Modified: 08/25/2018, Pawan Panwar, MSOE

    CHANGE LOG
    ===============   08/25/2018   ===============
    -Formated as per the Guidelines.
    ================================================

    ===============   08/07/2018   ===============
    -Initial release.
    ================================================
%}

% INITIALIZATION
% Read excel worksheet 20170809_Shell_Combo_Orthog_Run1234.xlsx to import
% experimental data
num = xlsread('20170809_Shell_Combo_Orthog_Run1234.xlsx');

% Allocate columns to corresponding variables and converting these
% variables into proper SI units for further analysis
N = convangvel(num(:,3),'rpm','rad/s');     % Pump speed [rad/s]
Q = 3.78541*num(:,6);                       % Pump outlet flow [l/min]
Pi = convpres(num(:,12),'psi','pa');        % Pump inlet pressure [pa]
Po = convpres(num(:,11),'psi','pa');        % Pump outlet pressure [pa]
Tin = convtemp(num(:,14),'F','K');          % Temperature of fluid at pump inlet [F]
P = Po-Pi;                                  % Differential pressure [pa]
```

```
Dmax = 45;                                  % Geometric displacement of the pump [cc/rev]
Bmax = 18.4;                                % Max swashplate angle [deg]
z = 9;                                      % Number of reciprocating pistons [#]
Ap = (pi/4)*(11.45E-03)^2;                  % Area of a piston [m^2]
r = (67E-03)/2;                             % Radius of pitch circle [m]
B = num(:,17)*Bmax;                         % Swashplate angle [deg]
D = z*Ap*r.*tand(B)/pi;                     % Actual pump displacement (m^3/rad)
Tpth = P.*D;                                % Theoretical pump torque [N-m]
Tp = convlength(num(:,4),'ft','in')*0.112985;% Actual pump torque [N-m]

% DETERMINE FLUID PROPERTIES AS A FUNCTION OF TEMPERATURE AND PRESSURE
% Operating parameters
FluidNum = 2; % Type 1, 2, 3, or 4 respectively for fluids PP10D, PP11D, PP12D, or PP13D

% Get all the fixed parameters of the fluids
[FldPar,Fld] = FluidParameters(FluidNum);

% Call FluidPropModel() function to determine fluid properties
[FldPro] = FldPropModel(Fld,convtemp(Tin,'K','C'),P);

% Constant Parameters for XTO10 fluid
rho = FldPro.rho;                           % Density of the fluid [kg/m^3]
nu = FldPro.nu;                             % Kinematic viscosity of the fluid [m^2/s]
mu = FldPro.mu;                             % Dynamic viscosity of the fluid [Pa.s]
Keff = FldPro.Keff;                         % Effective bulk modulus of the fluid [Pa]

% DEFINE ALL REGRESSION TERMS FROM TABLE 1
% Term for flow model
Q1 = P./mu; Q2 = N.*D; Q3 = N.^2;

% Pressure driven laminar flow loss
Q4 = D.*(P./(2*pi.*mu)); Q6 = (P./mu)*max(D); Q7 = P./(mu.*N);
Q8 = Q1; % Same as Q1
Q9 = Po./(mu);

% Pressure driven turbulent flow loss
Q10 = (D.^(2/3)).*sqrt(2*P./rho);
Q11 = sqrt(P./(mu.*N));
Q12 = sqrt(P./(rho));
Q13 = rho.*((N.^3)./P);
Q14 = sqrt(Po);

% Compressibility terms
Q15 = D.*P./Keff; Q16 = P.*N.*D; Q17 = P.*N.*D./Keff;
Q18 = N.*P./Keff; Q19 = (1-Po./Keff).*D.*N; Q20 = N;
Q21 = P; Q22 = P.*D./mu; Q23 = P.*(D.^2)./mu;


% Terms for torque model
% Viscous friction
T1 = mu.*N.*D;
T2 = mu.*N./P;
T3 = mu.*N;
```

```
% Turbulent friction
T4 = rho.*(D.^(5/3)).*(N.^2)./(4*pi);
T5 = mu.*(N.^2);
T6 = rho.*(N.^2);

% Coulomb or boundary friction
T7 = D.*P./(2*pi);
T8 = D.*(Po-20.*Pi)./(1+(N./1.81).^2.35);
T9 = sqrt(mu.*N./P);
T10 = P.^2;
T11 = mu.*N./P;
T12 = Tpth;        % Ideal torque [N-m]

% MODEL GENERATION
% Ask user to generate model for either flow or Torue
l = input('Enter 1 for flow model or 2 for torque model = ');

if l == 1 % If user want to generate flow models
    % Define n x m matrix containing m independent variables or flow model terms of size
n x 1
    R = [Q1 Q2 Q3 Q4 Q6 Q7 Q8 Q9 Q10 Q11 Q12 Q13 Q14 Q15 Q16 Q17 Q18 Q19 Q20 Q21 Q22
Q23];

    % Define 1 x m row vector containing labels of each independent variables or flow
model terms in string format
    termNam = {'P/mu', 'N*D', 'N^2', 'D*(P/2*pi*mu)', '(P/mu)*Dmax', 'P/(mu*N)',
'(P/mu)', 'P2/mu',...
        '(D^2/3)*sqrt(2P/rho)', 'sqrt(P/(mu*N))', 'sqrt(P/rho)', '(rho/P)*N^3',
'sqrt(P2)',...
        'D*P/K', 'P*N*D', 'P*N*D/K', 'N*P/K', '(1-P2/K)*D*N', 'N', 'P', 'P*D/mu',
'P*(D^2)/mu'};

    % Calling BestSubsetReg.m user defined function to conduct best subset regression
analysis
    [models,modelstats,Treg] = BestSubsetReg(Q,R,termNam,1E-100,5,0.99,0.45,10);

    % To save Treg table which constains models that satisfy selection criteria
    filename = 'TestCell2_PumpFlowModels.xlsx';       % Name of excel file that will be
created to store Treg
    writetable(Treg,filename,'Sheet',1,'Range','A1'); % Writing Sheet1 of created excel
file

else % If user want to generate torque models
    % Define n x m matrix containing m independent variables or torque model terms of
size n x 1
    R = [T1 T2 T3 T4 T5 T6 T7 T8 T9 T10 T11];

    % Define 1 x m row vector containing labels of each independent variables or torque
model terms in string format
    termNam = {'mu*N*Vth', 'mu*N/P', 'mu*N', 'rho*(Vth^5/3)(N^2)/(4*pi)', 'mu*(N^2)',
'rho*(N^2)',...
        'Vth*P/(2*pi)', 'Vth*(Po-20*Pi)/(1+(N/1.81)^2.35)', 'sqrt(mu*N/P)', 'P^2',
'mu*N/P', 'Tpth'};
```

```
    % Calling BestSubsetReg.m user defined function to conduct best subset regression
analysis
    [Treg]=BestSubsetReg(Tp,R,termNam,1E-50,4,0.90,15,10);

    % To save Treg table which constains models that satisfy selection criteria
    filename = 'TestCell2_PumpTorqueModels.xlsx';     % Name of excel file that will be
created to store Treg
    writetable(Treg,filename,'Sheet',1,'Range','A1'); % Writing Sheet1 of created excel
file
end
```

Appendix F: MATLAB Function for Best Subset Regression

```
function [Treg] = BestSubsetReg(Y,X,Xlabels,alpha,maxTerm,minR2,maxS_err,maxVIF)
% [Treg] = BestSubsetReg(Y,X,Xlabels,alpha,maxTerm,minR2,maxS_err,maxVIF)
%
% DESCRIPTION
% This function conduct the best subset regression and the multiple linear regression
analysis
% to select the best combination of terms, and determine their coefficients, respectively
% based on the selection scriteria which are confident interval, number
% of terms in the model, R-squared value and standard error of the model,
% and VIF value of each coefficients
%
% REQUIRED ARGUMENTS
% Y          : n x 1 column vector of the variable of which the model need to be
generated
% X          : n x m matrix containing m independent variables of size n x 1
% Xlabels    : 1 x m row vector containing labels of each independent variables in string
format
% alpha      : Confidence interval in fraction
% maxTerm    : Maximum numbers of independent variables terms above which all the models
will be discarded
% minR2      : Minimum R-squared value below which all the models will be discarded
% maxS_err   : Maximum Standard error value above which all the models will be discarded
% maxVIF     : Maximum Variance Inflation Factor (VIF) value above which all the models
will be discarded
%
% OPTIONAL ARGUMENTS
% No optional argument.
%
% OUTPUT VARIABLES
% Treg       : All the possible models with stats which satisfy the selection criteria
%
% REQUIRED FUNCTIONS (USER-DEFINED)
% MLinReg.m
% ExpressIntoEqn.m


% Initialization
count = 0;
k = 0;
[n m] = size(X);
for i = 1:size(X,2)
    % Get all possible combinations of the input factors
    c = combnk(1:size(X,2),i);

    % loop over each possible combination
    for j = 1:size(c,1)
        inmodel = ones(size(c(j,:)));

        % Only allow specified maximum number of terms and less than 1 number
        % of terms combination to search for best combination for generating model
```

```
        if (size(X(:,c(j,:)),2) == maxTerm | size(X(:,c(j,:)),2) == maxTerm-1)
            count = count+1;        % To keep track of the count of the model

            % If user want to generate model with just a single trem than
            % conduct simple regression analysis because stepwise
            % regression will not work for just one term
            if length(inmodel) == 1

[Models{count}.b,Models{count}.bint,Models{count}.r,Models{count}.rint,stats] =
regress(Y,[X(:,c(j,:)) ones(size(Y))]);
                Models{count}.R2 = stats(1); Models{count}.fstat = stats(2);
Models{count}.pval = stats(3); Models{count}.ErrVar = stats(4);
                Models{count}.count = count; Models{count}.NumVar =
length(Models{count}.b)-1;
                Vmtrx = [X(:,c(j,:)) Y]';
                [b SE t Models{count}.vif Models{count}.S_err Models{count}.s_sqd R_sqd]
= MLinREG(Vmtrx);

                % To display
                ModelStats(count,2) = Models{count}.NumVar;         % Number of terms
                ModelStats(count,3) = Models{count}.R2;             % R-squared value
                ModelStats(count,4) = Models{count}.S_err;          % Standard error
                ModelStats(count,5) = max(Models{count}.vif);       % Max of VIF

            else % If more than one terms than conduct stepwise regression analysis

[notused,Models{count}.se,Models{count}.pval,Models{count}.inmodel,Models{count}.stats,Mo
dels{count}.nextstep,Models{count}.history] =
stepwisefit(X(:,c(j,:)),Y,'inmodel',inmodel,'display','off');

[Models{count}.b,Models{count}.bint,Models{count}.r,Models{count}.rint,stats] =
regress(Y,[X(:,c(j,:)) ones(size(Y))]);%just to get the model coef, resid, etc in same
format
                Models{count}.R2 = stats(1); Models{count}.fstat = stats(2);
Models{count}.pval = stats(3); Models{count}.ErrVar = stats(4);
                Models{count}.count = count; Models{count}.NumVar =
length(Models{count}.b)-1;
                Vmtrx = [X(:,c(j,:)) Y]';
                [b SE t Models{count}.vif Models{count}.S_err Models{count}.s_sqd R_sqd]
= MLinREG(Vmtrx);


                % To display into Treg
                ModelStats(count,2) = Models{count}.NumVar;         % Number of terms
                ModelStats(count,3) = Models{count}.R2;             % R-squared value
                ModelStats(count,4) = Models{count}.S_err;          % Standard error
                ModelStats(count,5) = max(Models{count}.vif);       % Max of VIF
            end


            % Check whether model satisfy all the selection criteria or not
            if all(Models{count}.pval<alpha & Models{count}.R2 >= minR2 &
Models{count}.S_err <= maxS_err & Models{count}.vif <= maxVIF)
                Sigfact(count) = 1;     % Check for all significant factors
```

```
                k = k+1
                ModelStats(count,1) = k;
            else
                Sigfact(count) = 0;
            end

            % To display count of the model into Treg
            ModelStats(count,6) = count;

            % Determine AIC value as AIC = N ln(ESS/N)+2*number of parameters and
intercept
            ModelStats(count,8) = size(X,1)*log(ModelStats(count,1)/size(X,1))+2*(i+1);

            % Store more parameters in models
            Models{count}.facts = Xlabels(c(j,:));                      % Level of each
term
            Models{count}.string = ExpressIntoEqn(Models{count});       % Model equation
with coefficients
            Models{count}.X = X(:,c(j,:));
            ModelStats(count,7) = string(ExpressIntoEqn(Models{count}));
            Equation(count,1) = string(ExpressIntoEqn(Models{count}));
        end
    end
end

% Get only the significant models and sort them by their AICs
inds = find(Sigfact);
[useless,inds2] = sort(ModelStats(inds,end));
ModelStats = ModelStats(inds(inds2),:);
for i = 1:length(inds)
    terminate{i} = Models{inds(inds2(i))};
    terminate2{i} = Equation{inds(inds2(i))};
end

% Check if there are any significant models at all or not
if exist('terminate')
    Models = terminate;
elseif exist('terminate2')
    Equation = terminate2;
else
    Models = [];
    Equation = [];
end
Equation = Equation';

% calculate the delAIC value which is the each model's AIC minus value the
% mininum AIC value
delAIC = ModelStats(:,end)-min(ModelStats(:,end));

% Compute the wieghts of the delAICs
AICweight = exp(-delAIC/2)/sum(exp(-delAIC/2));
ModelStats = [ModelStats delAIC AICweight];

% Output results in a tabular format which contains the selection criteria
```

```
Treg =
table(ModelStats(:,1),ModelStats(:,2),ModelStats(:,3),ModelStats(:,4),ModelStats(:,5),Mod
elStats(:,6),...
    Equation, ModelStats(:,8), ModelStats(:,9), ModelStats(:,10), ...
    'VariableNames',{'k' 'NumberofVariables' 'Rsquared' 'StdError'  'MaxofVIF' 'count'
'Model' 'AIC' 'delAIC' 'AICweight'});
Treg = sortrows(Treg,[4, 5]);

% HERE THE FOLLOWING STRUCTURED PARAMETERS ARE:
% Models     : All the possible models including the ones which don't satisfy selection
criteria
% ModelStats : Stats of all possible models including the ones which don't satisfy
selection criteria
end


function [b SE t VIF StdErr Ssqd Rsqd] = MLinREG(Vmtrx)
% [b SE t VIF StdErr Ssqd Rsqd] = MLinREG(Vmtrx)
%
% DESCRIPTION
% This function conduct Multiple regression using least squares.
%
% REQUIRED ARGUMENTS
% Vmtr is a data array contains both dependent and indepent variables
%
% OPTIONAL ARGUMENTS
% No optional argument.
%
% OUTPUT VARIABLES
% b     :   row of cofficients
% SE    :   row of standard error for the coefficient
% t     :   row of the t statistic for the cofficient
% VIF   :   row of the VIF for the coefficient
% StdErr:   standard error for the model
% Ssqrd :   Error variance
% Rsqd  :   R^2
%
% REQUIRED FUNCTIONS (USER-DEFINED)
% NO user defined function is required.

% To check if the constant is required to be considered in regression analysis
[m,n] = size(Vmtrx);      % Size of the matrix Xd
Y = Vmtrx(m,:)';
X = [ones(n,1) Vmtrx(1:m-1,:)'];

% Constant coefficient vector
b = (inv(X'*X))*X'*Y;
b = b.';

% Error sum of squares (SSE): It measures the departure of the observed
% Y-values from the ones predicted by the model.
SSE = Y'*(eye(n)-(X*(inv(X'*X))*X'))*Y;
Ssqd = SSE/(n-m+1);
```

```
% Regression sum of squares (SSR): It measures the departure of the
% regression line from horizontal.
SSR = b*X.'*Y-(1/n)*(transpose(ones(n,1))*Y).^2;

% Total sum of squares (SSTO): The total amount of variation in the
% independent variable Y is measured by the sum of squared deviation of the
% Y-value from their mean.
SSTO = Y.'*Y-(1/n)*(transpose(ones(n,1))*Y).^2;

% Error sum of squares (SSE): It measures the departure of the observed
% Y-values from the ones predicted by the model.
SSE =  SSTO-SSR;

% Determine R-squared value for the model
Z = (1/n)*ones(n);
Rsqd = (Y'*((X*(inv(X'*X))*X')-Z)*Y)/(Y'*(eye(n)-Z)*Y);

% Determine the standard error for the coefficient
SE = sqrt(diag(Ssqd*(inv(X'*X))));
SE = SE.';

% Determine t-statistic for the cofficient
t = b./SE;

% Compute Variance inflation factor (VIF)
for j = 2:m
    Yn = X(:,j);
    Xn = X(:,[1 2:j-1,j+1:m]);
    R_sqr(j-1) = (Yn'*(Xn*(inv(Xn'*Xn))*Xn'-Z)*Yn)/(Yn'*(eye(n)-Z)*Yn);
end
VIF = 1./(1-R_sqr);                         % Variance inflation factor
VIF = [0 VIF];

% Compute standard error of the model
Resi = Y - (X*(inv(X'*X))*X')*Y;       % Residual
vari = var(Resi);                      % Variance of residual
[e, f] = size(Vmtrx');                 % Size of transpose matrix Xd
StdErr = sqrt(Resi'*Resi/(e - f));     % Standard error of the model
end


function ModelEqn = ExpressIntoEqn(Model)
% ModelEqn = ExpressIntoEqn{Model}
%
% DESCRIPTION
% This function give a string representation of a particular model equation.
%
% REQUIRED ARGUMENTS
% Model   : It is structure variable that contain both the coefficients and
%         labels of the factors
%
% OPTIONAL ARGUMENTS
% No optional argument.
%
```

```
% OUTPUT VARIABLES
% ModelEqn : contains model's equation in string format
%
% REQUIRED FUNCTIONS (USER-DEFINED)
% NO user defined function is required.

ModelEqn = [];  % Create a vector to store model's euqtaions in string form
Model.facts{end+1} = '';  % The intercept doesn't need to be called anything

% Loop through all the constant coefficient terms of the model
for i = 1:length(Model.b)

    % To give equation a symbolic expression by using bracket and
    % multiplication symbol or nothing
    if i<length(Model.b) % If it is not the last coefficient put the following symbol
        symb1 = '*(';
        symb2 = ')';
    else                  % If it is the last coefficient put nothing as symbol
        symb1 = '';
        symb2 = '';
    end

    % Now combine constant coefficient with the label of the factors
    if Model.b(i)<0
        coeffWfact{i} = [num2str(Model.b(i)) symb1 char(Model.facts(i)) symb2];
    else
        coeffWfact{i} = ['+' num2str(Model.b(i)) symb1 char(Model.facts(i)) symb2];
    end
end

% Now express all therms and coeffiicent as a equation
for i = 1:length(coeffWfact)
    ModelEqn = [ModelEqn char(coeffWfact{i})];
end
end
```

Engineering

Capstone Report Approval Form

Master of Science in Engineering – MSE

Milwaukee School of Engineering

This capstone report, titled "Modeling of Axial Piston Pump Input Torque and Output Flow Rate using MATLAB® Simulink," submitted by the student Pawan Panwar, has been approved by the following committee:

Faculty Co-Advisor: _____ Date: _____

Dr. Daniel Williams, Ph.D. 08/27/2018

Faculty Co-Advisor: _____ Date: _____

Paul Michael, B.S., M.B.A. 08/27/2018

Faculty Member: _____ Date: _____

Professor Gary Shimek, M.L.I.S. 08/27/2018